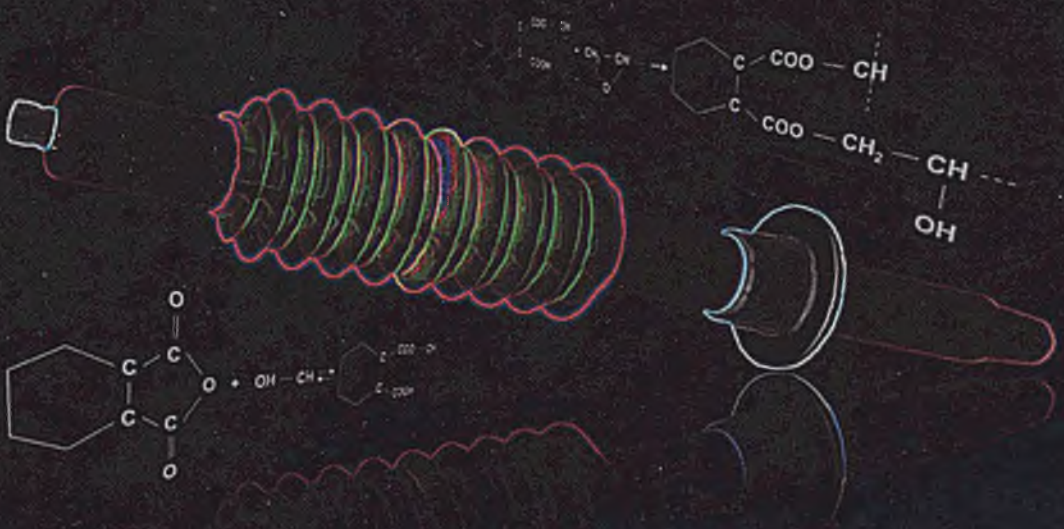


Lukasz Matysiak

Experimental Analysis and Inverse Approach in Numerical Modelling of Curing Process of Composite Materials

Ph.D. Thesis



Lukasz Matysiak

**Experimental Analysis and Inverse
Approach in Numerical Modelling
of Curing Process of Composite
Materials**

Ph.D. Thesis

Institute of Thermal Technology
Faculty of Energy and Environmental Engineering
Silesian University of Technology
Gliwice, Poland, 2014



Author:

Lukasz Matysiak
ABB Corporate Research
Starowislna 13A
31-038 Krakow
Poland
e-mail: lukasz.matysiak@pl.abb.com

Supervisors:

Professor Andrzej J. Nowak
Silesian University of Technology, Gliwice, Poland
e-mail: andrzej.j.nowak@polsl.pl

Doctor Zbigniew Bulinski
Silesian University of Technology, Gliwice, Poland
e-mail: zbigniew.bulinski@polsl.pl

Silesian University of Technology
Faculty of Energy and Environmental Engineering
Institute of Thermal Technology
Konarskiego 22
44-100 Gliwice
Poland

Polish title of the Ph.D. Thesis:

**Badania Eksperymentalne oraz Numeryczna Analiza Odwrotna Procesu
Utwardzania Materiałów Kompozytowych**

© Copyright 2014 by Lukasz Matysiak

ISBN 978-83-61506-24-9

CONTENTS

Introduction	5
1. The first part	11
2. The second part	17
3. The third part	23
4. The fourth part	29
5. The fifth part	35
6. The sixth part	41
7. The seventh part	47
8. The eighth part	53
9. The ninth part	59
10. The tenth part	65
11. The eleventh part	71
12. The twelfth part	77
13. The thirteenth part	83
14. The fourteenth part	89
15. The fifteenth part	95
16. The sixteenth part	101
17. The seventeenth part	107
18. The eighteenth part	113
19. The nineteenth part	119
20. The twentieth part	125
21. The twenty-first part	131
22. The twenty-second part	137
23. The twenty-third part	143
24. The twenty-fourth part	149
25. The twenty-fifth part	155
26. The twenty-sixth part	161
27. The twenty-seventh part	167
28. The twenty-eighth part	173
29. The twenty-ninth part	179
30. The thirtieth part	185
31. The thirty-first part	191
32. The thirty-second part	197
33. The thirty-third part	203
34. The thirty-fourth part	209
35. The thirty-fifth part	215
36. The thirty-sixth part	221
37. The thirty-seventh part	227
38. The thirty-eighth part	233
39. The thirty-ninth part	239
40. The fortieth part	245
41. The forty-first part	251
42. The forty-second part	257
43. The forty-third part	263
44. The forty-fourth part	269
45. The forty-fifth part	275
46. The forty-sixth part	281
47. The forty-seventh part	287
48. The forty-eighth part	293
49. The forty-ninth part	299
50. The fiftieth part	305
51. The fifty-first part	311
52. The fifty-second part	317
53. The fifty-third part	323
54. The fifty-fourth part	329
55. The fifty-fifth part	335
56. The fifty-sixth part	341
57. The fifty-seventh part	347
58. The fifty-eighth part	353
59. The fifty-ninth part	359
60. The sixtieth part	365
61. The sixty-first part	371
62. The sixty-second part	377
63. The sixty-third part	383
64. The sixty-fourth part	389
65. The sixty-fifth part	395
66. The sixty-sixth part	401
67. The sixty-seventh part	407
68. The sixty-eighth part	413
69. The sixty-ninth part	419
70. The seventieth part	425
71. The seventy-first part	431
72. The seventy-second part	437
73. The seventy-third part	443
74. The seventy-fourth part	449
75. The seventy-fifth part	455
76. The seventy-sixth part	461
77. The seventy-seventh part	467
78. The seventy-eighth part	473
79. The seventy-ninth part	479
80. The eightieth part	485
81. The eighty-first part	491
82. The eighty-second part	497
83. The eighty-third part	503
84. The eighty-fourth part	509
85. The eighty-fifth part	515
86. The eighty-sixth part	521
87. The eighty-seventh part	527
88. The eighty-eighth part	533
89. The eighty-ninth part	539
90. The ninetieth part	545
91. The ninety-first part	551
92. The ninety-second part	557
93. The ninety-third part	563
94. The ninety-fourth part	569
95. The ninety-fifth part	575
96. The ninety-sixth part	581
97. The ninety-seventh part	587
98. The ninety-eighth part	593
99. The ninety-ninth part	599
100. The hundredth part	605

Contents

Acknowledgments	9
Nomenclature	11
1. Introduction	17
1.1. Background.....	17
1.2. Literature review.....	20
1.3. Thesis objectives.....	25
1.4. Thesis outline.....	28
2. Electrical bushings	31
2.1. Technology of Resin Impregnated Paper bushings.....	31
2.2. Insulation system	34
2.3. Impregnation process.....	38
3. Mathematical modelling and determination of the kinetics of curing reaction	43
3.1. Mathematical modelling of the kinetics of curing reaction	43
3.2. Experimental determination of the kinetics of curing reaction.....	45
3.3. Determination of the curing kinetics as an inverse problem.....	49
3.3.1. Fundamentals of inverse analysis	49
3.3.2. Developed inverse methodology	51
3.3.2.1. Particle Swarm Optimization.....	54
3.3.2.2. Levenberg-Marquardt algorithm.....	56
4. Virtual experiment of curing process	61
4.1. General concept	61
4.2. Mathematical modelling of curing process.....	63
4.3. Numerical modelling of curing process.....	66
4.3.1. Model geometry.....	66

4.3.2.	Computational mesh and time-step.....	67
4.3.3.	Initial and boundary conditions	68
4.3.4.	Material properties.....	70
4.4.	Inverse calculations of the kinetics of curing reaction.....	72
4.5.	Validity of the results of inverse calculations	77
4.5.1.	Study on the influence of geometry and mesh.....	77
4.5.2.	Study on the influence of boundary conditions	80
4.5.3.	Analysis of error influence	81
4.6.	Sensitivity analysis.....	87
5.	Experimental investigation of curing process	97
5.1.	Goals and assumptions.....	97
5.2.	Experimental stand.....	98
5.3.	Research samples and experimental procedure.....	101
5.4.	Experimental results.....	103
5.4.1.	Course of curing reaction at different monitoring points.....	103
5.4.2.	Influence of sample structure.....	105
5.4.3.	Influence of heating conditions	107
5.4.4.	Influence of moisture in paper	108
5.4.5.	Mould temperature.....	109
6.	Experimental validation of the curing modelling approach	111
6.1.	General concept.....	111
6.2.	Mathematical modelling of the composite curing.....	112
6.3.	Numerical modelling of curing experiments.....	115
6.3.1.	Geometrical models	115
6.3.2.	Computational meshes and numerical time-steps.....	116
6.3.3.	Initial and boundary conditions	118
6.3.4.	Material properties.....	120
6.4.	Numerical simulations of pure heat and mass transfer	124
6.4.1.	Fitting of numerical model	125

6.4.2. Influence of mesh resolution and time-step size.....	125
6.4.3. Influence of the location of monitoring points	127
6.5. Numerical simulations of curing process.....	129
6.5.1. Inverse calculations of the kinetics of curing reaction	130
6.5.2. Results of inverse calculations	134
7. Conclusions and further work.....	141
7.1. Conclusions.....	141
7.2. Further work	144
Appendix	147
Bibliography	149
Abstract.....	157
Streszczenie.....	161

Acknowledgments

This thesis would have never been prepared without the help of many people.

Firstly, I would like to express my sincere thanks and gratitude to my supervisors, Professor Andrzej J. Nowak and Doctor Zbigniew Bulinski from Institute of Thermal Technology at Silesian University of Technology in Gliwice, Poland for their great guidance, support, patience and time devoted to me during the preparation of this thesis.

Additionally, I would like to direct many thanks to Doctor Zbigniew Bulinski for conducting Differential Scanning Calorimetry measurements and to Institute of Thermal Technology at Silesian University of Technology for testing equipment used in these experiments.

I am also truly grateful to Doctor Marek Florkowski, Director of ABB Corporate Research Centre in Cracow, Poland both for financial support as well as for making the laboratory equipment, computational and software resources available to me.

I would like to emphasize the priceless contribution to this thesis made by my colleagues from Manufacturing Mechanics and Materials Science Group at ABB Corporate Research Centre. This thesis would be surely of less significance without the fruitful discussions and valuable advices given especially by Doctor Robert Sekula and Krzysztof Kasza.

I wish to thank to Rafal Ziemski and Artur Falkowski from ABB Corporate Research Centre for their help in carrying out the part of experimental work described in this thesis.

I appreciate the help of Maciej Niebylski, Tomasz Swietoniowski and Sylwester Jarosinski in the software development that was used for the purpose of inverse calculations.

I would also like to show my appreciation to my whole family, especially to my wife Renata, for a great understanding, support and belief in me that I got from them during the work on this thesis.

Finally, I am indebted to all the people not listed here who contributed to this thesis preparation.

Nomenclature

Latin symbols

A, A_1, A_2	Arrhenius frequency factor, 1/s
B_1, B_2	function coefficient
c_1	cognitive parameter (personal learning factor)
c_2	social parameter (social learning factor)
C	inertial resistance tensor, 1/m
d_p	diameter of particles constituting the packed bed, m
$d_{p,j}$	diameter of pores in a given direction j , m
D_j	viscous resistance coefficient in a given direction j , 1/m ²
D	viscous resistance tensor, 1/m ²
E	total energy, J/kg
E_a	activation energy, J/kmol
E_1, E_2	activation energy, K
f	function
g	function
\mathbf{g}	vector of gravitational acceleration, m ² /s
G	objective function, K ²
H_t	heat of curing reaction generated until time t , J/kg
H_Σ	total heat of curing reaction, J/kg
IF	improvement factor, %
J_i	sensitivity matrix (Jacobian matrix) in a given iteration i
J_i^R	matrix of relative sensitivity coefficients in a given iteration i , K
k	Arrhenius reaction rate coefficient, 1/s
k_{02}	coefficient of the kinetics model of curing reaction
k_1	externally catalysed rate constant, 1/s
k_2, k_3	autocatalytic rate constant, 1/s
l_j	length of packed bed in a given direction j , m
m	mass, kg

M	mean
$NORMSINV()$	Microsoft Office function returning the inverse of the standard normal cumulative
p	pressure, Pa
P	parameter of the kinetics model of curing reaction
PF	perturbation factor, %
$\dot{q}_{v,r}$	volumetric heat source due to curing reaction, W/m^3
Q_{EVS}	Equivalent Size Skewness parameter
r_1, r_2	random number between 0 and 1
R	universal gas constant equal to 8314.47, $J/(kmolK)$
$RAND()$	Microsoft Office function returning a random number between 0 and 1 (evenly distributed)
S_{cell}	area of mesh cell, m^2
S_{eq}	maximum area of an equilateral cell that has identical circumscribing radius as that of mesh cell, m^2
S	vector of momentum source term expressing pressure drop due to flow through porous material, N/m^3
SD	standard deviation
t	time, s
T	temperature, K
T_i^{est}	matrix of the estimated temperatures in a given iteration i , K
T^{meas}	matrix of the measured temperatures (measured experimentally or generated virtually in simulated measurement), K
u	inertia weight
v_h	heating rate, K/min
v_i^p, v_{i+1}^p	vector of velocity of a given particle p in a given iteration i
v_{max}	vector of the maximum velocity values
V	volume, m^3
w_j	component of the velocity vector in a given direction j , m/s
w	velocity vector, m/s
x^{bp}	vector of the best position found by a given particle p
x^{bs}	vector of the best position found by a swarm
x_i, x_{i+1}	vector of the parameters values in a given iteration i

$\mathbf{x}_i^p, \mathbf{x}_{i+1}^p$ vector of position of a given particle p in a given iteration i

Abbreviations

CFD	Computational Fluid Dynamics
DMA	Dynamic Mechanical Analysis
DMTA	Dynamic Mechanical Thermal Analysis
DSC	Differential Scanning Calorimetry
FTIR	Fourier Transform Infrared
FVM	Finite Volume Method
GUI	Graphical User Interface
IRACKLIS	InveRse Approach in Curing Kinetics anaLysis
MDR	Moving Die Rheometer
NMR	Nuclear Magnetic Resonance
ODR	Oscillating Disc Rheometer
OIP	Oil Impregnated Paper
PISO	Pressure-Implicit with Splitting of Operators
PSO	Particle Swarm Optimization
RBP	Resin Bonded Paper
RIP	Resin Impregnated Paper
SF6	sulphur hexafluoride
SVD	Singular Value Decomposition
TMA	Thermomechanical Analysis

Greek symbols

α	degree of curing
$\dot{\alpha}$	curing rate, 1/s
β	independent variable
ϕ	dependent variable
γ	porosity
ϑ_i	damping parameter in a given iteration i
κ	damping parameter modifier
λ	thermal conductivity, W/(mK)
μ	dynamic viscosity coefficient, kg/(ms)

ρ	density, kg/m^3
Ω_i	damping matrix in a given iteration i

Subscripts

b	number of temperature level
c	length of epoxy resin chain
$cell$	cell
e	effective
f	fluid
fin	final
har	hardener
i	number of iteration
ini	initial
k	number of sampling time instance
l	number of sampling point
$meas$	measure
mix	mixture
p	pores
res	resin
s	solid

Superscripts

bs	best of a swarm
bp	best of a given particle p
est	estimated
K	total number of measurement points
L	total number of sampling time instances
m, m_1, m_2	curing reaction order
max	maximum
$meas$	measured
min	minimum
n, n_1, n_2	curing reaction order
p	particle

T transpose

Mathematical symbols

∇ gradient operator

∇^2 Laplacian operator

1. Introduction

1.1. Background

People have got used so much to an unlimited access to electricity that no one thinks nowadays, when plugging in e.g. home use devices into the socket, how the electrical energy is generated, transformed, stored and/or finally transmitted. Meanwhile, a huge number of different electrical devices act “behind” the socket to ensure a reliable, constant and safe access to the power. Among them generators, power transformers, distribution transformers, switchgears or transmission lines can be found to quote only few examples. A common denominator for all apparatuses constituting the power network is an extremely high requirement for their operational safety that can only be guaranteed by a reliable electrical insulation.

This concerns also electrical bushings that are used to transmit current at high potential through a grounded enclosure of an electrical equipment including among others the mentioned earlier power transformers, distribution transformers, switchgears, but also circuit breakers, power capacitors and shunt reactors [1, 2, 3, 4]. The role of bushing electrical insulation is to withstand the voltage at which it is applied to avoid overvoltage that can lead to a flashover in the insulation and to the failure not only of the bushing, but also for example of a few million dollars’ worth power transformer. For this reason there is a high demand for a failure-free insulation system in electrical applications.

Resins have been used for this purpose from the very beginning of bushings technology. The first bushings with dry type insulation involving Bakelite (resin-coated) paper and aluminium foils with outer porcelain insulator, so-called Resin Bonded Paper (RBP) bushings, appeared already at the beginning of 20th century. Later on, an increasing voltages determined changes in the electrical insulation design. Today, the newest and dominant protective solutions used in bushings are based on paper impregnated either with mineral oil known as Oil Impregnated Paper (OIP) insulation or with epoxy resin system called Resin Impregnated Paper (RIP) insulation. The second technology, gaining bigger and bigger market share, utilizes different grades of epoxy systems to form the electrically insulating layer.

The reason for great interest of bushings society in epoxy resins, which can be observed recently, are their excellent properties including dielectric strength, good volume resistivity, low dissipation factor, low shrinkage during curing, good adhesion, high mechanical strength and, finally, ability to retain all

these properties under varying ambient conditions [5]. It should be stressed that electrical, thermal and mechanical characteristics of epoxy resin must be tailored to the specific application requirements and, hence, the material properties are usually modified by addition of fillers. Most commonly, particulate inorganic fillers like silica are used for this purpose. Fillers addition increases hardness, lowers shrinkage during curing, diminishes the heat coming from the exothermic curing reaction lowering in this way the risk of material overheating, adds opacity and colour, improves other general processing and performance parameters, but also decreases the overall material cost [5].

Unfortunately, fillers presence in epoxy systems complicates the material processing. One of the common threats is the possibility of filler sedimentation during the epoxy casting process, what happens especially in case of high components like bushings for high-voltage applications. Sedimentation effect causes non-uniform filler distribution leading to anisotropic properties of the electrical insulation [6]. Meanwhile, an optimum filler content ensuring the best electrical, thermal and mechanical characteristics is usually strictly defined for the specific application and material under consideration [7, 8]. Too big deviations from this optimum filler concentration, even only in some regions, can result in the insulation failure. For this reason filler sedimentation issue was one of the factors influencing the mentioned evolution of the bushings design. It played an important role in the introduction of Kraft paper that, wound with aluminium foils on aluminium or copper rod and impregnated with epoxy system, constitutes the structure of the condenser cores in modern bushings [9]. One of the functions fulfilled by Kraft paper is to prevent the filler sedimentation during the processing of epoxy system.

Relatively complex structure and big dimensions of high-voltage RIP bushings is only one of the reasons making the production process extremely demanding. Even bigger difficulty is caused by a great number of physical and chemical phenomena occurring during the curing process of the resin-paper composite insulation. One can find among them the following: mass flow including flow through the porous structure of the crepe paper, heat transfer in fluids and solids, thermal expansion, thermal and chemical shrinkage of epoxy resin, stresses generation and relaxation, phase change of epoxy system because of the exothermic polymerization reaction. This chemical reaction is one of the most critical issues influencing the processing of epoxy resins. The course of this process is strongly coupled with heat transfer. On the one side, the cross-linking reaction requires heat for activation and the rate of this reaction is dependent on temperature. On the other side, the transformation of the liquid epoxy resin into highly-cross linked solid body generates big amounts of heat, what can lead to local overheating and, as a consequence, to degradation of the insulation

properties. Therefore, the understanding and control of the curing process is a matter of big significance.

As in any other product, the design and manufacturing process of high-voltage RIP bushings can be analysed and possibly improved. A common engineering practice is to apply experiments for this purpose, but such solution is usually unfounded in case of high-voltage bushings due to significant costs and time needed to perform experiments on these devices. Moreover, it is typical that experimental trials require interruption in production and, hence, factories do everything they can to avoid such situations. An interesting alternative can be computer simulations that have already been used for four decades in modelling of physical processes in scientific research and in the analysis and design of engineered systems. The most extensive development of the modelling and simulation-based design has been observed during the last thirty years, when numerical methods became mature enough and numerical modelling was raised to the rank of science. At the same time, the processors capacity and computer memory offered by modern computing units increased enormously. This development has met in time with growing competition in many technological industries like automotive, air, military, medical or energy one to quote only few examples. This forced engineers to search for fast and cost-efficient methods of designing and optimization of products and their manufacturing processes. It was found then that the application of computer modelling instead of or together with experiments lowers the cost and time of bringing new products to the market. Moreover, this computer-aided approach can be executed without or with minimized interference into production process on contrary to experiments.

The observed bigger and bigger popularity of computer simulations in solving engineering problems confirms their undoubted advantages and, simultaneously, stimulates reflexion on how accurate and reliable are results obtained by numerical analyses. This issue is of vital importance especially in case of industrial simulations, since the reliability, robustness and safety of some of the computationally-based designs are high-consequence systems that cannot be ever tested [10]. Meanwhile, their failure can have significant safety, legal and liability consequences. In this connection, it is critical to perform credibility analysis (known also as verification and validation analysis) [11] of numerical approach applied to solve industrial problems. For better understanding it can be noticed that each numerical analysis consists of three components, i.e. model, code and simulation. Basically, one implements model into the computer code and then uses this code to perform the numerical simulation which yields values further used in engineering analysis [12]. Hence, it is extremely important to examine errors in the model and code as well as in the simulations results by applying verification and validation procedure. More precisely, verification

determines if the programming and computational implementation of the conceptual model is correct. At this stage the potential computer programming errors and numerical errors (round-off error, iterative error, discretization error) can be excluded. The verification assessment is done either through the comparison of simulation results to exact analytical ones (if such benchmarks exist) or by checking if the solution fulfils the governing equations constituting the mathematical model of the considered problem. In turn, validation assessment determines if the computational simulation agrees with physical reality and for that the science in the models is tested through the comparison with experimental results. Based on the output of credibility analysis one can assess uncertainties and recognize possible sources of errors in the developed numerical approach. This, in turn, allows one to decide if they are on acceptable level and, consequently, if computer simulations based on such an approach can be applied to solve engineering problems with reasonable confidence.

Computational modelling with both verification and validation assessments can certainly be applied to improve particular stages of the manufacturing process of high-voltage RIP bushings which eventually results in improvement of the whole production process. What has already been done and what new directions can be investigated in this context is presented in the next section.

1.2. Literature review

High level of complexity of the curing process, discussed before and connected with the plurality of physical and chemical phenomena acting simultaneously, is also reflected in the numerical modelling of that process. According to [13] the standard set of governing equations (mass conservation equation, Navier-Stokes equation and energy equation) must be supplemented with additional model to reflect the kinetics of curing reaction of epoxy system. Formula proposed by Kamal-Sourour [14, 15] is most often used for this purpose in case of thermosetting materials. In this approach the kinetics of polymerization reaction is represented by the model consisted of several parameters that are determined individually for a given material. The modelling of the curing process of composite structures like in case of crepe paper impregnated with epoxy system is even more complicated, since the mathematical model must be developed further to include the influence of the porous body presence on the mass and heat transfer mechanisms in the considered system as well as on the course of curing reaction.

There is a plenty of experimental methods being used in practice that allows describing the characteristics of curing reaction. It is worth noticing that

none of the existing techniques is capable of measuring the polymerization process directly. Hence, the relations between the course of curing reaction and the properties of investigated material (mechanical, thermal or dielectric) are usually used to define the curing kinetics [16]. One can find the following experimental methods among the ones applied for the analysis of the curing kinetics: Differential Scanning Calorimetry (DSC), Oscillating Disc Rheometer (ODR), Moving Die Rheometer (MDR), Mooney viscometer, specific curemeters [17], swelling measurements [18], Dynamic Mechanical Thermal Analysis (DMTA) [19], Dynamic Mechanical Analysis (DMA) [20], Thermomechanical Analysis (TMA) [21], Fourier Transform Infrared (FTIR) [22], Nuclear Magnetic Resonance (NMR) [23], (di)electrical [24] and ultrasonic measurements [25]. One of the most popular measurement methods used to determine the curing kinetics of thermosetting materials like epoxy resins is DSC [26, 27, 28]. However, DSC technique is limited by small sample size reaching usually a few milligrams what complicates the preparation of specimens, especially anisotropic ones like in case of crepe paper impregnated with epoxy system. It is also doubtful if the results obtained in small scale measurements are valid for much bigger and complex geometries like a few meters long high-voltage RIP bushings.

The performed literature survey revealed that the determination of the kinetics of phase change process, similar to the curing of epoxy resins, can also be defined as a subject of inverse analysis. It should be explained that the literature on inverse problems in general is so extensive that only selected publications are shortly described in the following part of this subchapter. One of the interesting papers found is the work of Brizaut et al. [16], where the curing process of a rubber is considered. The experimental stand used in the validation procedure allowed authors to bring the problem to one-dimensional case. The energy effects of the curing reaction were reflected in the internal heat source term of energy equation. The applied model of polymerization reaction consisted of several parameters. The goal of the proposed inverse analysis was to find some parameters of the curing reaction model, whereas the remaining ones were determined based on DSC experiments. The parameters were searched within the inverse approach by matching the results of temperature measurements recorded during experiment with the outcome of numerical calculations done with the use of thermal model of the considered process. The iteration procedure led to a good agreement between the measured and the calculated temperatures, and, the parameters values were consistent with these determined in the calorimetric measurements.

Another application of inverse analysis was presented in the publication of Majchrzak et al. [29], who deals with the problem of binary alloy solidification during a foundry process. The inverse procedure was applied to find one of the

parameters constituting the model of the kinetics of solidification reaction. It is worth stressing that the alloy was modelled as a homogenous material and, again, the effects of the solidification phenomenon were reflected in the mathematical model as internal heat sources in the energy equation. The goal defined in the inverse procedure was to find the parameter value minimizing the difference between the measured and the calculated temperatures. However, instead of performing real experiment, numerical simulation with known value of the sought parameter was used to generate the reference data (so-called simulated measurement). Further, the value of the sought parameter was perturbed and such modified numerical model was tuned in few iterations to find eventually the parameter value, which was close to the reference one. Additionally, authors performed an error analysis by introducing artificial perturbations to the reference data and the developed methodology turned out to be effective also in this case.

Meanwhile, Szeliga et al. [30] used inverse analysis to identify the coefficients of three models describing the properties of microalloyed niobium steel, i.e. rheological models of ferrite and austenite and phase transformation model of ferrite. Dilatometric and plastometric experiments were conducted in order to record the reference data utilized further in inverse calculations. Temperatures and volume fractions of phases were measured in dilatometric experiment, while loads were measured during plastometric experiment. Direct numerical model was developed to simulate the mentioned measurements, including model describing the flow stress of the considered material. The mentioned coefficients present both in the rheological models and phase transformation model were calculated in inverse analysis by minimizing the difference between the experimental data and values computed in numerical simulations. Authors reported satisfactory agreement between the experimental and numerical results proving the effectiveness of the proposed inverse procedure.

One of only few papers presenting the solution of inverse problem formulated for composite material in the form of carbon reinforced epoxy resin is the publication of Skordos et al. [31]. Authors developed direct numerical model of the investigated process in the first stage of this work. For this purpose the curing experiment and thermal properties measurements were conducted. Next, the results of simulations carried out using simplified one-dimensional and full three-dimensional models were compared. Good agreement in results allowed authors to use the simplified simulation in the inverse calculations utilising genetic algorithm. In the first approach the proposed inverse methodology was used to optimize the duration of the curing process controlling simultaneously the level of thermal gradients generated in the material during the curing progress. In another application the developed inverse procedure was

employed to find the parameters of the function describing the influence of curing degree and temperature on thermal conductivity of the composite system. The inverse calculations were supported with temperature measurements carried out during the mentioned curing experiment. Authors stated that the application of inverse procedure gave satisfactory effects. In the first analysed case the duration of the curing process was shortened excluding at the same time the possibility of residual stresses generation. The second application of inverse analysis was also successful. In this case the results of numerical simulation, run with the function parameters determined in inverse manner, were in a good agreement with the outcome of computer simulation defined based on experimental data recorded during the curing experiment and on the measurements of thermal properties of the investigated composite material.

In turn, the Jarny's publication [32] presents the solution of several inverse problems focusing on determination of thermophysical properties of different materials like metallic alloys, thermoplastics, thermoset polymers and composites. The first study described in this paper concerned the heat conduction process through semi-infinite isotropic medium having constant thermal properties. Inverse calculations supported with temperature measurements were performed in order to determine thermal conductivity and thermal diffusivity of the material. Next, the heat transfer mechanism through finite orthotropic composite material in the form of thermoset reinforced with fibres was analysed. Inverse algorithm was proposed to define the value of thermal conductivity and specific heat of the mentioned composite. Temperature measurements were again used as additional information needed to perform the inverse analysis. In further considerations author dealt with more complex problems, as dependence of thermal properties on temperature was included, both in case of isotropic and orthotropic materials. In the first case, inverse methodology and temperature measurements were applied to determine thermal conductivity of isotropic material. The same method was also used for different materials like thermoset material after polymerization, thermoplastic material under moulding conditions and metallic alloys. In case of orthotropic material, both two-directional specific heat and thermal conductivity was sought by using inverse algorithm and temperature recordings during curing experiment performed for fibre reinforced epoxy resin. Author reported very good agreement of the obtained thermal properties with the results got by using conventional methods like DSC and guarded hot plate measurements. Finally, the last research described in the article concerned determination of the specific heat, thermal conductivity and curing rate for exemplary material transformed during the phase change process (e.g. solidification for thermoplastics, cooling for alloys and curing for thermosets). The biggest difficulty was the dependence of all mentioned variables on

temperature and, additionally, on degree of transformation. Two experimental strategies were discussed allowing one to get rid of this coupling and to make the properties calculation simpler. The first method assumed measurement of thermal conductivity and specific heat at temperatures just before and just after the phase transformation process. In case of the curing kinetics it was proposed to perform DSC measurements on thin sample to avoid temperature gradient inside the sample. The curing kinetics model developed in this way was applied in computer simulation to calculate temperature distribution in the considered system. The obtained agreement between numerical results and experimental ones was on a very good level. Furthermore, optimization of the heating cycles during the analysed phase transformation process was defined as a subject of inverse analysis.

Another interesting work concerning inverse methods and kinetics, but this time of a drying process of a crepe paper, was presented in the publication of Nowak et al. [33]. In the described work authors dealt with a complex issue, since initial and parameter estimation inverse problems were coupled and solved simultaneously. Two information sought within the inverse study was the initial moisture distribution within the considered material and the evaporation constant embedded in the kinetics model describing the drying process of the analysed system. A substantial part of this research was drying experiment done on a laboratory-scale bushing, made among others of the mentioned crepe paper in the form of coil. This experiment provided information about temperatures during the drying process of the tested system. The measured data were next utilised as an input for inverse calculations that were done with the use of Levenberg-Marquardt algorithm. The goal of inverse analyses was to match the measured temperatures with the estimated temperatures by fitting the value of the evaporation constant and the initial moisture distribution within the paper coil. The calculated temperatures were obtained in the simulations based on the developed numerical model of the paper drying process. It is worth stressing that three approaches to approximate the initial moisture distribution were proposed and tested. Generally, they were based on different functions approximating the initial moisture field and the parameters of these functions were searched in the mentioned inverse analyses. The results reported by authors were promising, although it was concluded among others that poor conditioning of the considered problem could be improved by application of regularization techniques. Such an approach was a subject of the publication of Bulinski et al. [34], where authors continued the research described above. Generally, the idea of the applied Tikhonov-type regularization algorithm was to put constraints on the solution. In the first approach the value of the evaporation constant was constrained, whereas in the second case the total water mass evaporated during the drying process was

restricted. For that purpose the drying experiment was repeated and the amount of water evaporated from the system was roughly measured. Authors reported that the results obtained by combining Levenberg-Marquardt algorithm with Tikhonov-type regularization method improved the solution convergence and led to more reliable results.

1.3. Thesis objectives

The performed literature review revealed that the curing process of epoxy resin influences the manufacturing and, consequently, the quality of composite electrical insulation in high-voltage RIP bushings. For this reason understanding and proper control of the process is of vital importance, but, according to the literature search, there are no effective experimental methods that would allow one to analyse the curing process directly during the bushings production. It seems that numerical modelling can be an interesting alternative, but in this case the kinetics of curing reaction must be known to model the process in a reliable way. Meanwhile, it is questionable if the curing kinetics characterized experimentally based on few milligrams samples like in DSC measurement, is representative for much bigger and complex (composite) structures of the RIP bushing insulation. Simultaneously, it was reported in literature that the unknown kinetics of phase change process, similar to that of epoxy resin curing, can be found as a solution of inverse heat transfer problem. However, it seems that such an approach in case of composites curing as well as numerical modelling of that process is not a fully explored field of science.

The conclusions described above led to the hypothesis saying that, firstly, the curing process of resin-paper composite system can be modelled in numerical simulations. The second statement is that the kinetics of curing reaction occurring in such a structure can be determined with satisfying engineering accuracy by combining inverse methods with computer simulations and thermal experiments, done on the real composite sample and serving as an additional information needed to solve the inverse problem. It is believed that the proposed approach could fill the gap connected with the mentioned lack of methods allowing one to investigate and possibly optimize the curing process of composite insulation in high-voltage RIP bushings.

The main goal of the presented work, defined to prove the formulated hypothesis, is twofold, i.e. to develop the numerical model allowing one to simulate and analyse the curing process of epoxy resins in composite structures and to work out the inverse methodology of determination of the kinetics of curing reaction of composite bodies. Achievement of these two targets forced

additional tasks that had to be accomplished within the framework of this thesis, namely:

- choice of mathematical model of the kinetics of curing reaction of epoxy resin,
- definition of the example and simplified problem of curing process of the epoxy resin-based casting system, build-up of its mathematical and numerical models, solution of that problem for the known curing kinetics data (referred to as virtual experiment),
- implementation of the optimization algorithms into the inverse methodology and development of software automating the inverse calculations,
- application of the developed inverse methodology and the model and data used in the virtual experiment to calculate the curing kinetics of the analysed epoxy system,
- sensitivity analysis performed within the inverse analysis mentioned above to define among others the optimum location of sensors during curing experiments that were done for a similar system as the one analysed in the virtual experiment,
- assessment of the validity of the results obtained in inverse analyses in terms of the influence of geometry, mesh, boundary conditions and uncertainties in the input data,
- design and preparation of experimental stand, procedure and samples for curing experiments,
- execution of temperature measurements during the curing experiments run on three kinds of samples, i.e. epoxy resin without hardener, epoxy resin with hardener and, finally, resin-paper composite,
- build-up of mathematical and numerical models of all three experiments,
- assessment of the validity of the results obtained in numerical simulations done for the epoxy resin without hardener in terms of discretization errors (influence of mesh resolution and time-step size) and with respect to influence of the location of monitoring points,
- inverse analyses aimed at determination of the curing kinetics of the epoxy resin with hardener and of the resin-paper body,
- assessment of the validity of the curing kinetics calculated in inverse analyses for both systems mentioned above.

The general idea standing behind the developed inverse methodology is to combine three things to determine the kinetics of curing reaction, i.e. optimization algorithms (Levenberg-Marquardt and Particle Swarm Optimization known also as PSO), temperature measurements done during the curing process of the considered sample and computer simulations of that

process. In this approach the coupling between the exothermic effect of the cross-linking process and temperatures in the analysed system is utilized. The goal of the inverse procedure is to match temperatures measured experimentally with temperatures calculated in the numerical simulation of the experiment by optimizing the parameters of the curing kinetics model that constitutes an input of the numerical simulation. The effectiveness of the developed inverse methodology was verified in two ways. In the first one the mentioned virtual experiment of the epoxy system curing was performed, i.e. the results generated in the computer simulation with the known (assumed) curing kinetics constituted the measured data (simulated measurement), while in the second approach this synthetic measured data were substituted with the outcome of temperature measurements done during the real curing experiments.

The numerical models used in these investigations were created in CFD commercial software ANSYS Fluent that was selected due to its versatility resulting from a big number of available mathematical models and because of the possibility of implementing additional user-defined models. In this way it was possible to extend the standard set of governing equations (Navier-Stokes equation, mass continuity equation and energy equation) with the model describing the kinetics of curing reaction to get the full picture of the curing process in numerical simulations. Furthermore, modelling of the porous structure in the resin-paper composite required additional effort in terms of special treatment of the curing kinetics and with respect to physical properties of the material in the composite region, again offered by ANSYS Fluent.

As already mentioned, in case of experimental study three different samples were investigated. In the first experiment the epoxy resin without hardener was considered to avoid the influence of the curing reaction on heat transfer. Based on that the numerical model describing the heat and mass transfer mechanisms was developed and constituted the reference for the simulations including the curing related effects. The measurements done for the next two samples, i.e. the epoxy resin with hardener and the crepe paper impregnated with the mixture of epoxy resin and hardener, were used to capture differences in the course of curing process in homogenous and composite structures. The results of these two experimental runs were used to develop numerical models describing the curing process of both systems and as the input in inverse calculations of the curing kinetics models.

1.4. Thesis outline

The presented thesis starts with the list of nomenclature. The main part of this thesis is organized in seven chapters that are briefly described below.

Chapter 1 constitutes introduction to the subject of this work. More particularly, background of this thesis, its objectives and outline are included in this part.

Chapter 2 provides basic information about electrical bushings, with the focus on high-voltage RIP bushings having composite electrical insulation. One can find in this chapter description of the bushing structure with details concerning the mentioned insulation system. Besides that the bushings manufacturing process is explained including information about the curing phenomenon taking place during impregnation process.

The beginning part of chapter 3 describes the principles of the mathematical modelling of the kinetics of curing reaction. In further part of this chapter two methods allowing one to determine the curing kinetics data are presented. One of them is DSC experimental technique that is dedicated to the investigations of the curing kinetics of homogenous samples. The second method is the inverse approach developed within this thesis that enables determination of the kinetics of curing reaction both for homogenous and composite materials. In this part both fundamentals of inverse analysis are provided and the architecture and the principle of working of the applied inverse methodology is explained.

Chapter 4 is devoted to the virtual experiment that was executed in order to check the correctness of the mathematical mechanism used in the developed inverse methodology. The chapter starts with description of the governing equations constituting the mathematical model of the curing process of homogenous sample. Next, details of the numerical model are provided in the form of the analysed geometry, the applied numerical mesh, the specified material properties and the defined initial and boundary conditions. The key part of chapter 4 is the discussion concerning the results of inverse calculations of the model parameters of curing kinetics. Furthermore, the numerical study of the validity of the obtained curing kinetics data, done for modified geometries (consequently also numerical meshes) and boundary conditions, as well as the findings of the error influence analysis, done for the developed inverse methodology, are addressed in this section. Finally, the outcome of the sensitivity analysis performed for the investigated problem can be found in the final part of chapter 4.

Chapter 5 relates to the experimental study conducted within the thesis. The measurement stand, materials samples and experimental procedure used during laboratory tests are described. The goal of the measurements was triple.

Firstly, they provided data needed to validate the simulation approach. Secondly, it was possible to verify if and how the course of curing of the resin-paper composite differs from the polymerization of standard casting system in the form of the epoxy resin with hardener. Finally, it allowed verifying how the heating conditions influence the course of curing process.

Chapter 6 is devoted to the experimental validation of the inverse methodology proposed within the thesis. The mathematical approach to the modelling of the curing of composite structure is presented in the first part of this chapter. Besides that the geometry, initial and boundary conditions as well as physical properties of the materials used in numerical calculations are discussed. The findings related to the resolution of computational mesh, to the size of time-step and to the location of temperature monitoring points are also presented. Finally, the main part of this chapter is the analysis of results of inverse calculations performed to determine the curing kinetics data for the mixture of epoxy resin and hardener and for the composite structure, in both cases based among others on the laboratory experiments constituting the subject of chapter 5.

Chapter 7 summarizes the presented thesis and recommends further steps that could be taken as a continuation of the thesis.

In the final part of this document Appendix section can be found, where information about the content of CD attached to this thesis is included. Next, the Bibliography cited in this work is listed according to the appearance order. The last section includes Abstract of the thesis prepared in English and Polish languages.

2. Electrical bushings

2.1. Technology of Resin Impregnated Paper bushings

Electrical bushings are present at almost each stage of the power transmission and distribution path (see Figure 2.1), since their purpose is to transmit electrical power into or out of enclosure (forming grounded barrier) of an electrical apparatus (refer to Figure 2.2) like transformers, circuit breakers, shunt reactors and power capacitors [2]. The current flow in a bushing is realized through an insulated conductor that must be capable of carrying rated current without overheating the adjacent insulation. In turn, the main role of the insulation in a bushing is to withstand the voltage level at which it is applied preventing in this way from flashovers or partial discharges that could cause the failure of a bushing and, moreover, other elements of the power grid system like e.g. power transformer.

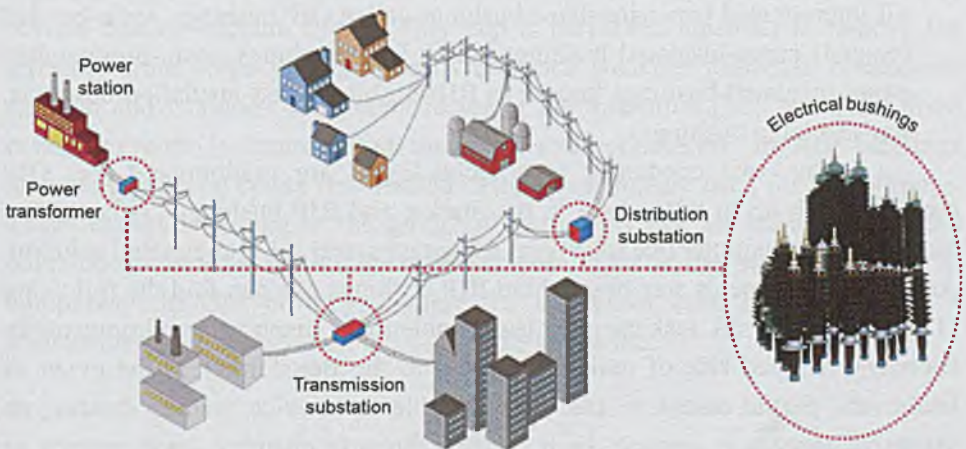


Figure 2.1: Electrical bushings as a part of power transmission and distribution systems [35, 36].

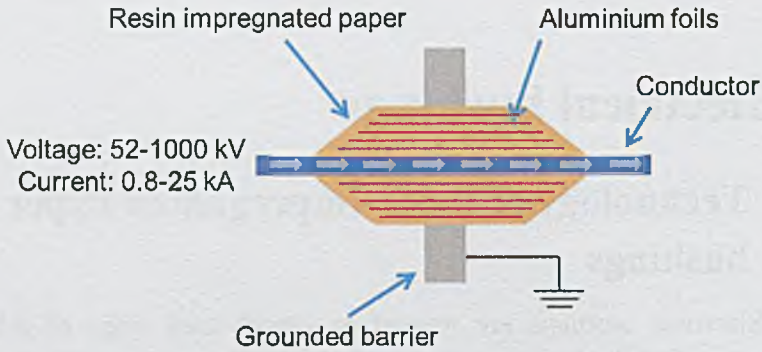


Figure 2.2: The principle of working of electrical bushing [3].

Wide application of electrical bushings results in a significant diversity of the bushings technologies. There are three main classification criteria applicable to bushings industry [2], namely:

- bushing application influencing the insulating media on the bushings ends (air-to-oil, air-to-air or in case of special applications air-to-gas (sulphur hexafluoride – SF₆), gas-to-oil, oil-to-oil),
- bushing construction (solid/bulk type or capacitance-graded/condenser type),
- bushing insulation (air-insulated bushings, oil-insulated/oil-filled bushings, oil-impregnated paper-insulated bushings called OIP bushings, resin-bonded (coated) paper-insulated bushings called RBP bushings, resin-impregnated paper-insulated bushings known as RIP bushings, cast-insulation bushings, gas-insulated bushings).

Today, two condenser type technologies are predominant, i.e. OIP bushings with up to 80% share in the market and RIP bushings [3] becoming more and more popular due to several advantages over oil-impregnated solution. Among the arguments standing behind RIP bushings one can find the following [37]: no risk of oil leakage and less problematic disposal (environmentally friendly), reduced risk of moisture ingress to the transformer in the event of flashovers, partial discharge free up to double the service voltage creating an extensive margin in service, high thermal strength ensuring large margin to ageing in service, self-extinguishing properties, high mechanical strength and reduced weight resulting in improved earthquake withstand, flexible design, possible storage and service in any position and, finally, easier installation.

The structure of the bushing condenser core is presented schematically in Figure 2.3. During the production a web of crepe paper with conductive inserts (most often in the form of aluminium foils) is wound on a conductor. The precise location of aluminium screens is of high significance, since this determines the

grading of the electric field and, consequently, facilitates controlling of the electrical stresses.

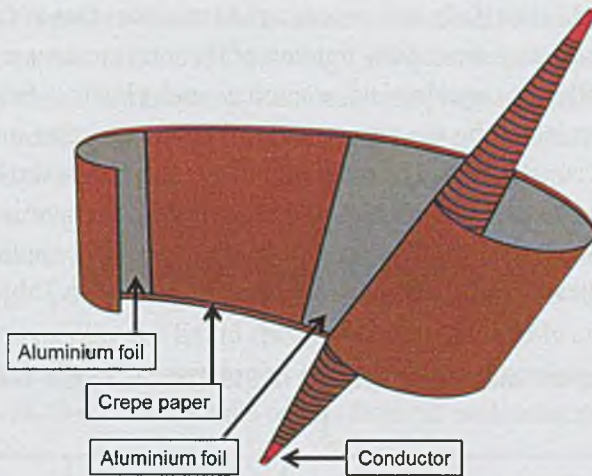


Figure 2.3: The structure of the condenser type bushing [3].

The consecutive stages of the RIP bushing production are presented in Figure 2.4. The winding operation is followed by the drying process consisted of several heating-vacuum cycles. This step is performed in order to remove the moisture from crepe paper, since its presence weakens dielectric breakdown strength and increases dissipation factor of the insulation [38]. Next, the dried condenser core is impregnated under vacuum conditions. In RIP bushings technology special epoxy resin-based casting systems are used for this purpose. These materials belong to the group of thermosets that are cured in elevated temperature to form the solid condenser core. This is the main difference in comparison to OIP bushings, where the condenser core is immersed in a transformer grade mineral oil throughout its entire life.

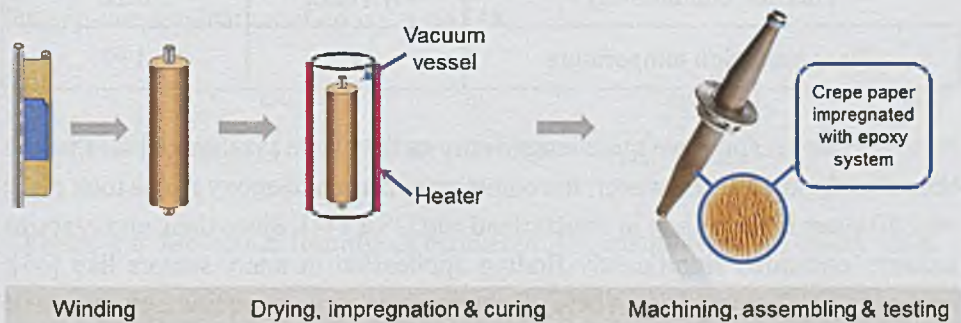


Figure 2.4: The main steps in the bushings production [39, 40, 41].

2.2. Insulation system

The insulation part of the condenser core of RIP bushings consists of a crepe paper, aluminium foils and impregnation medium that is the predominant component constituting about 80% fraction of the total condenser core mass [42, 43]. Consequently, the mechanical, electrical and physical behaviour of this composite is dominated by the properties of the impregnation medium that is a mix of different constituents. The main ingredient is epoxy resin, but other fillers like hardener and accelerator are also added to tailor the properties of the casting system and to fit in this way the requirements of specific application. Typical material properties of such RIP composite body are listed in Table 2.1.

Table 2.1: Typical material properties of the RIP condenser core composite [43].

Property	Unit	Value
Colour	-	Brown
Density	kg/m ³	1270
Tensile strength	MPa	88
Elongation at break	%	2.5
Dielectric constant (at 50 Hz)	-	3.9
Dissipation factor (at 50 Hz)	-	< 0.005
Modulus of elasticity	MPa	4800
Coefficient of thermal expansion	1/K	$45 \cdot 10^{-6}$
Thermal conductivity	W/(mK)	0.26
Glass transition temperature	°C	139

Epoxy resins have quite long history as they were synthesized for the first time already in 1891. However, the commercialization of epoxy resins took place over 50 years later, mainly in Switzerland and USA [44]. Since then, epoxy resins industry expanded significantly finding application in many sectors like [45]: coatings (50%); composites (18%) for aerospace, process equipment, structural and other end uses; construction (13%); electronics/electrical (8%); adhesive/tooling (6%). The worldwide production in 2012 achieved the level of

2.24 million tons per year (80% ÷ 95% of this production belongs to bisphenol A-based epoxy resins) [46], while the projected production volume in 2017 is at the level of 3.03 million tons per year [47]. The popularity of epoxy resins comes, on the one side, from their excellent mechanical, thermal, chemical and electrical properties and, on the other side, from a big variety in these properties offered by different epoxy resin formulations. Such tailored properties can be achieved in case of epoxy resins by addition of different types of additives like fillers, accelerators and so on.

The chemical definition says that epoxy resin is a chemical compound possessing at least two epoxy groups (refer to Figure 2.5) in the molecule that are able to undergo polymerization reaction (also known as curing reaction) transforming irreversibly the liquid epoxy resin into the highly cross-linked solid body. High reactivity of epoxy group (called oxirane) containing one oxygen atom bonded with two carbon atoms results from its molecular structure [11].

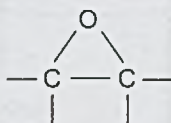


Figure 2.5: Epoxy group.

The production of epoxy resin starts with the reaction of two compounds, namely bisphenol A and epichlorohydrin. Bisphenol A is a chemical product formed by combination of one acetone unit with two phenol groups. The reaction between these two basic ingredients removes unreacted phenol and acetone and attaches two glycidyl groups to form a standard epoxy resin known as diglycidyl ether of bisphenol A (called also DGEBA). Its molecular formula is presented in Figure 2.6, where the parameter c describes the length of the DGEBA chain and informs about degree of polymerization [11]. The c value varies between 0 and 25 and indicates the viscosity (higher value means higher viscosity) determining the end-use application of epoxy resin [48].

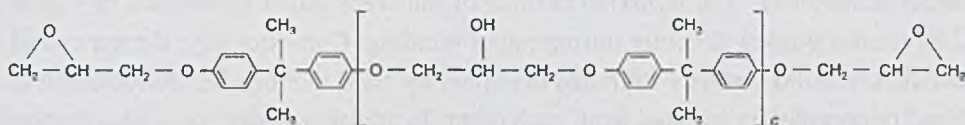


Figure 2.6: Molecular formula of bisphenol A + epichlorohydrin epoxy resin.

DGEBA epoxy resin is the main component of many impregnation systems used in electrical industry. One of the examples is the commercial epoxy

resin-anhydride system offered by Hexion Specialty Chemicals, i.e. EPIKOTE™ Resin 04820 + EPIKURE™ Curing Agent 860. This casting system was used in the experimental part of this thesis. EPIKOTE™ Resin 04820 consists in 25% ÷ 50% of DGEBA, in more than 50% of epoxide derivatives and in less than 10% of methylenedianiline [49], while EPIKURE™ Curing Agent 860 consists in more than 50% of hexahydrophthalic anhydride and in 25% ÷ 50% of methylhexahydrophthalic anhydride [50] (molecular formulas are presented in Figure 2.7). Easy processing and very good mechanical, thermal and electrical characteristics (refer to Table 2.2) make this material an ideal solution among others for the impregnation of a crepe paper in high-voltage electrical bushings produced in RIP technology.

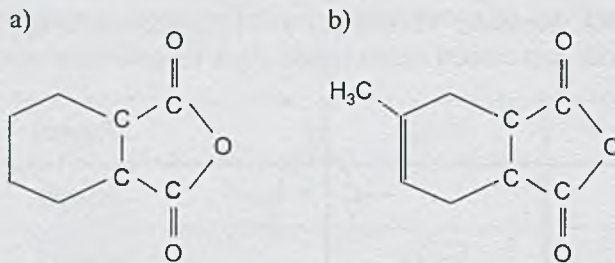


Figure 2.7: The ingredients of EPIKURE™ Curing Agent 860: hexahydrophthalic anhydride – a) and methylhexahydrophthalic anhydride – b).

As already mentioned, crepe paper and aluminium foils constitute about 20% of the total mass of the bushing condenser core (the mass fraction of aluminium foils is small, since the foils thickness is below 0.02 mm). The main role of the crepe paper is to provide electrical insulation on one hand and to form the mechanical structure of the condenser core on the other hand. In addition to that the paper wound tightly on the conductor keeps the aluminium foils in a desired position. This is extremely important, since aluminium layers must be located in very precise axial and radial positions in order to provide the proper grading of electric field during the bushing operation and to control the electric stress in this way. The wrinkled surface of the crepe paper (presented in Figure 2.8) creates porous structure during paper winding. Consequently, the paper coil consists of solid matrix with pores occupied by fluid that can be interconnected, blind or completely isolated from each other. In addition to that some distribution of the pores size and diversity in their shapes exists. It might be even surprising that the porosity of crepe paper is at the level of about 80% [51, 52]. This means that 80% of the paper coil volume in electrical bushing is occupied by pores, while solid matrix constitutes only 20%. Selected physical properties of cellulose

and aluminium representing the paper coil and foils respectively are gathered in Table 2.3.

Table 2.2: Selected material properties of EPIKOTE™ Resin 04820 + EPIKURE™ Curing Agent 860 mixture after curing [53].

Property	Unit	Value
Flexural strength	MPa	105 ÷ 155
Tensile strength	MPa	60 ÷ 80
Young's modulus	GPa	2.815 ÷ 4.092
Impact strength	J/m ²	1700 ÷ 5700
Compressive strength	MPa	125 ÷ 135
Density	kg/m ³	1220
Glass transition temperature	°C	125 ÷ 135
Coefficient of thermal expansion	10 ⁻⁶ /K ⁻¹	45 ÷ 55
Thermal conductivity	W/(mK)	0.15-0.25
Specific heat	J/(kgK)	1380 ÷ 1420
Electric strength	kV/m	24000 ÷ 32000
Dissipation factor at 50 Hz and 25°C	-	0.004
Dissipation factor at 1000 Hz and 25°C	-	3.23
Relative permittivity at 50 Hz and 25°C	-	0.008
Relative permittivity at 1000 Hz and 25°C	-	3.22

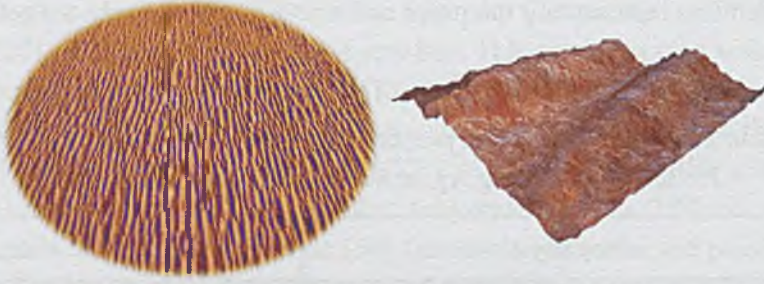


Figure 2.8: Microscopic view on the structure of crepe paper [39].

Table 2.3: Selected physical properties of cellulose and aluminium [51, 54].

Property	Unit	Cellulose	Aluminium
Density	kg/m ³	1550	2790
Specific heat	J/(kgK)	1340	873
Thermal conductivity	W/(mK)	0.335	134

2.3. Impregnation process

Basically, the impregnation of the condenser core of RIP bushing consists of filling and curing stages. It is extremely demanding technology that requires a high degree of competence in the area of process control, both in terms of the process setup (parameters settings) and in the area of material science (material selection and tailoring of its properties). Meanwhile, there are no direct measurement methods allowing one to learn the process and to gain the mentioned expert knowledge. Simultaneously, this production step is of high significance from the product quality perspective, since any imperfection in the condenser core could lead to break-down of the device during its operation.

For this reason the impregnation of the condenser core of high-voltage RIP bushing is performed in vacuum casting technology. There are two main issues that make the vacuum technology superior in comparison to standard casting process conducted under ambient conditions. First of all, vacuum lowers the risk of air traps formation during the impregnation step. Secondly, vacuum technology offers bigger freedom in terms of the product geometry that can be manufactured.

The scheme of typical automated vacuum casting plant is presented in Figure 2.9. Basically, in the vacuum casting technology, the condenser body of RIP bushing is inserted into the steel or paper mould that is placed inside the

vacuum vessel. The vessel is heated with electric heaters and the paper coil is dried during repeatable heating-vacuum cycles. The vacuum conditions are kept after the last drying cycle and the impregnation process starts. The casting system (usually preheated to lower the viscosity and to make the impregnation process easier) is poured into the mentioned paper or steel container with the condenser body inside. Pressure gradients arising inside the material intensify the penetration of epoxy system through the porous structure of the paper coil as shown in Figure 2.10. When the impregnation process is finished, the vacuum is broken and additional heating stage starts. The mechanism of heat convection is activated thanks to atmospheric pressure inside the vacuum vessel and in this way the mould with the impregnated bushing body inside is heated effectively. In turn, rising temperature of the bushing condenser core initiates and accelerates the cross-linking process of the epoxy resin-based casting system.

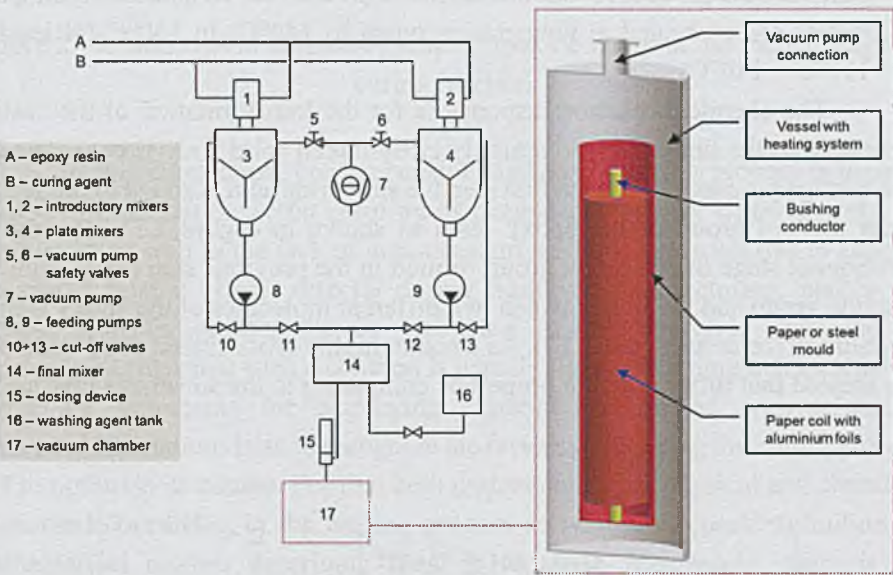


Figure 2.9: The scheme of automated vacuum casting plant [11, 55].

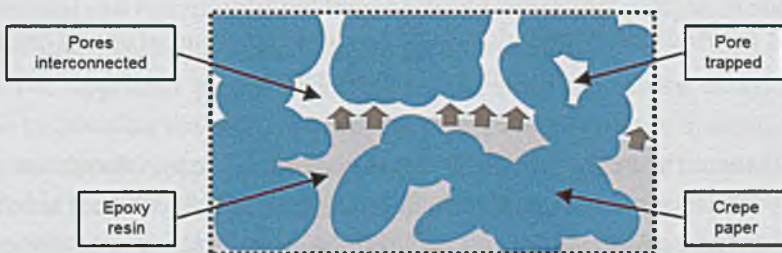


Figure 2.10: The flow of epoxy system through the porous structure of crepe paper.

According to information possessed from the material supplier the recommended procedure for the production of RIP bushings by using the mentioned Hexion casting system is the following [53]:

- degas epoxy resin and curing agent separately under vacuum at the level between 1 mbar and 5 mbar and in temperature equal to $50^{\circ}\text{C} + 80^{\circ}\text{C}$,
- mix the components with the following ratio: 100 parts-by-weight of resin and 85 parts-by-weight of hardener,
- fill the mould with the mixture under vacuum conditions and in temperature in the range of $60^{\circ}\text{C} + 100^{\circ}\text{C}$ (the filling pressure should be between 5 mbar and 10 mbar above the level applied during the ingredients degassing),
- gel the casting system inside the mould at $60^{\circ}\text{C} + 100^{\circ}\text{C}$ over a period of at least 24 hours (up to 48 hours),
- remove the product from the mould,
- post-cure the product for another 20 hours (at least for 10 hours assuming that inserts are preheated at temperature equal to 140°C) in 150°C (at least in $130^{\circ}\text{C} + 140^{\circ}\text{C}$).

The chemical reaction responsible for the transformation of the casting system from the liquid state to a highly cross-linked solid body is considered as a two-stage process [11]. In the first step the anhydride acid is added to the second order alcohol group of the epoxy resin as shown in Figure 2.11. During the subsequent stage the carboxyl group formed in the previous step reacts with the epoxide group and the link between two different molecules of the epoxy resin is established (refer to Figure 2.12). As a result, highly cross-linked solid structures are created that differ much in properties comparing to the substrates mixture.

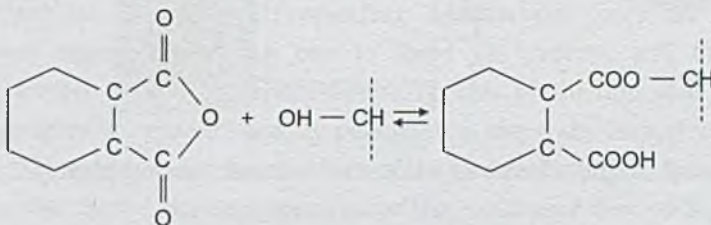


Figure 2.11: Addition of anhydride acid to alcoholic group of epoxy resin in the first stage of curing reaction.

It should be mentioned that the course of the phase transformation process of epoxy resin-based casting systems is strongly coupled with heat transfer. On the one side, curing reaction is induced by heat and its rate depends on temperature and curing degree, while, on the other side, the reaction progress results in heat generation. This relationship is even more complicated when

considering the presence of crepe paper in the body being cured. Consequently, the control of polymerization process is of vital importance, since too low amount of heat could lead to too slow or incomplete curing, while too high temperatures caused by the exothermic effects of the reaction can be the reason for degradation of the insulation properties. In addition to that one can encounter also other problems like e.g. wrong propagation of the curing front or the formation of weld lines (places where two curing fronts meet each other) weakening the mechanical characteristics of the insulation.

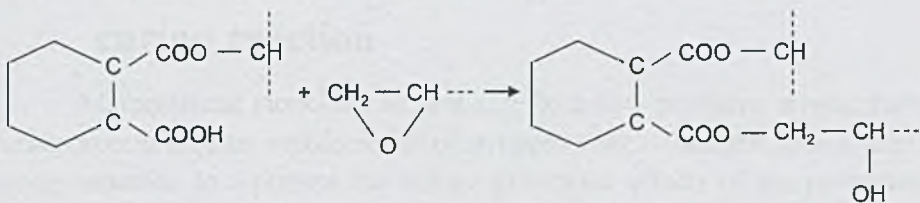


Figure 2.12: Addition of carboxyl group to epoxide group in the second stage of curing reaction.

In this connection, comprehensive analysis of curing process is usually needed to work out the setup ensuring its trouble-free course. Unfortunately, its complexity as well as the lack of measurement methods, allowing one to capture the curing related effects directly during bushings manufacturing, makes the process analysis problematic in the sense of trial-and-error experimental approach. Besides that such a solution is usually time-consuming and expensive. These are arguments for employing experiments assisted with advanced numerical simulations both to recognize the factors influencing the curing process and to optimize its course. For that both understanding of physical and chemical phenomena occurring in the casting process as well as accurate definition of mathematical models describing them is required. Meanwhile, there is no information how the presence of crepe paper influences the course of the cross-linking reaction of epoxy system. The other not fully explored subject is the mathematical and numerical modelling of curing process of composite bodies like in case of crepe paper impregnated with epoxy system.

The approach proposed in this thesis, utilizing among others inverse analysis to calculate the kinetics of curing reaction in composite systems, aims to fill the mentioned gaps. The general concept of this inverse methodology is presented in the next chapter, together with the basics of mathematical modelling of the kinetics of curing reaction and of DSC measurement as a standard method of the curing kinetics determination.

3. Mathematical modelling and determination of the kinetics of curing reaction

3.1. Mathematical modelling of the kinetics of curing reaction

Mathematical modelling of heat and fluid flow problems arising during curing process requires consideration of an appropriate volumetric source term in energy equation to represent the energy generation effects of the progressing chemical reaction. This heat source term $\dot{q}_{v,r}$ varies in time and with position during the reaction course. It is a common practise to link this term with the total heat of reaction H_{Σ} (also known as enthalpy of reaction) and degree of curing α [56, 57, 58, 59, 60] that are coupled by the equation below through the amount of heat generated from the beginning of the reaction till time t denoted as H_t :

$$\alpha = \frac{H_t}{H_{\Sigma}} \quad (3.1)$$

The curing rate $\dot{\alpha}$ can be obtained by differentiating the equation above with respect to time t :

$$\dot{\alpha} = \frac{1}{H_{\Sigma}} \frac{dH_t}{dt} \quad (3.2)$$

Finally, considering Equations (3.1) and (3.2), the heat source term $\dot{q}_{v,r}$ can be defined as:

$$\dot{q}_{v,r} = \rho \dot{\alpha} H_{\Sigma} \quad (3.3)$$

where ρ stands for the material density.

There are plenty of kinetics models available in literature, e.g. [16, 60, 61, 62], that characterize the curing of thermosetting materials like epoxy resins. The origin of them is the general formula describing the kinetics of a single-stage curing reaction that is expressed as [11, 63]:

$$\dot{\alpha} = \frac{\partial \alpha}{\partial t} = k(T)f(\alpha)g(\alpha, T) \quad (3.4)$$

where $k(T)$ is the Arrhenius reaction rate coefficient depending exponentially on temperature T , $f(\alpha)$ is the functional dependent only on the actual value of the curing degree α and $g(\alpha, T)$ term is always assumed to be equal to 1 [11, 63].

The simplest expression formulated according to Equation (3.4) is the n -th order reaction model describing the curing rate $\dot{\alpha}$ as:

$$\dot{\alpha} = k(1 - \alpha)^n \quad (3.5)$$

where superscript n stands for the order of chemical reaction, while the Arrhenius reaction rate coefficient k is calculated in the following way:

$$k = A \exp\left(-\frac{E_a}{RT}\right) \quad (3.6)$$

where A represents the Arrhenius frequency factor, E_a stands for the activation energy and R denotes the universal gas constant.

Much more popular model of the curing kinetics is the equation combining n -th order and autocatalytic reactions that was proposed by Kamal [60, 64]:

$$\dot{\alpha} = k_1(1 - \alpha)^n + k_2\alpha^m(1 - \alpha)^n = (k_1 + k_2\alpha^m)(1 - \alpha)^n \quad (3.7)$$

where k_1 is the externally catalysed rate constant related to n -th order reaction, k_2 is the autocatalytic rate constant related to autocatalytic reaction and both are calculated according to Equation (3.6), whereas power m refers to the order of chemical reaction.

It is worth noticing that the Kamal's formulation describes one-stage curing reaction. This kind of reaction is characterized by one peak resulting from the exothermic effects of occurring chemical reaction that can be captured e.g. in DSC measurements. In case of multi-stage curing reactions the curing kinetics model has to be extended with additional terms representing the subsequent steps of the reaction. According to [11], the Hexion casting system used in the

experimental part of this thesis cures in a two-stage manner. For this reason the model describing the curing kinetics of this material consists of few models representing simple chemical reactions. The first stage of curing reaction is represented by autocatalytic reaction and the second step is modelled by combining autocatalytic and n -th order reactions:

$$\dot{\alpha} = k_1 \alpha^{m_1} (1 - \alpha)^{n_1} + k_2 \alpha^{m_2} (1 - \alpha)^{n_2} + k_3 (1 - \alpha)^{n_2} \quad (3.8)$$

where k_3 is the externally catalysed rate constant related to n -th order reaction, while powers m_1 , m_2 , n_1 and n_2 refer to the orders of chemical reactions.

After simple mathematical transformations, Equation (3.8) takes the following form:

$$\dot{\alpha} = k_1 (1 - \alpha)^{n_1} \alpha^{m_1} + k_2 (k_{02} + \alpha^{m_2}) (1 - \alpha)^{n_2} \quad (3.9)$$

where k_{02} is the coefficient of kinetics model of curing reaction that correlates k_2 and k_3 parameters.

Eventually, combining Equations (3.6) and (3.9), one obtains the formula expressing the kinetics of two-stage curing reaction that includes all parameters of the model:

$$\begin{aligned} \dot{\alpha} = A_1 \exp\left(-\frac{E_1}{T}\right) (1 - \alpha)^{n_1} \alpha^{m_1} \\ + A_2 \exp\left(-\frac{E_2}{T}\right) (k_{02} + \alpha^{m_2}) (1 - \alpha)^{n_2} \end{aligned} \quad (3.10)$$

where A_1 and A_2 are the Arrhenius frequency factors corresponding respectively to the first and the second stage of curing reaction, while E_1 and E_2 stand for the activation energies expressed in K (after division of activation energy expressed in J/kmol by universal gas constant expressed in J/(kmolK)).

3.2. Experimental determination of the kinetics of curing reaction

One can notice that the curing kinetics models consist of material characteristic parameters that must be determined in order to describe the curing reaction of the considered casting system accurately and reliably. Usually, experimental methods like DSC, ODR, DMTA or NMR, quoting only few examples, can be used for this purpose as already discussed in subchapter 1.2, although none of them allows measuring the curing kinetics directly. One of the

most popular methods is dynamic DSC experimental technique (presented schematically in Figure 3.1) that is applied especially often in the analysis of the cross-linking process of epoxy systems.

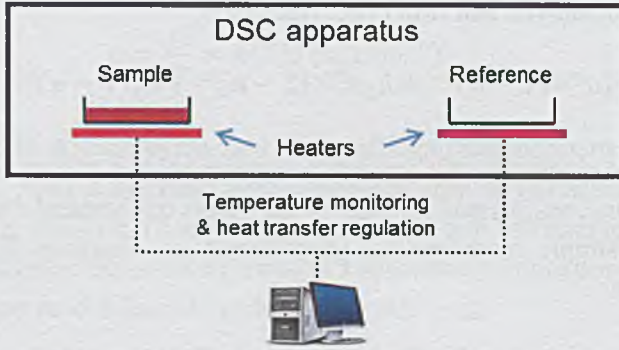


Figure 3.1: The scheme of DSC measurement stand.

In a single run of dynamic DSC analysis two samples (the reference and the investigated one) are heated with the same constant heating rate v_h , which is equivalent to the constant increase of the sample temperature T in time t :

$$v_h = \frac{dT}{dt} = \text{constant} \quad (3.11)$$

The instantaneous heat flow to both samples is measured in time and it is assumed that this heat flow is proportional to the rate of reaction. It means that the heat flow is on the stable level when the reaction does not progress. This can be observed in Figure 3.2 presenting exemplary results of DSC run. When the curing reaction starts and the heat is generated inside the investigated sample, smaller amount of heat must be provided to the curing sample to keep the same heating rate as in the reference one. This difference in the heat flow is visualized in the form of characteristic peaks on DSC curve. The shape of this curve (more precisely the number of peaks) informs about the character of curing reaction and helps to choose the appropriate curing kinetics model.

Integrating DSC curve with respect to time the area of peak (coloured area in Figure 3.2) can be calculated, which refers to the overall heat of reaction H_Σ :

$$H_\Sigma = \int_{t_{ini}}^{t_{fin}} \frac{dH_t}{dt} dt \quad (3.12)$$

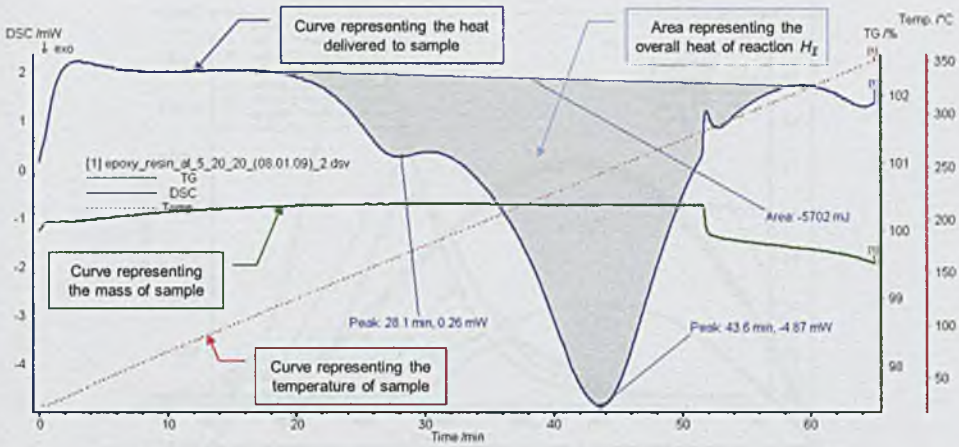


Figure 3.2: Example of readings taken during DSC measurement done for epoxy system sample [60].

As mentioned before, the constant heating rate applied during DSC run means constant increase of temperature in time unit. In this connection, the relationship between heat flow and time can be easily converted to the graph showing the heat flow rate in dependence on temperature. Exemplary DSC results (after data processing) are presented in this form in Figure 3.3 (solid lines). Such data representation is then used in non-linear regression analysis to find the best fit of the curing kinetics model (including function and its parameters) to the experimental results. Next, the found model is used to predict the curing kinetics and the modelled data is presented in Figure 3.3 as symbols. One can also notice that the shape of DSC curve for different heating rates is similar, however the location and the height of peaks depends strongly on the heating rate. Moreover, this means that the total heat of reaction H_T calculated according to Equation (3.12) is variable and changes with the heating rate v_h :

$$H_T = H_T(v_h) \quad (3.13)$$

Since the heat source term expressed by Equation (3.3) is influenced by the value of the overall heat of reaction, it is absolutely essential to perform a series of DSC measurements for different values of the heating rate in order to model accurately the thermal effects of curing reaction.

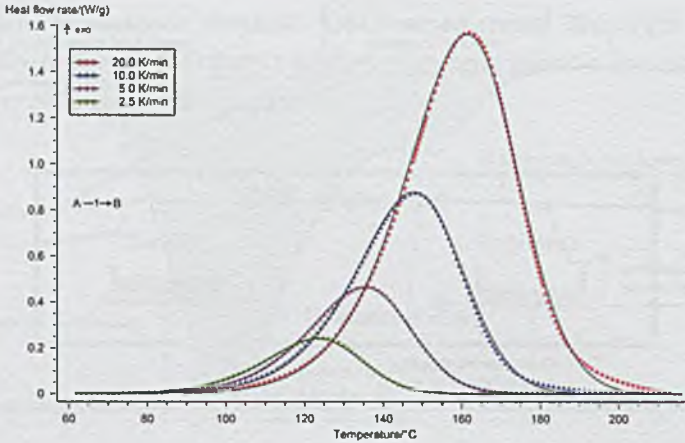


Figure 3.3: Heat flow rate vs. temperature observed during DSC measurement with different heating rates applied (continuous lines represent experimental data, while symbols depict the result of data fitting) [65].

It is also useful to present the results of DSC measurements in the form of relationship between the curing rate and degree of curing for different values of the heating rate as shown in Figure 3.4. This can be done by combining Equation (3.1) with Equation (3.2) and by utilizing data represented by Figure 3.3.

Furthermore, results presenting the function $\dot{\alpha} = f(\alpha, v_h)$ can be modified to illustrate the influence of degree of curing and temperature on the curing reaction rate as illustrated in Figure 3.5.

In spite of many advantages of calorimetric measurements one should be aware that this experimental technique has also some limitations. One of the biggest obstacles is a small sample size (few milligrams) and problematic preparation of specimen representative for bigger and more complicated geometries. Consequently, experimental analysis of the curing kinetics with DSC is usually restricted to simple and homogenous structures. These limitations are all the more valid for composite structures like in case of insulation in the form of crepe paper impregnated with epoxy system that can be found in high-voltage RIP bushings. To overcome the restrictions above, an alternative method allowing one to determine the curing kinetics both for homogenous and composite bodies has been developed within the framework of this thesis. The proposed approach is explained in details in the subsequent subchapters.

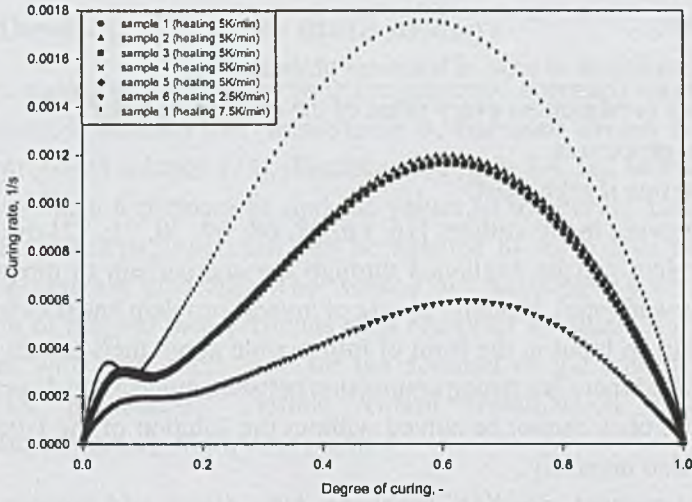


Figure 3.4: The curing rate vs. degree of curing observed during DSC measurement with different heating rates applied [60].

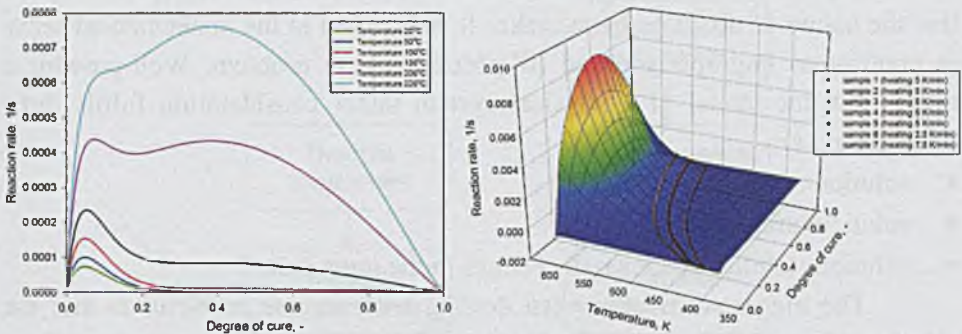


Figure 3.5: The curing rate in dependence on degree of curing and temperature in 2D (left) and 3D (right) representation [60].

3.3. Determination of the curing kinetics as an inverse problem

3.3.1. Fundamentals of inverse analysis

The majority of problems in engineering practice belong to the group of direct problems, when one predicts effects having full information about their causes. It is important that unique solution of direct problem can only be found if the required minimum set of input data exists. It is referred to as uniqueness conditions and includes information about [66, 67]:

- geometry,
- initial conditions in case of transient problems,
- boundary condition on every point of the domain boundary,
- material properties,
- source terms if such exist.

Following many authors [16, 66, 67, 68, 69, 70, 71, 72] the concept of inverse problem can be explained through the comparison to direct one (also known as forward one). Namely, in case of inverse problem one tries to determine causes having an input in the form of information about their effects. It must be emphasized that there is a strong connection between inverse and direct problems, since the first ones cannot be solved without the solution of the latter ones and sometimes also inversely.

The concept dividing problems into direct and inverse group in dependence on the kind of information sought and on the basis for this search is not the only one. More intuitive and lucid is distinction between the mentioned problems proposed by Jacques Hadamard in 1902 [66, 67, 68, 70]. He noticed that the nature of direct problem makes it well-posed in the mathematical sense in contrast to improperly posed (ill-posed) inverse problem. Well-posedness means that the model of a physical system under consideration fulfils three conditions, i.e.:

- solution existence,
- solution uniqueness,
- solution stability under small changes in the input data.

The biggest difficulty when dealing with inverse problems is that the solution of such problem can lead to meaningless result if at least one of the conditions mentioned above is not fulfilled. In this connection, each improperly posed inverse problem must be reformulated to become well-posed approximated problem. In other words, special techniques must be implemented to damp the errors affecting the solution of inverse problem. This reformulation can be done by using e.g. regularization or stochastic techniques that have been intensively developed within the last fifty years, contributing to the popularization of inverse analysis. Generally, regularization techniques require introduction of additional information to deal effectively with the ill-posed problem or to prevent overfitting of the problem solution, while stochastic methods utilize random search mechanisms when looking for the optimum of objective function. The concept of regularization appears in many techniques used today quoting the least-squares method as one of the simplest form of them. Such methods can be loosely divided into three main subgroups, i.e. optimization, filtering and iterative techniques [73].

3.3.2. Developed inverse methodology

The main goal when developing the presented approach was to eliminate the restrictions of standard DSC measurements, discussed already in subchapter 3.2. In the proposed solution [74], illustrated in Figure 3.6, one solves an inverse parameter estimation problem to find the values of the curing kinetics model, although the developed approach can be adapted to solve also other inverse parameter estimation problems. The worked out methodology constitutes the combination of thermal measurements with computer simulations of the curing process and with algorithms used for the solution of the considered inverse problem, i.e. probabilistic Particle Swarm Optimization technique and deterministic Levenberg-Marquardt method.

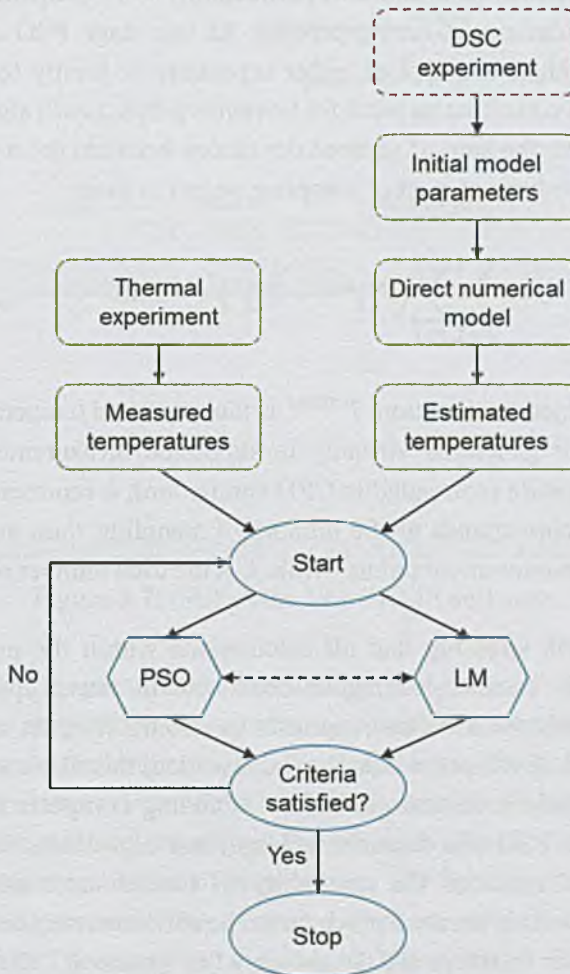


Figure 3.6: The principle of working of the developed inverse methodology of the curing kinetics determination.

In the presented approach DSC experiment is an optional step that can be taken to measure the curing kinetics of investigated sample and the obtained information can be applied as a starting point for the inverse procedure. In turn, thermal experiment provides information about dependent variable field that is required when solving an inverse problem. In this case temperatures measured during curing process are these additional input data.

At this point a strong two-directional coupling of the curing kinetics with temperature is utilized. According to Equation (3.4) temperature value influences directly the rate of curing reaction and, in addition to that, cross-linking process results in significant heat generation affecting temperature field (refer to Figure 3.2 and Equation (3.12)). Consequently, the goal defined in the inverse procedure is to find iteratively the values of the curing kinetics model parameters by matching temperatures determined experimentally with temperatures computed in the CFD simulations of curing process. At this stage PSO and Levenberg-Marquardt algorithms are applied either separately or jointly (e.g. results from PSO calculations constitute an input for Levenberg-Marquardt algorithm and vice versa) to minimize the sum of squared deviations between the measured and the calculated temperatures at a set of sampling points in time:

$$G = \sum_{k=1}^K \sum_{l=1}^L (T_{k,l}^{meas} - T_{k,l}^{est})^2 \rightarrow \min \quad (3.14)$$

where G is the objective function, T^{meas} is the measured temperature (measured experimentally or generated virtually in simulated measurement), T^{est} is the estimated temperature (computed in CFD simulation), k represents the sampling point number, l corresponds to the number of sampling time instance, K is the total number of measurement points, while L is the total number of sampling time instances.

It is worth stressing that all calculations within the proposed inverse methodology are done by using a dedicated in-house application called IRACKLIS (stands for InveRse Approach in Curing Kinetics anaLysis). This software has been developed within the framework of this thesis and it allows one to automate the whole inverse procedure including computer simulations and calculations with PSO and Levenberg-Marquardt algorithms. This benefits in time-savings and excludes the possibility of human error during repeatable actions executed within iterative procedure. The software user is obliged to define via Graphical User Interface (GUI), presented in Figure 3.7, the input data like the initial curing kinetics data, measured temperatures, CFD model and the settings of optimization algorithms (refer to Figure 3.8). Next, the computational

part is done automatically until reaching one of the specified criteria (the maximum number of iterations or the value of objective function). Finally, the results are generated both in text and graphical form.

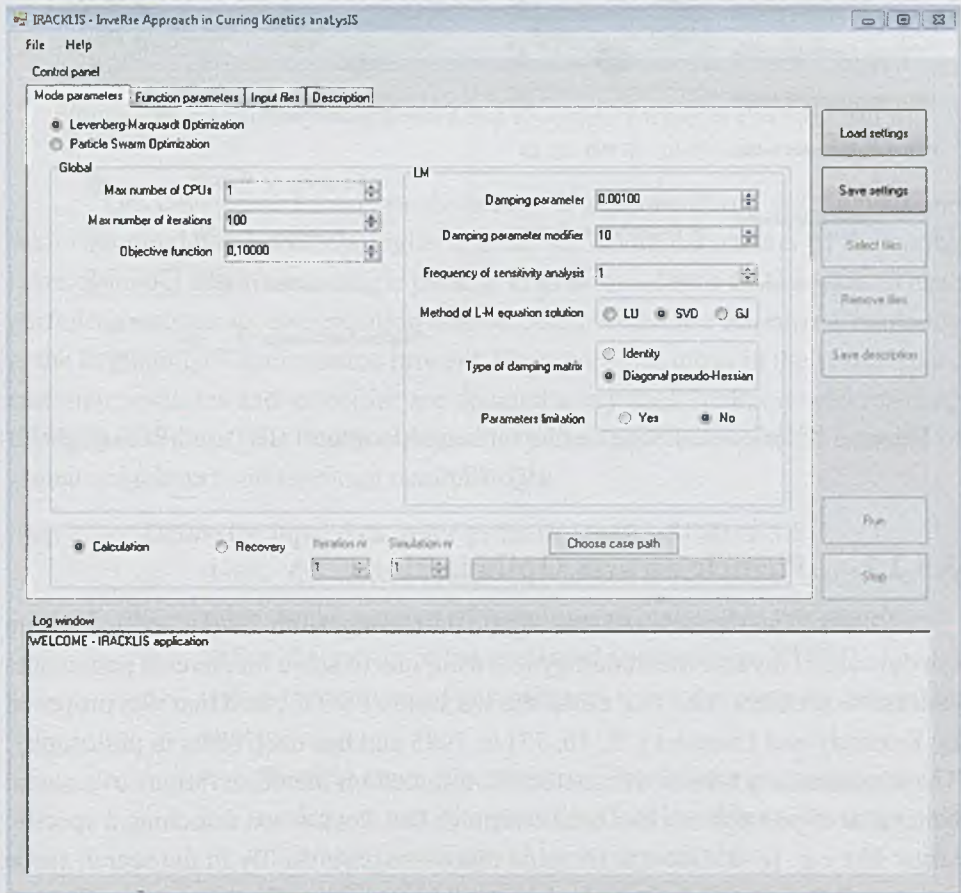


Figure 3.7: GUI of the IRACKLIS software.

Besides the mentioned calculations automation, the other major advantage of the proposed solution is that temperature measurement is relatively simple experimental technique (especially comparing to DSC) that can be applied without the restrictions related to the analysed system complexity or dimensions. For example, temperature recordings can be made directly during the casting process of electrical insulation of high-voltage RIP bushing. In this way, in the proposed inverse procedure, the measured data are strongly coupled with the analysed product geometry and process parameters. Meanwhile, DSC measurement can only be conducted for a few milligrams sample and, hence, might not be representative when modelling the destination system. Nevertheless,

DSC experiment can be used as a part of the developed methodology to determine the initial curing kinetics model that is further fitted by means of inverse analysis.

The image shows two side-by-side panels of software settings. The left panel is for the Levenberg-Marquardt (LM) algorithm, and the right panel is for the Particle Swarm Optimization (PSO) algorithm.

LM Settings:

- Damping parameter: 0.00100
- Damping parameter modifier: 10
- Frequency of sensitivity analysis: 1
- Method of L-M equation solution: LU SVD GJ
- Type of damping matrix: Identity Diagonal pseudo-Hessian
- Parameters limitation: Yes No

PSO Settings:

- Particle range generator: 5 One per set All per set
- Particle percentage generator: 5 One per set All per set
- Cognitive factor: 1.00000
- Social factor: 1.00000
- Inertia factor: 0.95000
- Neighbourhood topology: 3 Local Global

Figure 3.8: Selected settings of Levenberg-Marquardt (left) and PSO (right) algorithms.

3.3.2.1. Particle Swarm Optimization

As already mentioned, two optimization algorithms were applied within the developed inverse methodology allowing one to solve the inverse parameters estimation problem. The first one is the stochastic PSO method that was proposed by Kennedy and Eberhart [75, 76, 77] in 1995 and has deep roots in philosophy. The idea standing behind this method is founded on the observations of a social behaviour of populations like bees swarm or fish flock when searching a specific target like e.g. food. One can imagine that these particles fly in the search space trying to find the specified target and interchange information between each other to make this search more effective. In this way the particle being the closest to the target informs the other population members about its position, so they modify the flight trajectory to become closer to the target increasing in parallel the success probability of the whole population. The core of the PSO method constitutes the system of information exchange between particles and some of the most popular ones are presented in Figure 3.9. Basically, global method assumes that each particle sees all remaining population members, while in ring or star method this visibility is limited only to selected neighbours.

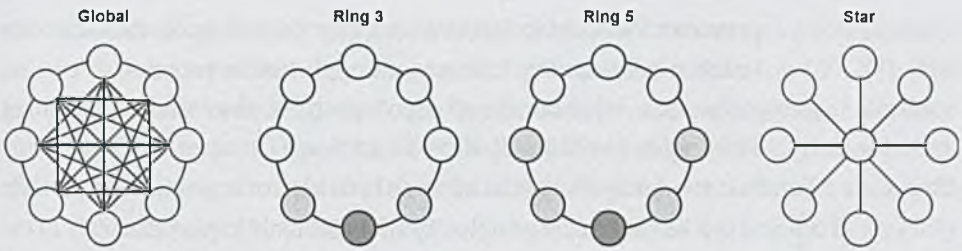


Figure 3.9. Exemplary neighbourhood topologies used in PSO algorithm.

The developed inverse methodology is equipped both with global and with ring neighbourhood topologies and the set of the parameters of the curing kinetics model constitute a single particle in this case. In the PSO approach each particle possesses its own position and velocity, which are initialized randomly at the beginning of optimization process. Next, particles move in the search space and their positions and velocities are updated every each iteration until reaching the defined criteria. The iteration procedure is described below on the example of global neighbourhood topology used [78, 79]:

- Step 1. Define the input data (refer to the right side of Figure 3.8)
- a. define the initial vector of position of a mother particle x_i^p (i refers to the number of iteration and equals 0 at this stage)
 - b. define the matrix of the measured temperatures T^{meas}
 - c. define the number of particles and select the particles generation strategy
 - ‘Particle range generator’ or ‘Particle percentage generator’ – randomize particles according to allowable values range or to allowable percentage change respectively
 - ‘One per set’/‘All per set’ – change only one parameter or all parameters of the curing kinetics model respectively
 - d. define the vector containing the maximum velocity values v_{max} (the maximum allowable change of the parameters values)
 - e. define the value of cognitive (called also personal learning factor) c_1 and social (known also as social learning factor) c_2 parameters (cognitive parameter indicates how much a particle should follow its best trajectory, whereas social parameter defines how much a particle should follow the swarm best trajectory)
 - f. define the value of inertia weight u that controls the velocity of a particle and determines the contribution rate of a particle

previous velocity to its new velocity providing in this way the balance between exploration and exploitation process)

g. define the neighbourhood topology (global or one of the local topologies like Ring 3, Ring 5 and Star)

Step 2. Generate randomly the initial vector of position of a given child particle x_i^p and the initial vector of velocity of a given child particle v_i^p

Step 3. Calculate the value of objective function G_i^p for each particle p according to Equation (3.14) and compare to the lowest objective function found so far by a given particle G^{bp} and by a swarm G^{bs}

a. if $G_i^p < G^{bp}$ then update the vector of the best position of a given particle $x^{bp} = x_i^p$

b. if $G_i^p < G^{bs}$ then update the vector of the best position of a swarm $x^{bs} = x_i^p$

Step 4. Check the stopping conditions

a. Terminate if satisfied

b. Continue if not satisfied

Step 5. Increase the number of iteration i

Step 6. Assign random value (in the range between 0 and 1) to parameters r_1 and r_2

Step 7. Update the vector of velocity of a given particle v_{i+1}^p according to equation below:

$$v_{i+1}^p = uv_i^p + c_1 r_1 (x^{bp} - x_i^p) + c_2 r_2 (x^{bs} - x_i^p) \quad (3.15)$$

Step 8. If $v_{i+1}^p > v_{max}$ then limit the vector of velocity of a given particle $v_{i+1}^p = v_{max}$

Step 9. Update the vector of position of a given particle x_{i+1}^p according to equation below and go to Step 3

$$x_{i+1}^p = x_i^p + v_{i+1}^p \quad (3.16)$$

3.3.2.2. Levenberg-Marquardt algorithm

The second optimization algorithm that constitutes the basis of the proposed inverse methodology is the deterministic Levenberg-Marquardt algorithm. The core of this techniques was derived by Levenberg in 1944, but nearly twenty years later, in 1963, Marquardt modified the Levenberg's approach making the method more efficient in solving ill-conditioned problems. Since that

modification the Levenberg-Marquardt algorithm can be treated as a combination of two different methods, i.e. Steepest Descent and Gauss-Newton [80, 81]. The predominance of one of these techniques depends on the progress of iteration process. The Steepest Descent approach dominates in case of diverging solution, since it is more stable algorithm than the Gauss-Newton one, although slower. In turn, the Gauss-Newton method converges quicker at the cost of lower stability and, hence, is used when the objective function decreases in consecutive iterations, i.e. when the risk of instabilities occurrence is lower. The minimization of the objective function by the Levenberg-Marquardt algorithm is done iteratively according to the procedure described below [66]:

- Step 1. Define the input data (refer to the left side of Figure 3.8)
- a. define the vector of initial parameters values x_i (i refers to the number of iteration and equals 0 at this stage)
 - b. define the matrix of the measured temperatures T^{meas}
 - c. define the initial value of the damping parameter ϑ_i determining whether the Steepest Descent method or the Gauss-Newton method dominates at the beginning of the iterative procedure
 - d. define the value of the damping parameter modifier κ that changes the value of the damping parameter ϑ_i every iteration as explained in Step 7
 - e. define the frequency of sensitivity analysis calculation
 - f. select the method (LU, SVD or Gauss-Jordan) to solve the Levenberg-Marquardt equation (refer to Equation (3.18))
 - g. select the type of the damping matrix Ω_i (can take the form of 'Identity' matrix or 'Diagonal pseudo-Hessian')
 - h. choose to limit or not the parameters values
- Step 2. Calculate the matrix of the estimated temperatures T_i^{est}
- Step 3. Calculate the objective function G_i according to Equation (3.14)
- Step 4. Check the stopping conditions
- a. Terminate if satisfied
 - b. Continue if not satisfied
- Step 5. Calculate the sensitivity matrix (known as Jacobian matrix) J_i , containing sensitivity coefficients of the sought parameters for different sampling points and sampling time instances, according to equation below:

$$J_i = \frac{\partial T_i^{est}}{\partial x_i} \quad (3.17)$$

Step 6. Update the vector of the parameters values \mathbf{x}_{i+1} according to equation below:

$$\mathbf{x}_{i+1} = \mathbf{x}_i + [\mathbf{J}_i^T \mathbf{J}_i + \vartheta_i \mathbf{\Omega}_i]^{-1} \mathbf{J}_i^T (\mathbf{T}^{meas} - \mathbf{T}_i^{est}) \quad (3.18)$$

where superscript T stands for transpose matrix.

Step 7. Calculate the value of a new objective function G_{i+1} according to Equation (3.14)

- a. if $G_{i+1} < G_i$ then accept the new parameters values and update the damping parameter value $\vartheta_i = \frac{1}{\kappa} \vartheta_i$ making the Levenberg-Marquardt algorithm more similar to the Gauss-Newton method
- b. if $G_{i+1} \geq G_i$ then reject the new parameters values, update the damping parameter value $\vartheta_i = \kappa \vartheta_i$ making the Levenberg-Marquardt algorithm more similar to the Steepest Descent method and go to Step 6

Step 8. Check the stopping conditions

- a. Terminate if satisfied
- b. Continue if not satisfied

Step 9. Increase the number of iteration i and go either to Step 5 or to Step 6 (depending on the chosen frequency of the sensitivity analysis calculation)

It is worth noticing that different numerical methods can be used to solve the set of non-linear equations expressed by Equation (3.18). One of the most popular techniques is the LU decomposition, however this approach fails when the approximated Hessian matrix $\mathbf{J}_i^T \mathbf{J}_i$ is nearly singular meaning that it cannot be inverted [82]. In such a case other methods that are resistant to the problem of matrix singularity can be applied. One can find among them such numerical techniques like SVD or Gauss-Jordan with pivoting [83].

The most time consuming operation of the optimization procedure described above is the so-called sensitivity analysis that plays an important role both in solving of inverse parameters estimation problems and in designing of measurements [66, 84]. On the one side, sensitivity analysis allows estimating how the unknown parameters influence the solution of the considered problem. Based on that knowledge, the places with the biggest impact of the parameters changes on the solution can be detected and the best location of sensors during experiment can be selected. On the other side, the placement of sensors in the regions sensitive to the parameters changes improves the conditioning of inverse problem. Information about the parameters significance can also be used to judge the model uncertainty caused by the doubtful parameters values.

The main point of sensitivity analysis is the calculation of the mentioned sensitivity matrix J_i (refer to Equation (3.17)) that consists of so-called sensitivity coefficients that are determined for each unknown/estimated parameter. In the mathematical meaning, sensitivity coefficients are partial derivatives of the solution with respect to the investigated model parameter, assuming simultaneously constant values of the other model parameters [85]. In this way it can be easily observed how the change in a given parameter value modifies the problem solution (temperature field in the considered case). Basically, small value of sensitivity coefficient indicates that large changes in the parameter value yield small changes in the solution [66]. In such case the estimation of the unknown parameter value is difficult, since broad range of the parameter values give the same or very similar results. Furthermore, in case of small sensitivity coefficients values the approximated Hessian matrix $J_i^T J_i$ (refer to Equation (3.18)) is usually singular or nearly singular and the inverse problem is then ill-conditioned. Summing up, large values of sensitivity coefficients are desired, but not always possible.

The other important aspect is the mutual dependence between sensitivity coefficients. The optimum situation is when sensitivity coefficients are linearly-independent. This means the case when only one parameter determines results at a specific measurement point and in a limited neighbourhood of this point, whereas the other analysed parameters are not significant there [86].

Sensitivity coefficients can be determined by using different approaches like e.g. direct analytic solution, the solution of boundary value problem, finite difference approximation etc. [66]. In the considered case the central difference scheme was combined with numerical differentiation by means of computer simulations based on Finite Volume Method (FVM). The advantage of central difference method is its second order accuracy (on the equidistance mesh), but at the cost of computational time. In this approach the determination of sensitivity coefficient for one parameter requires two simulations, what means that the total number of simulations needed to compute the whole sensitivity matrix is twice bigger than the total number of the sought parameters of the curing kinetics model.

The other type of sensitivity coefficient that is useful when performing sensitivity analysis is the so-called relative sensitivity coefficient and the matrix of relative sensitivity coefficients J_i^R is expressed by the following equation:

$$J_i^R = x_i \left(\frac{\partial T_i^{\text{est}}}{\partial x_i} \right) \quad (3.19)$$

Generally, relative sensitivity coefficients allow one to compare the impact of different parameters on the problem solution. In other words, they inform how the solution behaves when the parameter is modified (keeping unmodified values of the remaining parameters) by a given relative fraction. In this way the most critical parameters can be identified from a group of the model uncertainties [85].

4. Virtual experiment of curing process

4.1. General concept

The inverse methodology developed within the framework of this thesis and described in the previous chapter was applied to find the parameters of the curing kinetics model of the epoxy resin-based casting system. The main goal of this study was to check the reliability and efficiency of the proposed approach as well as to compare the effectiveness of the implemented optimization algorithms, i.e. PSO and the Levenberg-Marquardt method.

For this purpose a kind of virtual curing experiment was proposed instead of performing real thermal measurements. More precisely, experimental input required by the developed inverse methodology was substituted with data generated in CFD simulation of curing process (compare Figure 3.6 with Figure 4.1), performed for the known parameters of the curing kinetics model that were determined earlier in DSC measurement. These numerical results in the form of temperature field constituted the measurement data in inverse analysis. In the next step, the original parameters of the curing kinetics model (measured in DSC) were perturbed and such virtually prepared curing kinetics model was used in CFD simulation to calculate the temperature field (further referred to as estimated temperatures). These data were treated as a starting point of inverse procedure. Next, inverse calculations were applied to fit the perturbed parameters of the curing kinetics model to get good matching between the measured temperatures (generated in the simulation run with the original values of the parameters) and the estimated temperatures (calculated for the perturbed parameters values).

It is worth stressing that the approach described above resulted in the commitment of so-called inverse crime. Basically, inverse crime appears when virtually produced measurement data is generated by the same model that is used in inverse analysis [87, 88, 89]. In such strategy the influence of discretization errors is ignored what often leads to unreal and optimistic results of inverse calculations. In the considered case the same geometry, numerical mesh, initial condition, boundary conditions, material properties and mathematical models were employed to generate the measured and the estimated data. Nevertheless, the commitment of inverse crime was justified at this stage of considerations, since this approach guaranteed that the obtained results were not influenced by the errors of numerical modelling origin or by the measurement related errors (the measurement data were generated virtually). This was important, since it was possible in this way to verify reliably the correctness of the mathematical

mechanism used in inverse analysis, to judge its credibility in solving of parameters estimation problem and to eliminate the possible computer programming errors. It is also worth adding that the results of sensitivity analysis done within this part of calculations (refer to subchapter 4.6) were utilized to design the experiments (to define an optimum number and location of temperature sensors) following this theoretical study that are described in chapter 5.

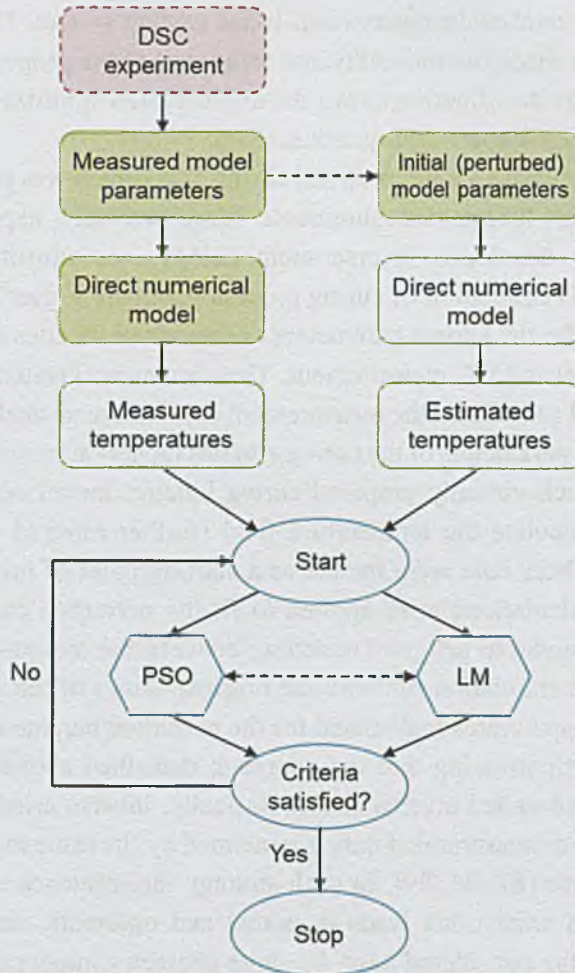


Figure 4.1: The modified inverse procedure applied in the virtual experiment study (colour-filled boxes indicate changes made in comparison to the original concept of the inverse methodology).

Meanwhile, the efficiency of the implemented inverse algorithms was verified within other analysis that was done avoiding inverse crime by applying different numerical mesh to generate the synthetic measurement data than used in inverse calculations. Moreover, the influence of perturbations, introduced intentionally to the virtually generated measurement data (in the form of temperatures) to simulate measurement errors, was investigated in this part and the outcome of these considerations is described in subchapter 4.5.3.

4.2. **Mathematical modelling of curing process**

It has already been explained in subchapter 2.3 that the impregnation process in vacuum casting technology consists of two main stages, i.e. filling of the mould with the casting system and polymerization of the casting system. The scope of interest in this thesis is limited to the modelling of the curing process with the focus on the kinetics of curing reaction. Consequently, the filling stage was excluded from considerations during the process modelling within the proposed virtual experiment of curing process. In addition to that, it was assumed for the sake of simplicity that the mould is filled with homogenous material represented by the epoxy resin-based casting system and the other ingredients of the RIP bushings composite insulation like crepe paper and aluminium foils were eliminated from the analysis.

The simulation approach utilized within virtual curing experiment was based on ANSYS Fluent software (ver. 12.1) that is a general purpose CFD commercial code having broad physical modelling capabilities in the area of mass flow, turbulence, heat transfer and reaction problems. Besides the impressive set of built-in mathematical models, the capabilities of ANSYS Fluent can be extended by adding user-defined models [90]. From the numerical point of view the software is based on FVM technique. This means that the solution of the problem defined in simulation is searched by applying the control volume-based technique to convert the governing equations to the algebraic equations that can be solved numerically [90, 91]. This involves decomposition of the whole solution domain into the finite number of control volumes (or cells) and integration of the governing equations over the cells volumes to find the discrete values for each cell centre.

In spite of the introduced simplifications and assumptions, one has to deal with relatively complex problem when modelling the curing of the epoxy resin-based casting system. During the considered process epoxy system is heated up in time in order to induce and accelerate the cross-linking phenomenon. Additional effects related to temperature changes are variations in the epoxy system density that, consequently, impact also the material convective flow.

Furthermore, the mentioned phase transformation of casting system has exothermic nature resulting in heat generation. The phenomena mentioned above cause that the considered problem has an unsteady character. The other difficulty is that one has to solve in parallel the mass conservation equation, the Navier-Stokes equation and the energy equation including internal heat source. Moreover, the course of curing reaction must be traced by adding user-defined unsteady conservation equation. All governing equations constituting the mathematical model of the virtual curing experiment are described in details in the following part of this subchapter.

Because of the convective mass flow of epoxy system the solution must satisfy the continuity equation (mass conservation equation). It states that the overall mass of system is conserved and has the following form:

$$\frac{\partial \rho}{\partial t} + \nabla \cdot (\rho \mathbf{w}) = 0 \quad (4.1)$$

where ∇ is the divergence operator and \mathbf{w} is the vector of the fluid velocity. Generally, the first term on the left hand side of Equation (4.1) can be neglected in case of incompressible flows.

The convective motion of epoxy system, having laminar character, is expressed by the Navier-Stokes equation known also as the momentum equation, which is derived from the Newton's second law:

$$\frac{\partial(\rho \mathbf{w})}{\partial t} + \nabla \cdot (\rho \mathbf{w} \mathbf{w}) = \mu \cdot \nabla^2 \mathbf{w} - \nabla p + \rho \mathbf{g} \quad (4.2)$$

where μ is the dynamic viscosity coefficient, ∇^2 is the Laplacian operator, ∇p stands for the gradient of static pressure p and \mathbf{g} is the vector of gravitational acceleration. The left-hand side of the equation above includes accumulative (unsteady) and convective terms respectively, while the right hand side of the equation consists of diffusion term, of pressure gradient and of momentum source (body force) term due to gravity respectively.

Another governing formula constituting the presented approach is the energy equation, which ensures the conservation of energy and for fluids takes the following form:

$$\frac{\partial}{\partial t} (\rho E) + \nabla \cdot [\mathbf{w}(\rho E + p)] = \nabla \cdot (\lambda \nabla T) + \dot{q}_{v,r} \quad (4.3)$$

where E stands for the total energy and λ is the thermal conductivity. In this equation the left-hand side is sequentially composed of accumulative (unsteady) and advective terms, while the first term on the right-hand side is known as diffusive (or conductive) term and the second one is called generation term. It is worth stressing that the energy equation is simplified for solids, since the generation term is then neglected.

As already explained in subchapter 3.1, in this particular case, the generation term of the energy equation $\dot{q}_{v,r}$ describes the exothermic effect of curing reaction of epoxy system and is expressed according to Equation (3.3). For a single-stage curing kinetics model and combining Equation (3.3) with Equation (3.6) and Equation (3.7) this source term takes the following form:

$$\dot{q}_{v,r} = \rho \left(A_1 e^{\frac{-E_1}{RT}} + A_2 e^{\frac{-E_2}{RT}} \alpha^m \right) (1 - \alpha)^n H_\Sigma \quad (4.4)$$

where all parameters of the curing kinetics model, i.e. m , n , A_1 , A_2 , E_1 , E_2 , and the total heat of reaction H_Σ are material dependent and their values are searched by the application of inverse analysis developed within the framework of this thesis.

Finally, changes in the value of degree of curing are traced in the presented approach through the solution of additional unsteady conservation equation defined as below:

$$\frac{\partial(\rho\alpha)}{\partial t} + \nabla \cdot (\rho w\alpha) = \rho \dot{\alpha} \quad (4.5)$$

The problem formulated by Equations (4.1) ÷ (4.5) was solved numerically by the pressure-based solver, dedicated generally to solution of incompressible flow problems [92]. This solver solves the flow problem in a segregated manner by using pressure-velocity coupling algorithm. PISO scheme was applied for this purpose and this algorithm, based on the predictor-corrector approach, is recommended for transient calculations [92, 93]. Regarding discretization schemes, the first-order implicit time discretization was used for transient formulation [92, 94], while the first-order upwind discretization schemes [92, 94] were applied for the spatial discretization of the momentum and user-defined conservation equations. Finally, for the energy equation, the second-order accuracy upwind discretization scheme [92, 94] was utilized. The gradients evaluation was done in accordance to Green-Gauss Cell-Based scheme, which is generally less accurate on highly distorted meshes than Green-Gauss Node-Based and Least-Squares Cell-Based methods [92], but this was not a case in the

analysed problem. On the other side, the Green-Gauss Cell-Based scheme is superior to the other two schemes when considering the computational time [92]. Finally, one of the most universal methods, i.e. PRESTO! [92, 94], was chosen as a pressure discretization scheme.

4.3. Numerical modelling of curing process

4.3.1. Model geometry

The geometrical model used in the computer simulations of the virtual curing experiment is illustrated in Figure 4.2. It is relatively simple system consisting of cylindrical aluminium mould that is filled with epoxy resin. It is worth mentioning that the reason for choice of such geometry was twofold. Firstly, this geometry configuration allowed one to bring the analysed problem to 2D axisymmetric case and, in this way, to shorten the computational time needed to perform numerical simulation. This, in turn, was of high significance when considering the number of simulations needed in each iteration of inverse procedure, especially for the sensitivity matrix computation (refer to subchapter 4.6). Secondly, this geometry is very similar to the one used in the experimental part of this thesis that is described in chapters 5 and 6.

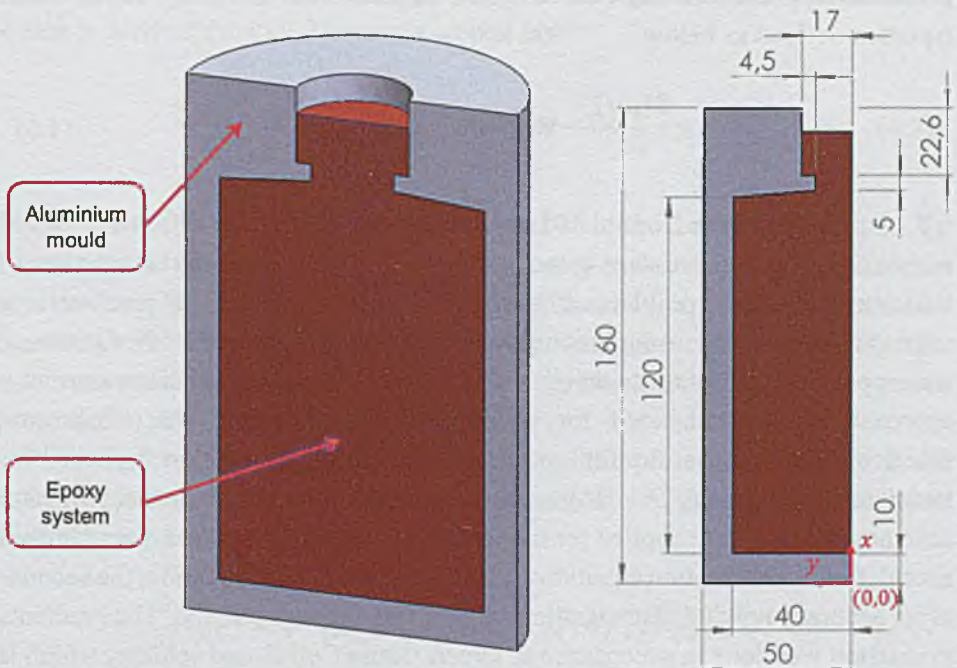


Figure 4.2: Half of the geometrical model in 3D representation (left) and 2D axisymmetric geometry (right) of aluminium mould filled with epoxy system.

4.3.2. Computational mesh and time-step

Discretization of the simplified 2D axisymmetric geometry of the analysed system was done in a commercial software GAMBIT (ver. 2.4) that was for a long time a dedicated pre-processor for Fluent solver (before market debut of ANSYS Workbench platform). Even now, GAMBIT is appreciated, especially for its simultaneous efficiency and simplicity in generating of 2D meshes. Basically, GAMBIT offers different meshing schemes when preparing 2D face meshes [95]. In the considered case, Quad Elements Scheme with Pave and Submap Type Scheme was used for the epoxy system regions and for the aluminium mould region respectively. In both cases the interval size-based spacing equal to 1.5 mm was applied. This resulted in the unstructured mesh consisted of 3533 quadrilateral elements that is presented in Figure 4.3. 1267 of these elements were located in the aluminium mould region, while 2266 cells were in the epoxy resin region. The mesh quality was judged based on one of the GAMBIT built-in methods, i.e. so-called Equivalent Size Skewness parameter that is defined as:

$$Q_{EVS} = \frac{(S_{eq} - S_{cell})}{S_{eq}} \quad (4.6)$$

where S_{cell} is the area of mesh element (cell) and S_{eq} is the maximum area of an equilateral cell that has identical circumscribing radius as that of the mesh element (by definition $0 \leq Q_{EVS} \leq 1$ and $Q_{EVS} = 0$ describes an equilateral, i.e. good quality element, while $Q_{EVS} = 1$ indicates completely degenerated, i.e. poor quality element).

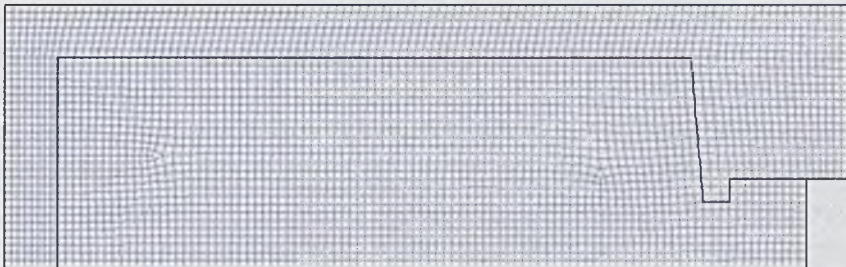


Figure 4.3: 2D numerical mesh generated in the GAMBIT software.

The results of the mesh quality investigation are gathered in Table 4.1. It can be noticed that all mesh elements were characterized by the Equivalent Size Skewness parameter in the range of $0 \div 0.4$ and only 10 elements were outside of

0 ÷ 0.2 region. For the best quality element the Equivalent Size Skewness was at the level of 1.30573e-10, while for the worst one it equalled to 0.385593. Moreover, mesh independence study (similar to the one described in subchapters 6.3.2 and 6.4.2) proved that the numerical solution is not influenced by the mesh resolution. It should also be mentioned that the performed tests with different time-step values allowed finding the optimum between the solution convergence/stability and computational time. Finally, time-step equal to 1 s was applied in all calculations.

Table 4.1: The quality of numerical mesh based on the Equivalent Size Skewness parameter.

Q_{EVS}^{\min}	Q_{EVS}^{\max}	Number of elements -	Number of elements %
0	0.1	2937	83.13
0.1	0.2	586	16.59
0.2	0.3	5	0.14
0.3	0.4	5	0.14
0.4	1.0	0	0

4.3.3. Initial and boundary conditions

Initial and boundary conditions defined in the computer simulations of the virtual curing experiment, described in Figure 4.4, were chosen in a way corresponding to some extent to the conditions in the real curing experiment (refer to chapter 5). As mentioned, the mould filling stage was excluded from considerations and, hence, the aluminium mould filled with epoxy system (see Figure 4.2) was treated as the starting point in all simulations. Equalized temperature at the level of 49.5°C was assumed in the mould and epoxy system regions as initial condition. The initial degree of curing was also uniform (equal to 4%) in the whole epoxy system region. However, it must be emphasized that this level of degree of curing was chosen based on the assumption that the considered epoxy system cures even when exhibited to ambient temperature. Boundary conditions of temperature type were applied to reflect the heating process inside electric oven. Time-dependent temperature profiles, presented in Figure 4.5, were assumed separately for external walls of the mould and of the epoxy system region. Finally, axisymmetric boundary condition was defined on the wall corresponding to the symmetry axis in the 3D geometry of the analysed system.

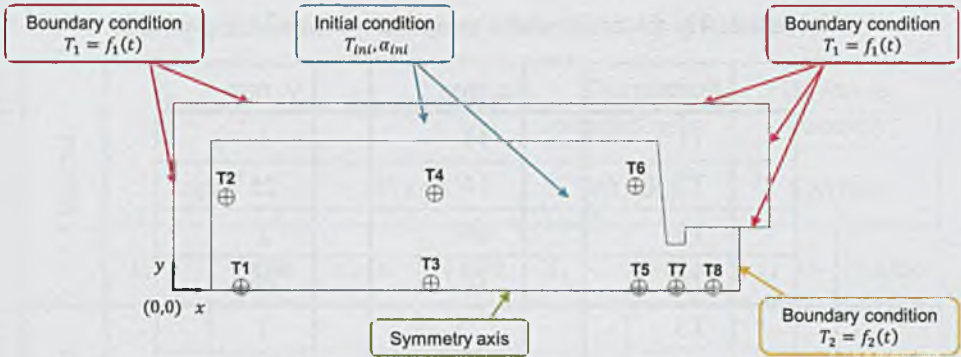


Figure 4.4: Definition of initial and boundary conditions.

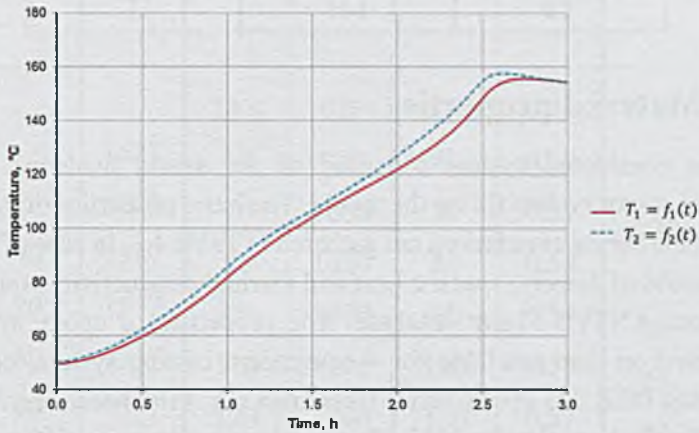


Figure 4.5: Temperature profiles defined as boundary conditions.

The course of curing reaction was monitored on the basis of temperature recordings taken at several points positioned as specified in Table 4.2. The locations of these virtual temperature sensors are also shown in Figure 4.4. It is worth stressing that only data from selected time instances gathered at point T3 and T5 were used in inverse analysis, since temperatures at these monitoring points were affected the most by the curing reaction progress. Temperatures recorded at the remaining points were used for the observation purposes and, for example, they allowed checking if the parameters of the curing kinetics model, optimized in inverse analysis, improve the agreement between the measured and estimated temperatures at the points that were not included in inverse analysis.

Table 4.2: The location of the temperature monitoring points.

Point	x , mm	y , mm
T1	18	1
T2	14	25
T3	69	2
T4	70	26
T5	125	1
T6	124	28
T7	135	1
T8	145	1

4.3.4. Material properties

The considered system consisted of the mould made of aluminium material and epoxy system filling the mould. The basic properties of the materials included in the curing simulations are gathered in Table 4.3. In case of aluminium constant values of density, specific heat and thermal conductivity were imported directly from ANSYS Fluent database. The properties of epoxy system were defined based on data available for 4-component casting system, consisted of Dow Corning DER 331 epoxy resin, Huntsman HY 1102 hardener, Amosil 510 filler and Curezol accelerator [96]. This insulation system is different than the one used in the experimental part of this thesis, although it finds its application among others in high-voltage bushings. The material data were expressed in this case in dependence on temperature with piecewise-linear function available in ANSYS Fluent that is defined according to the following equation [92]:

$$\phi(T) = \phi_b + \frac{\phi_{b+1} - \phi_b}{T_{b+1} - T_b} (T_{cell} - T_b) \quad (4.7)$$

where ϕ is the dependent variable corresponding in this case to the material property, b is the number of temperature level and T_{cell} denotes the temperature value in the cell belonging to the range $T_b \div T_{b+1}$.

Table 4.3: Material properties used in the curing simulations.

Material	Density		Specific heat		Thermal conductivity		Dynamic viscosity	
	kg/m ³		J/(kgK)		W/(mK)		kg/(ms)	
	T, °C	Value	T, °C	Value	T, °C	Value	T, °C	Value
Aluminium	-	2719	-	871	-	202.4	-	-
Epoxy system	0 ≤	1627	20 ≤	920	20 ≤	0.48		
	20	1607	40	940	40	0.50		
	40	1587	70	1000	70	0.53	≤ 30	32.0
	70	1557	80	1030	80	0.54	40	22.6
	80	1547	90	1070	90	0.54	60	12.7
	90	1537	100	1115	100	0.55	70	7.0
	100	1527	120	1200	120	0.57	80	4.4
	120	1507	140	1330	140	0.59	≥ 90	2.7
	≥ 130	1497	160	1350	160	0.61		
			180	1365	180	0.63		
		≥ 200	1370	≥ 200	0.65			

The kinetics of curing reaction was defined according to available results of DSC measurements performed for the mentioned 4-component casting system [96]. It resulted in the simplified version of the Kamal's model, where the term describing the n -th order reaction was neglected (zero values of A_1 and E_1 parameters) and only the autocatalytic term remained in the curing kinetics formula (refer to Equation (3.7)). The parameters of the curing kinetics model of the considered epoxy system are gathered in Table 4.4. One can notice that two different sets of parameters were used. The measured one was introduced to the model simulating the curing experiment, while the other one, referred to as initial, constituted the starting point for inverse analysis. It can be seen that the initial

parameter P_{ini} was generated simply by lowering the value of the measured parameter P_{meas} by perturbation factor PF defined as:

$$PF = \frac{(P_{meas} - P_{ini})}{P_{meas}} \cdot 100\% \quad (4.8)$$

Table 4.4: Measured and initial (perturbed) curing kinetics data.

Parameter	Unit	Measured value	Initial (perturbed) value	PF , %
A_1	1/s	0.0	0.0	0.0
A_2	1/s	478400.0	406640.0	15.0
E_1	K	0.0	0.0	0.0
E_2	K	8104.34	7942.2532	2.0
m	-	0.5016	0.4264	15.0
n	-	1.0363	0.8809	15.0
H_{Σ}	J/kg	112600.0	95710.0	15.0

4.4. Inverse calculations of the kinetics of curing reaction

Inverse calculations with the use of the developed methodology of the curing kinetics determination were the main part of the study referred to in this thesis as the virtual experiment of curing process. The goal of these investigations was to check if the mathematical mechanism standing behind the proposed methodology is correct. For this purpose two different cases were investigated. In the first one the Levenberg-Marquardt algorithm was used in inverse calculations, while in the second one the PSO method was applied.

The optimum configuration of both algorithms was worked in preliminary tests, where the coefficients of two mathematical functions (simple 3rd order polynomial and much more complicated non-linear multimodal Rastrigin's function) were determined in inverse analyses. The use of these functions allowed avoiding long computations related to the numerical simulations of the curing process. Next, the efficiency of Levenberg-Marquardt

and PSO algorithms was compared in inverse calculations aimed at determination of the parameters of the curing kinetics model. It is worth stressing that the same parameters of the curing kinetics model (refer to Table 4.4) were defined as a starting point of inverse procedure in both cases. The direct numerical model simulating the curing process, already described in subchapter 4.3, was also identical, similarly as the constraints imposed on iterative procedure. In total 10 iteration steps were allowed and the target objective function value expressed by Equation (3.14) was defined at the level of 0.01. Computational time needed to perform iterative step was also comparable in both cases and it lasted about 9 hours and 30 minutes (by using computer with single 3.0 GHz Central Processing Unit). The reason for this is that the number of particles (simulations) in the swarm in case of the PSO method was the same as the number of simulations required to determine the sensitivity matrix within the Levenberg-Marquardt optimization. It should also be stressed that the inverse calculations with the use of the PSO method were repeated two times to verify if the stochastic character of this algorithm influences its effectiveness.

The actual goal defined in the performed analyses was to minimize the value of the objective function, i.e. to match the measured and estimated temperatures, through the modification of the parameters constituting the curing kinetics model. In this connection, the efficiency of both investigated algorithms was judged in threefold manner. One of the aspects under consideration was simply the value of the objective function. The second investigated issue was the correlation between temperature fields from the simulation with the measured curing kinetics data and from the simulation with the curing kinetics obtained in inverse calculations. It is worth stressing that this correlation affected directly the value of the objective function. Finally, the third aspect was the agreement between the measured and the estimated values of the parameters of the curing kinetics model.

Figure 4.6 presents the value of the objective function in consecutive iterations of all inverse analyses performed. Basically, one can deduct from these results that the solution converged in case of the Levenberg-Marquardt method just after 6 iterations reaching the target value of the objective function below 0.01, while PSO did not succeed after reaching the maximum number of iterative steps. The final value of the objective function for the best run of the PSO-based inverse analysis was at the level of more or less 50, which is still a significant improvement taking into account that the initial value of the objective function was around 1600. It can also be concluded that the efficiency of the PSO algorithm was similar to the Levenberg-Marquardt optimization in the first iterations and, then, the supremacy of the latter method became evident. Finally, the comparison of the results obtained in three different runs of the PSO-based

inverse analysis confirmed that the course of iteration procedure is strongly affected by the stochastic nature of this method.

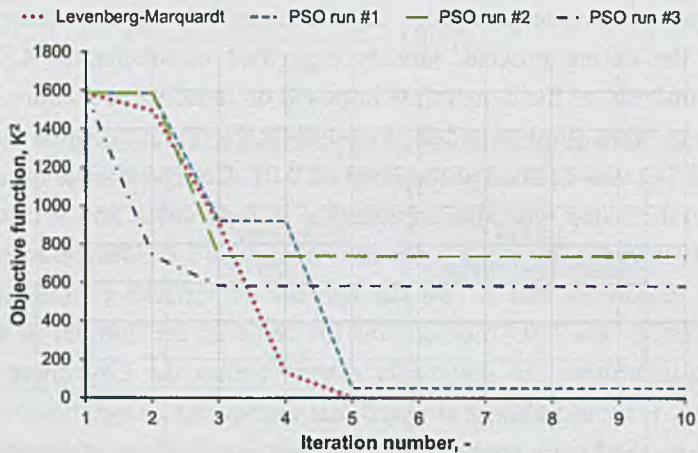


Figure 4.6: The value of the objective function in consecutive iterations.

As announced earlier, the second considered aspect, influencing the results judgment, was the agreement between the measured (generated in simulated measurement) and estimated temperature fields. According to Equation (3.14), the value of the objective function is directly linked with the level of this agreement. More precisely, the lower objective function the better correlation in terms of temperatures and vice versa. This dependence is confirmed by the results of all inverse analyses performed, but in case of the PSO-based calculations the results from the best run are only presented. Figure 4.7 depicts temperatures recorded at selected monitoring points, of which T3 and T5 were directly used in inverse analysis, while T1 and T4 were not a part of calculations. It should be stressed that the same improvement in the agreement of temperatures was observed for the remaining points, i.e. T2, T6, T7 and T8. One can notice based on these graphs that temperature curves obtained for the parameters found by using the Levenberg-Marquardt algorithm cover the curves got from the simulated measurement. Worse accuracy in terms of temperature can be observed in case of the results obtained for the PSO method and, as mentioned, this is reflected in higher value of the objective function (refer again to Figure 4.6). Nevertheless, the improvement in correspondence between the measured and the estimated data is also significant if compared to the initial agreement. Besides that it can be stated based on the discussed results that the optimized parameters of the curing kinetics model improved agreement of temperatures at all monitoring points (no matter if data gathered at these points were used in inverse analysis or not).

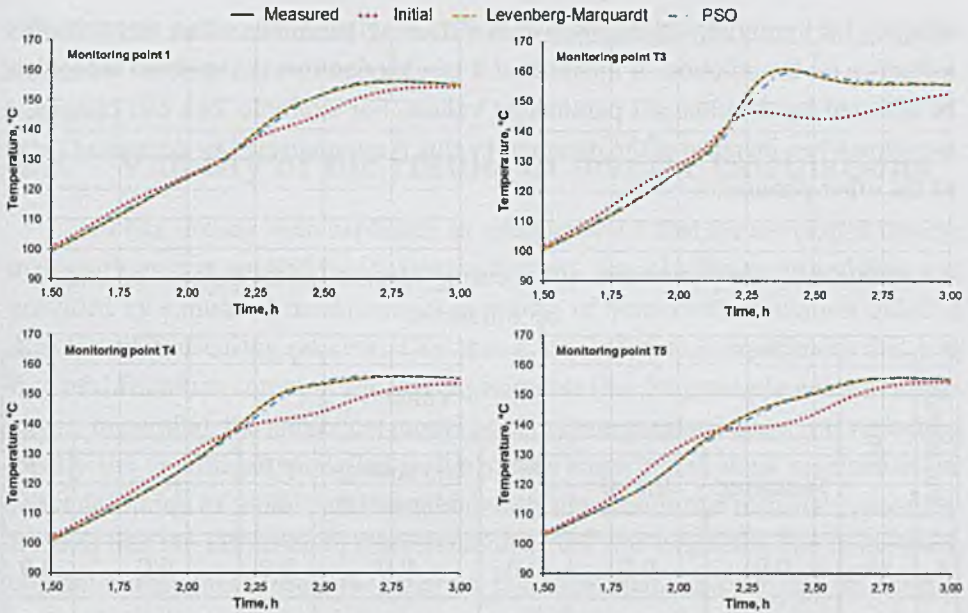


Figure 4.7: Temperature agreement at selected monitoring points before and after optimization.

The optimization results represented by the values of the parameters of the curing kinetics model are shown in Table 4.5. Plus sign next to the parameter value indicates that the optimized value is closer to the measured one than before the optimization. Meanwhile, minus sign means that the agreement between the parameter value, being searched in inverse analysis, and the measured one worsened comparing to the situation before optimization. Generally, the Levenberg-Marquardt optimization turned out to be superior also from this perspective when confronting with the best run of inverse analysis performed with the use of the PSO method. The values of four parameters were improved in inverse analysis based on the Levenberg-Marquardt approach and one parameter (A_2) had negative fitting effect. In turn, in case of the PSO method only two parameters values (E_2 and H_2) were improved when comparing the initial and final fitting to the measured values, while for the remaining three coefficients the optimization effect was negative. This is in line with the conclusion drawn based on the correlation between temperature fields as better agreement was obtained for the parameters calculated with the Levenberg-Marquardt approach.

Moreover, keeping in mind that the final objective function, obtained in calculations based on the Levenberg-Marquardt optimization, was very low, it can be stated that the kinetics of the considered curing process can be described by more than one set of the parameters values. This, in turn, shows that the investigated problem is ill-conditioned, since the result of inverse analysis is not

unique. Furthermore, it indicates that different parameters can have similar influence on the solution. It means that it can happen that the solution would not be affected by the changed parameters values. For example, one can imagine a situation when increase of the parameter value is compensated by decreased value of the other parameter.

Table 4.5: The parameters of the curing kinetics model before and after optimization.

Parameter	Unit	Value						
		Measured	Initial	PF %	Levenberg-Marquardt	PF %	PSO	PF %
A_1	1/s	0.0	0.0	0.0	0.0	0.0	0.0	0.0
A_2	1/s	478400.0	406640.0	15.0	367403.4 (-)	23.2	342439.0 (-)	28.4
E_1	K	0.0	0.0	0.0	0.0	0.0	0.0	0.0
E_2	K	8104.34	7942.2532	2.0	7995.7 (+)	1.3	8105.9 (+)	0.0
m	-	0.5016	0.4264	15.0	0.5130 (+)	-2.3	0.3149 (-)	37.2
n	-	1.0363	0.8809	15.0	1.0275 (+)	0.8	0.8546 (-)	17.5
H_T	J/kg	112600.0	95710.0	15.0	112591.3 (+)	0.0	112941.5 (+)	-0.3
G	K ²	✕	1585.403	✕	0.007	✕	50.007	✕

Summing up, the obtained results confirmed that the mathematical methodology applied in the developed approach works appropriately, i.e. it allows solving the inverse parameters estimation problem and improving in this way the dependent variable field (temperatures influenced by the parameters of the curing kinetics model). Apart from that the performed investigation revealed that the considered inverse problem is poorly conditioned, since the parameters values describing the curing kinetics are not unique. In other words, the course of the curing process can be described accurately by more than one set of the parameters of the curing kinetics model. Finally, the presented study showed that the optimized parameters of the curing kinetics model improve the correlation between the measured (generated in simulated measurement) and estimated

temperatures in the whole analysed system (not only at points, where the gathered data were used in inverse analysis).

4.5. Validity of the results of inverse calculations

It has already been explained in subchapter 4.1 that the developed inverse methodology was applied for idealistic situation. Namely, the measured data was provided by simulated measurement in a form of numerical simulation utilising direct model of curing process. This was a kind of virtual experiment that was free of difficulties common for real experiments like for example measurements errors. In parallel, the numerical model used in inverse calculations was reflecting ideally the conditions modelled in the virtual experiment, what resulted in the exact definition of initial condition, boundary conditions and material properties. Besides that the influence of discretization errors was neglected due to the same computational mesh used to generate the measurement data and in inverse calculations. It means that the only source of difference between the model used to simulate measurement and the one used in inverse analysis was the curing kinetics data in the form of the model parameters. In this connection, it was decided to perform a series of numerical tests in order to check the validity of the results obtained in inverse calculations.

4.5.1. Study on the influence of geometry and mesh

The goal of the first study was to verify if the values of the coefficients of the curing kinetics model, found in inverse analysis, are also valid for different geometries presented in Figure 4.8. In the first case the dimensions of the original geometry, shown in Figure 4.2, were simply scaled by a factor of 2, keeping simultaneously the same number of mesh elements as in the original model (3533 cells). Consequently, this operation resulted in the mesh coarsening, since the mesh element size was also enlarged by a factor of 2. The mesh topology remained the same as in the original model (refer to subchapter 4.3.2 and Figure 4.3). In the second design both the shape and dimensions of the geometry were changed. This caused also modifications in the numerical mesh, which this time was created in the whole volume according to Quad Elements Scheme with Pave Type Scheme (as shown in Figure 4.8) and consisted of 8661 cells (5160 elements in the casting system region and 3501 cells in the aluminium mould region). In this way the performed study can also be treated as a kind of analysis of the numerical mesh influence on results, since in case of both considered geometries the computational mesh differed from the original one.

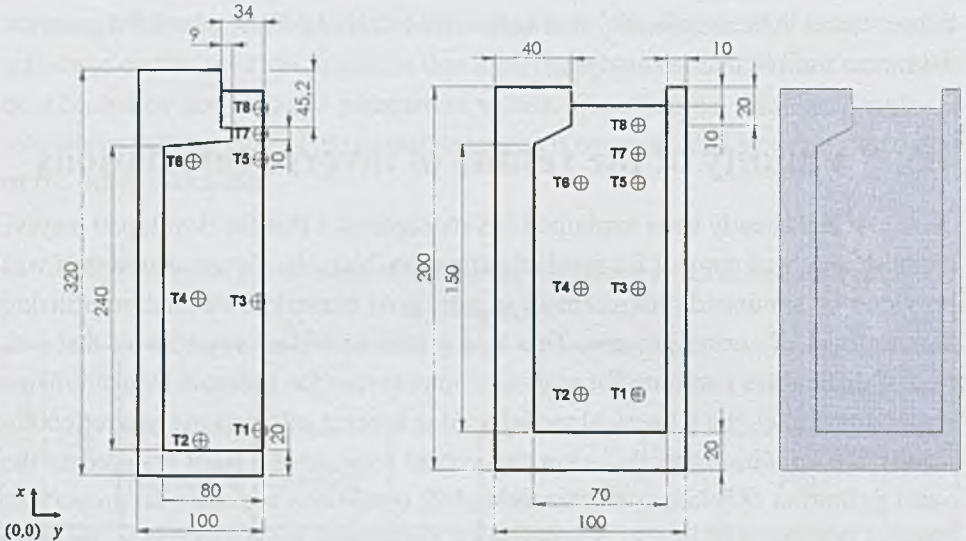


Figure 4.8: Scaled geometry (left) and modified geometry and mesh (right) used in the study on the influence of geometry and mesh.

Two numerical simulations were run for each of the modified geometries, one with the measured curing kinetics data and the second one with the coefficients of the curing kinetics model found in inverse analysis. The comparison of temperatures obtained in these computations is presented in Figure 4.9 and Figure 4.10. It should be mentioned that the location of monitoring points changed, comparing to the original geometry, due to the geometry modifications. In the first case the coordinates of monitoring points were only scaled by a factor of 2, while, for the modified geometry, the placement of monitoring points changed totally (refer to Figure 4.8 and

Table 4.6). In spite of the mentioned geometrical changes, the agreement between temperatures obtained for the measured and for the optimized parameters was on the same level as in case of the original geometry. Very good correlation was observed for the parameters determined with the use of Levenberg-Marquardt algorithm and slightly worse for the parameters calculated by PSO method. This proves that the validity of the parameters of the curing kinetics model, determined by using the developed inverse methodology, is independent on geometry and numerical mesh. In other words, the curing kinetics model developed for a specific geometry can also be used in case of different system assuming that the polymerization concerns the same casting material as the one used to determine the parameters of the curing kinetics model.

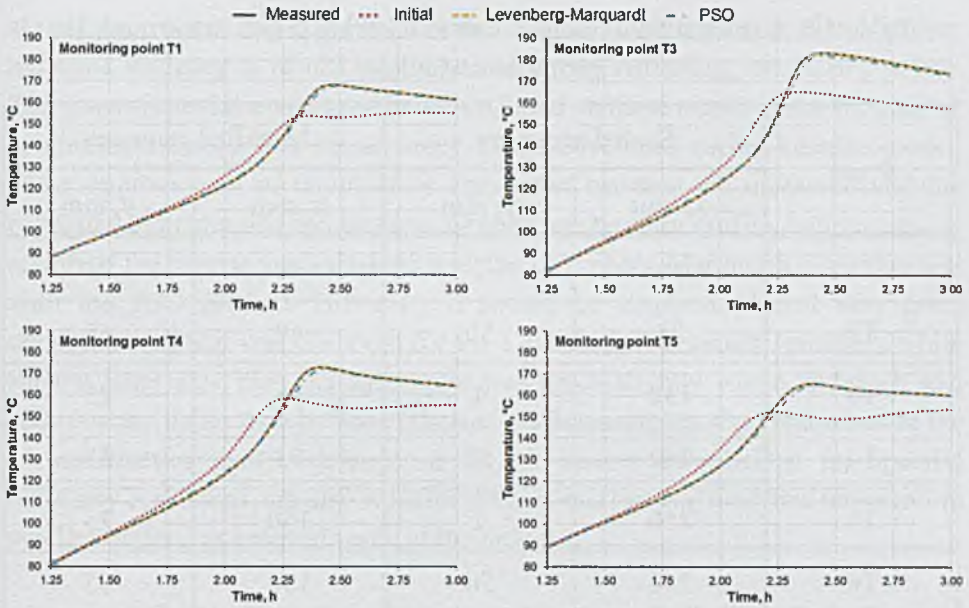


Figure 4.9: Temperature agreement observed for the scaled geometry with the curing kinetics data fitted for the original geometry.

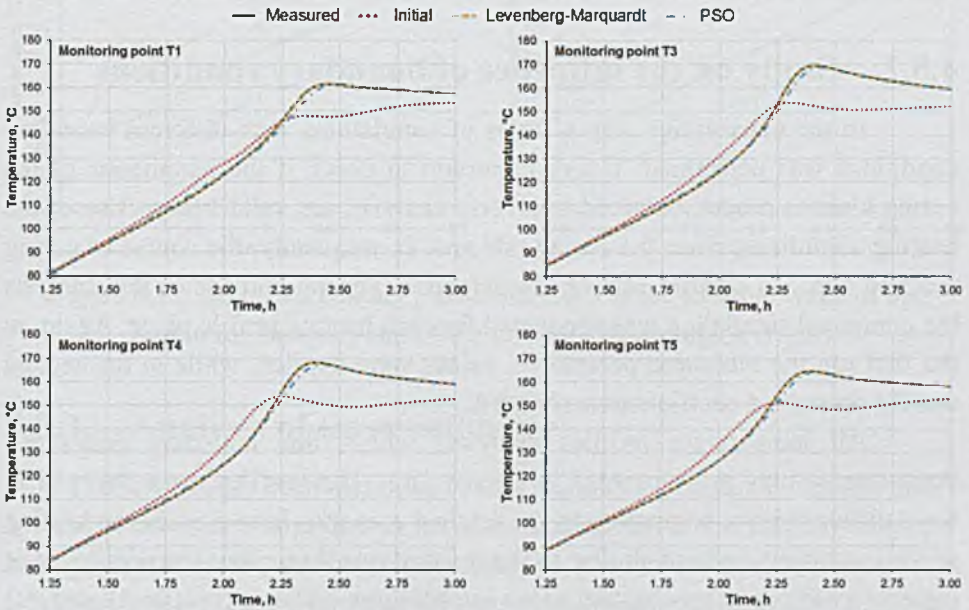


Figure 4.10: Temperature agreement observed for the modified geometry with the curing kinetics data fitted for the original geometry.

Table 4.6: The location of temperature monitoring points in the modified geometrical models.

Point	Scaled geometry		Modified geometry	
	x, mm	y, mm	x, mm	y, mm
T1	36	2	40	25
T2	28	50	40	55
T3	138	4	95	25
T4	140	52	95	55
T5	250	2	150	25
T6	248	56	150	55
T7	270	2	165	25
T8	290	2	180	25

4.5.2. Study on the influence of boundary conditions

In the consecutive step a series of simulations with different boundary conditions was performed. It was important to check if the parameters of the curing kinetics model, obtained in inverse analysis, are valid irrespective of the heating conditions, since the curing rate and, consequently, the course of curing reaction depends significantly on temperatures. For the purpose of this analysis the numerical simulation was conducted for each heating profile twice. Again, in the first run the measured parameters values were applied, while in the second one the optimized coefficients were used.

All temperature profiles analysed within this boundary conditions dependence study are presented in Figure 4.11. The profiles were changed in three different ways comparing to the original scenario. In two cases the heating curve character was kept similar to the original one, but either temperature was increased/decreased by constant value in each time instance (profile #1 and #2) or the heating rate was increased/decreased (profile #3 and #4). In the third case the character of temperature profile changed totally in terms of heating rate, temperature values and number of temperature peaks (profile #5).

The outcome of the presented study, related to the influence of boundary conditions, is illustrated in Figure 4.12. It is worth stressing that data calculated

at only one monitoring point is presented for each temperature profile, however the same tendency in results was observed for the remaining monitoring points. The general conclusion that can be drawn based on these results is that the heating conditions do not affect the accuracy of the developed curing kinetics model. Clear improvement of temperature agreement between the measured and the estimated temperatures can be seen for each temperature profile, both in case of results of the inverse analysis done with the Levenberg-Marquardt algorithm and with the PSO method. However, it should be emphasized that very good temperature fitting was observed for the Levenberg-Marquardt approach, while for the latter algorithm the agreement was again slightly worse, although still significantly better than before optimization. Summing up, the parameters of the curing kinetics model, determined in the inverse calculations for specific boundary conditions, are also valid for other scenarios with modified temperature profiles defined at external walls of the model.

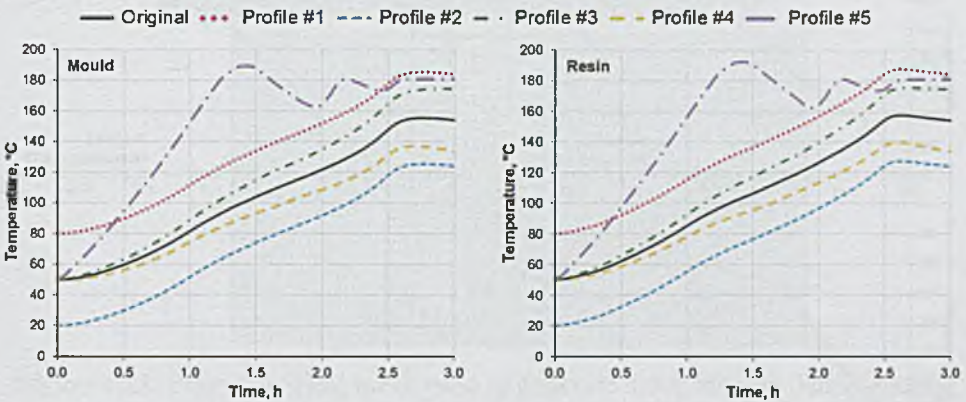


Figure 4.11: Modified heating profiles defined at the external walls of the mould region (left) and of the casting system region (right).

4.5.3. Analysis of error influence

It has already been mentioned at the beginning of chapter 4 that so-called inverse crime was committed in inverse calculations of the parameters of the curing kinetics model, done within the study referred to as the virtual experiment of curing process. This means that the same numerical model was used to prepare data describing the cause of curing reaction in the form of temperature field as the one employed during inverse calculations aimed at finding the coefficients of the curing kinetics model. More precisely, the numerical mesh, physical properties of materials, initial condition and boundary conditions were the same. The only difference between the model applied to simulate measurements and the

one utilized in the inverse procedure was the set of the parameters of the curing kinetics model. This idealistic approach allowed proving that the mathematical mechanism used in the inverse methodology works correctly and is free of the computer programming errors.

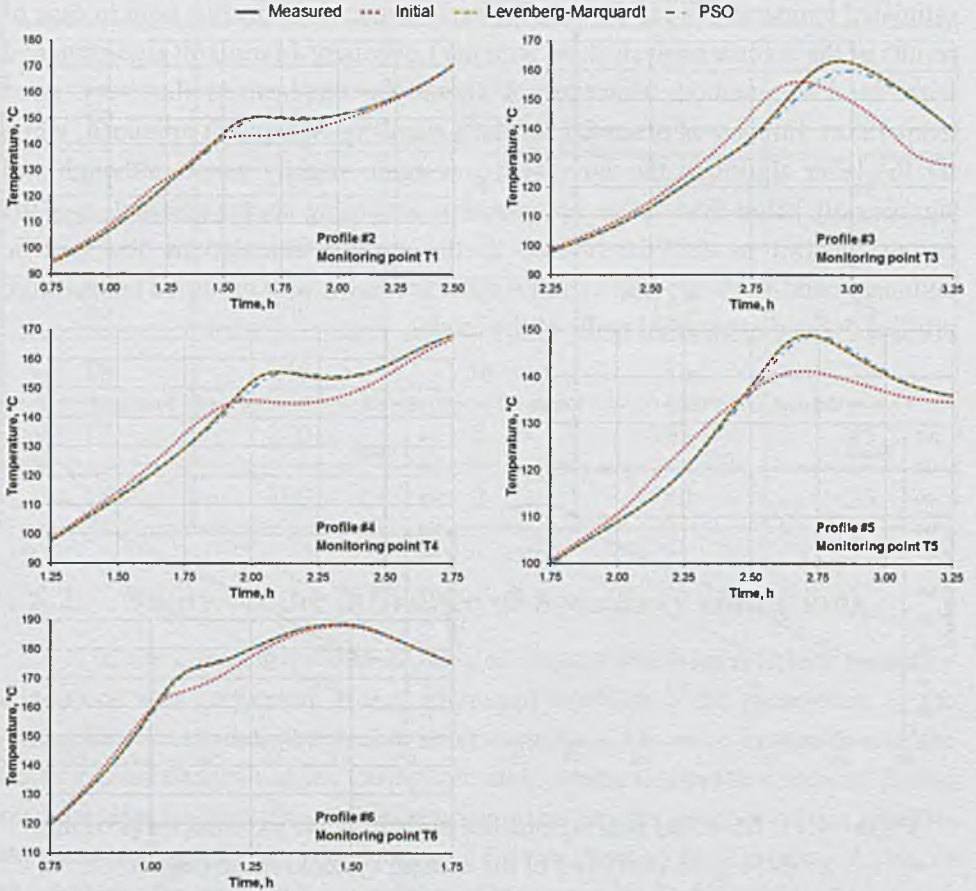


Figure 4.12: Temperature agreement observed for the modified boundary conditions with the curing kinetics data fitted for the original boundary conditions.

The main focus of the next step of investigations was the influence of error in the measured data on effectiveness of the developed inverse methodology. For this purpose perturbations, simulating measurements errors, were introduced into the information about the measured temperatures and two different series of inverse analyses were performed. In the first one the inverse crime was again committed, while in the second series the inverse formulation was deprived of this problem. This was done by applying much finer mesh in the

model used to generate the measured data, whereas the numerical mesh of the model applied during the inverse calculations was exactly the same as discussed in subchapter 4.3.2 and shown in Figure 4.3. The refined numerical mesh is presented in Figure 4.13. It consisted of 56528 cells (36256 in the epoxy resin region and 20272 in the aluminium mould region) and was prepared by double adaption of the original mesh. It means that the fine mesh had the same topology as in case of the based mesh (Quad Elements Scheme with Pave and Submap Type Scheme in the casting system region and aluminium mould region respectively).

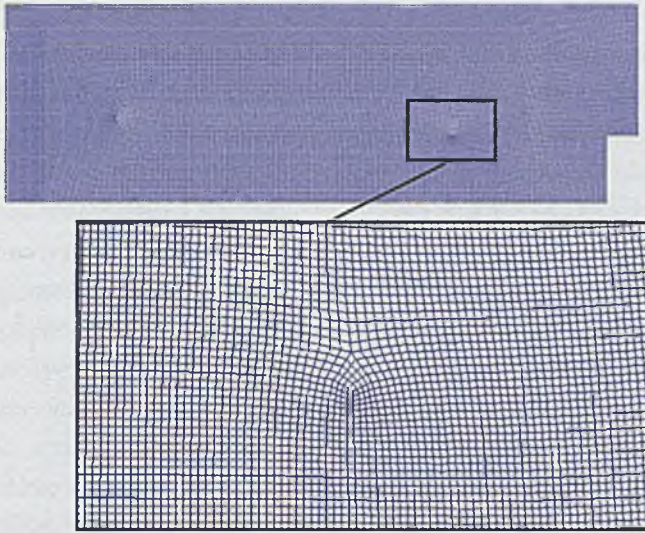


Figure 4.13: Fine numerical mesh used to generate the measured data avoiding inverse crime.

The main goal of the error influence analysis was to check how different levels of perturbations in the measured data affect the inverse problem solution. The errors were introduced into the measurement data by using built-in Microsoft Excel functions that compute a random number RN from the Gaussian distribution for a given standard deviation SD and mean M :

$$NORMSINV(RAND() \cdot SD) + M \quad (4.9)$$

where $NORMSINV()$ is a function that returns the inverse of the standard normal cumulative, $RAND()$ is a function that returns a random number between 0 and 1 (evenly distributed).

Basically, the function above generated random number from the Gaussian distribution with different levels of standard deviation (1%, 2%, 5%) and with the mean value corresponding to the original measured temperature for a given monitoring point and time instance. In this way, the mentioned perturbations, simulating measurements errors, were introduced to the information about the measured temperatures, as shown in Figure 4.14. This, in turn, allowed judging more reliably the efficiency and accuracy of the developed methodology. However, it is worth stressing that the error influence study was performed only by using the Levenberg-Marquardt approach, with the algorithm parameters tuned in comparison to the inverse analysis described in subchapter 4.4. The stochastic character of the PSO algorithm excluded the sense of performing the similar error influence analysis for this method, since the error influence on the solution could be diminished or enlarged by the mentioned randomness in the working principle of the algorithm.

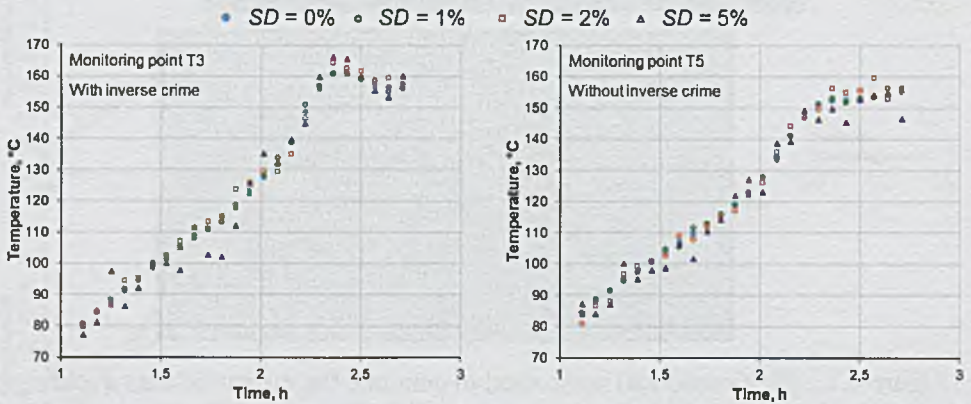


Figure 4.14: The level of perturbations in the measurement data depending on the value of standard deviation.

The influence of errors, introduced to the measured data, on the course of inverse analyses is illustrated in Figure 4.15. The left-hand side graph presents the objective function value in the consecutive iterations for the inverse calculations performed with different levels of perturbations in the measurement data and committing the mentioned inverse crime (further referred to as ‘inverse crime’ case). The right-hand side graph depicts analogous results obtained during inverse calculations without the inverse crime commitment (further referred to as ‘no crime’ case). Additionally, the included tables present the initial and final values of the objective function (G_{ini} and G_{fin} respectively) as well as the value of improvement factor IF , calculated according to the following equation:

$$IF = \frac{(G_{ini} - G_{fin})}{G_{ini}} \cdot 100 \tag{4.10}$$

Two main conclusions can be drawn based on the presented results. Firstly, the developed inverse methodology improved the correlation between the measured and the estimated temperatures in all analysed cases. Secondly, the methodology is sensitive to the error in the measurement data, however, this dependence is strongly affected by the error level and, as expected, increases with its value. One can also notice that the efficiency of the inverse methodology lowers more rapidly with the error growth in the ‘no crime’ case. The probable reason for that is the summation of the influence of two uncertainties, the one connected with different numerical meshes used during the measurement data generation and during the inverse calculations, and the second one resulting from the introduced error. Furthermore, it can be seen in the results obtained for the ‘no crime’ case that the final objective function value was relatively high even in the inverse analysis with the error-free measured temperatures. The analogous analysis performed for the ‘inverse crime’ case finished successfully reaching the target value of the objective function just after 4 iterations. Keeping in mind the conclusions above, it can be stated that much care should be taken both to prepare accurate numerical model of a considered problem and to minimize the measurement errors when collecting the measurement data for inverse calculations done with the use of the proposed inverse methodology. In this way the conditioning of the inverse problem under investigation can be better, increasing simultaneously the probability of the inverse calculations success.

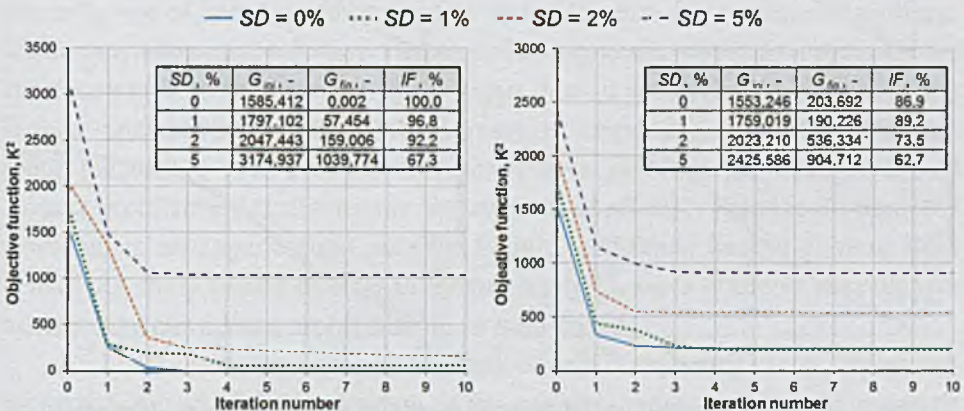


Figure 4.15: The convergence of the solution with (left) and without (right) commitment of inverse crime depending on the error in the measurement data.

The efficiency of the inverse methodology is also presented in Figure 4.16 and Figure 4.17 in terms of temperatures agreement, obtained at selected points, in dependence on the error level in the measurement data. Generally, it can be concluded that the correlation of temperatures follows the value of the objective function, i.e. the lower final value of the objective function the better fitting of temperatures. This relationship is quite obvious when analysing the way the objective function is calculated (refer to Equation (3.14)). One can also see that, in the ‘inverse crime’ case (refer to Figure 4.16), the matching between the measured and the estimated temperatures was significantly improved in all runs of inverse analysis, although the best and the worst fitting was obtained, respectively, for the calculations without errors and with the highest errors in the input data. The disagreement between the measured and the estimated temperatures was also clearly lowered in the ‘no crime’ case (see Figure 4.17), but the final fitting of temperatures was generally worse for each error level when comparing to the ‘inverse crime’ case. However, it seems that bigger discrepancy in the study based on the approach without inverse crime commitment is highly influenced by the difference in computational meshes applied in the numerical simulation acting as simulated measurement and in the computations performed within the inverse calculations.

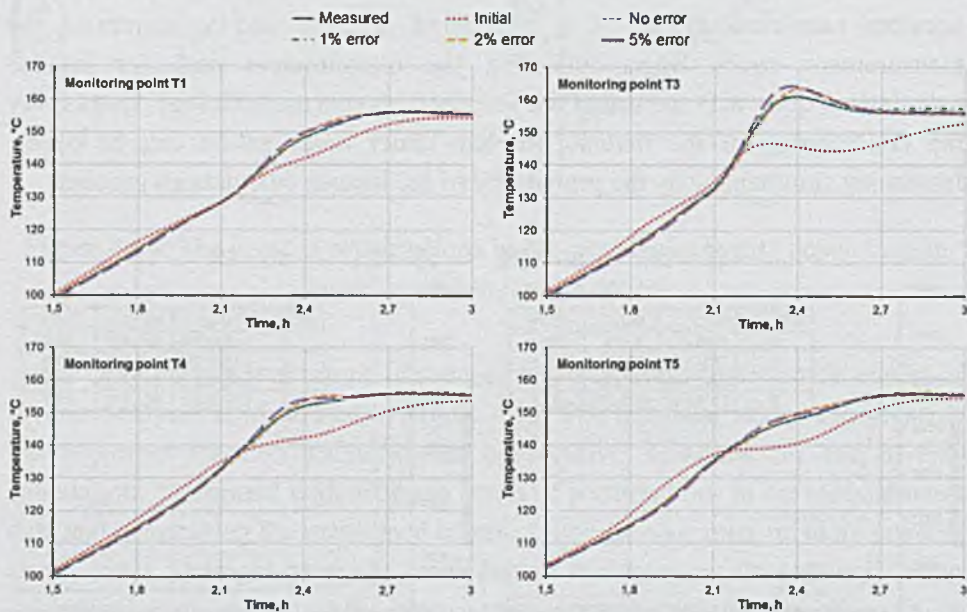


Figure 4.16: The influence of the error in the measurement data on temperatures agreement at selected monitoring points (with inverse crime committed).

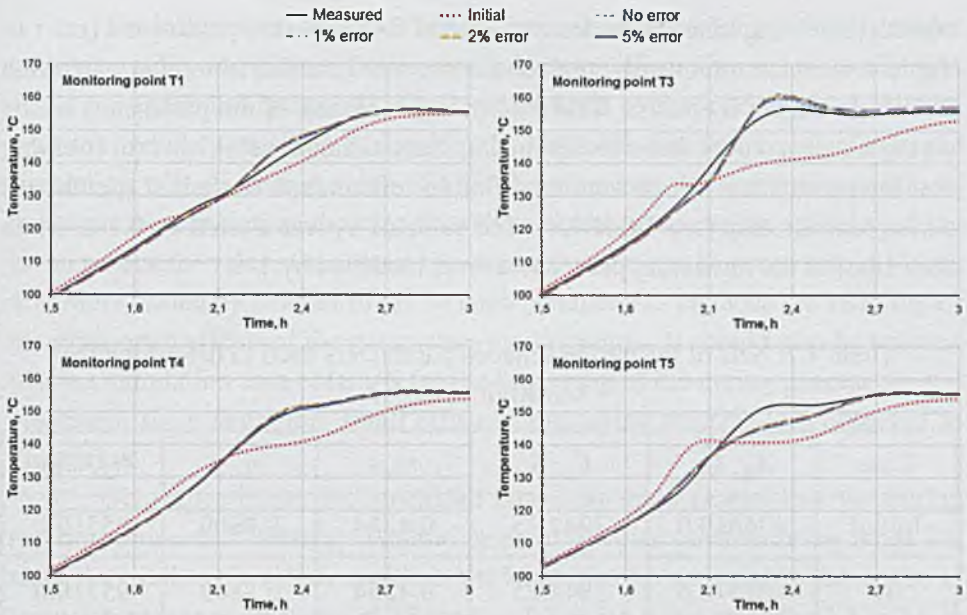


Figure 4.17: The influence of the error in the measurement data on temperatures agreement at selected monitoring points (without inverse crime commitment).

4.6. Sensitivity analysis

Sensitivity analysis was a part of inverse analysis performed with the use of Levenberg-Marquardt approach and described in subchapter 4.4. It was carried out every each iteration to determine the sensitivity matrix required to solve the parameters estimation problem, i.e. to find the values of the parameters of the curing kinetics model. Generally, sensitivity study provides information about the influence of investigated parameters on the solution of a considered problem. This knowledge can be further used to define locations, where the solution is the most sensitive to the changes in the input data. It is crucial when performing inverse analyses and planning measurements supporting inverse calculations, since the use of such strongly influenced data improves the conditioning of inverse problem and facilitates the observations of effects, related to the analysed problem, in an experimental manner. Finally, additional benefit coming from sensitivity study relates directly to inverse analysis, since it allows to recognize whether the considered problem is ill- or well-posed.

In this particular case, the matrix of sensitivity coefficients, informing about the impact of the parameters of the curing kinetics model on temperature field, was determined by using central difference scheme (refer to subchapter 3.3.2.2). Due to this method two computer simulations were needed to calculate sensitivity coefficients of a single parameter, according to Equation (3.17). The

considered curing kinetics model consisted of five non-zero parameters (refer to Table 4.4) and, consequently, ten simulations were needed in total to determine the whole sensitivity matrix. Table 4.7 presents all sets of the parameters of the curing kinetics model that were applied in these simulations. It is worth stressing that the parameters values were modified in reference to the initial (perturbed) curing kinetics data (see Table 4.4). The value of E_2 was altered by 0.1%, while the values of the remaining parameters were modified by 1%.

Table 4.7: Sets of the curing kinetics parameters used to determine the sensitivity matrix.

Case	A_2 , 1/s	E_2 , K	m , -	n , -	H_{Σ} , J/kg
Initial	406640.0	7942.25	0.4264	0.8809	95710.0
01	402573.6	7942.25	0.4264	0.8809	95710.0
02	410706.4	7942.25	0.4264	0.8809	95710.0
03	406640.0	7934.3109	0.4264	0.8809	95710.0
04	406640.0	7950.1955	0.4264	0.8809	95710.0
05	406640.0	7942.25	0.4221	0.8809	95710.0
06	406640.0	7942.25	0.4306	0.8809	95710.0
07	406640.0	7942.25	0.4264	0.8720	95710.0
08	406640.0	7942.25	0.4264	0.8897	95710.0
09	406640.0	7942.25	0.4264	0.8809	94752.9
10	406640.0	7942.25	0.4264	0.8809	96667.1

The influence of the value of each parameter of the curing kinetics model on temperature, at points referring to the location of monitoring points T3 and T5, is presented in Figure 4.18. Black dotted lines correspond to the simulation with the initial (perturbed) curing kinetics data. Blue solid curves refer to the simulation with decreased value of a given parameter, while red dashed curves represent the simulation showing how the solution reacts to the increase of the given parameter value. One should be aware that the results presented in Figure 4.18 were scaled by a factor of 10 for each parameter to enhance the visibility of the mentioned effects of the parameters modifications. It should also be stressed that the simulation data obtained for the beginning of the curing process are not presented, since negligibly small effect of the curing reaction was observed in this period.

Generally, it can be concluded based on these results that the curing reaction proceeded faster at monitoring point T5 than at monitoring point T3, since the exothermic effect, visible in the form of sudden change in the course of temperature curves, occurred at T5 for $t = 1.7 \div 2.4$ h and at T3 for $2.1 \div 2.6$ h. It can also be seen that the influence of the parameters values on temperature was initially (for $t = 1.5 \div 2.2$ h) bigger at point T5 than at point T3. Then the situation inverted. This can be connected with the way the curing front propagated, i.e. the reaction was probably initiated in the top regions of the mould, where the hottest portions of the casting system were present and, then, it proceeded downwards. Besides that it can be noticed that decreased value of A_2 parameter resulted in lower temperatures in the first part of the analysed time period (more or less until $t = 2.1$ h for both monitoring points), while in the remaining part temperatures were higher. Moreover, the highest temperatures obtained in the period, when the heat was released due to ongoing curing reaction, occurred later in case of lower value of A_2 parameter. In turn, for the increased value of A_2 parameter the reverse effects were observed and the influence of E_2 , m and n parameters on the solution was opposite to that detected for A_2 parameter. Finally, in case of H_2 parameter, two regions of different influence of the parameter value on the solution, characteristic for the other coefficients, were not observed. In this case the growth of the parameter value caused increase of temperatures in the prevailing part of the considered process, except the last period, where no dependence between the parameter value and the solution was detected.

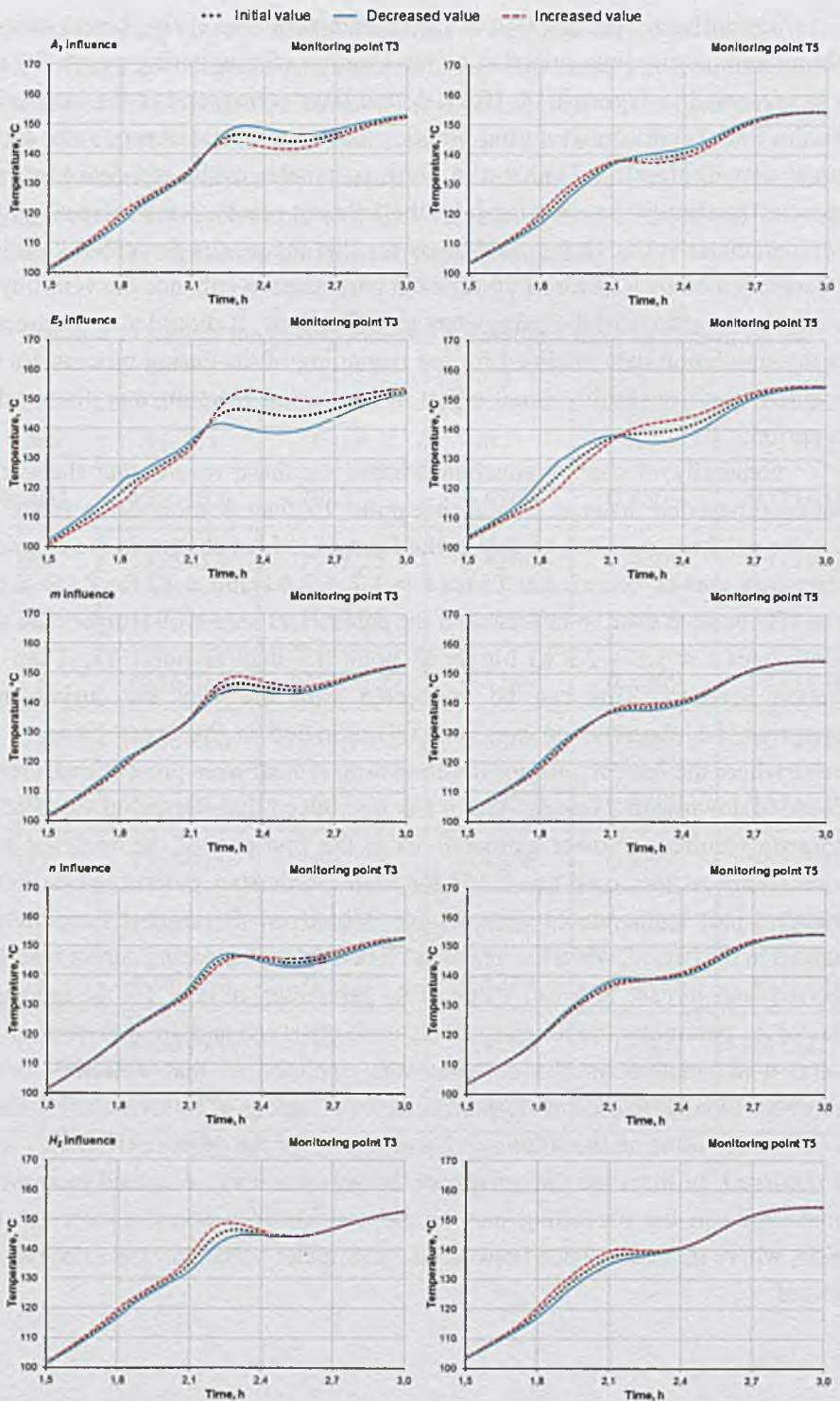


Figure 4.18: The dependence of temperature on the parameters of the curing kinetics model at points T3 and T5.

As mentioned, one of the main advantages of sensitivity analysis is that it allows checking whether the formulated inverse problem is ill- or well-conditioned. In the best situation the values of sensitivity coefficients, calculated according to Equation (3.17), are large and linearly independent of each other, i.e. only one parameter impacts the solution at a given location, while the remaining ones are meaningless there. Figure 4.19 presents the values of sensitivity coefficients obtained for the parameters of the curing kinetics model at all monitoring points for the selected time instances. Generally, each parameter influences temperature at each monitoring point which means that the condition of the parameters linear independence is not fulfilled and the investigated problem is ill-conditioned. Furthermore, the obtained values of sensitivity coefficients confirmed the observations made when analysing the results showing temperature dependence on the change of the parameters values. Positive sign standing in front of sensitivity coefficient means that the increase of the parameter value results in higher temperature at a given point and sampling instance. The opposite situation should be expected in case of the negative sensitivity coefficient, while zero value means no influence on temperature.

The other useful quantity calculated within sensitivity study is relative sensitivity coefficient that can be used to compare directly the influence of different parameters. In this way the most critical parameters can be chosen, i.e. these impacting the solution the most. One can notice, comparing Equation (3.17) with Equation (3.19), that relative sensitivity coefficient is simply a result of multiplication of the value of a sensitivity coefficient by a given parameter. It means that there is a direct relationship between these quantities and, therefore, one should expect exactly the same tendency in the change of relative sensitivity coefficients in time as in case of sensitivity coefficients. Figure 4.20 presents the values of relative sensitivity coefficients calculated for the parameters of the curing kinetics model at monitoring points T1 ÷ T8. It should be noticed that the left y axis corresponds to parameters A_2 , m , n and H_2 , while parameter E_2 is expressed in terms of the right y axis. It can be concluded based on these results that E_2 parameter was a dominating factor in the analysed case, affecting temperature to the greatest extent at all monitoring points. The values of relative sensitivity coefficients for this parameter were more or less one order of magnitude bigger than for the remaining parameters of the curing kinetics model. Nevertheless, the influence of the other parameters was also noticeable, especially in case of A_2 and H_2 , whereas parameters m and n turned out to be the least essential.

All results of the performed sensitivity analysis, discussed in the previous paragraphs, were focused on determining the most influential parameters of the curing kinetics model, based on data gathered at monitoring points that were

defined prior to the sensitivity study. However, one of the mentioned advantages of sensitivity analysis is the ability to recognize the most crucial locations considering the whole domain under investigation. This information can be further used in experiments designing, since it is easier to capture effects related to a given problem in regions, where the measured quantity is significantly influenced by investigated process or phenomenon. In this specific case the spatial representation of relative sensitivity coefficients, presented in Figure 4.21, was employed to observe if and possibly how the influence of a single parameter of the curing kinetics model changes in space and time as well as to compare the impact of the parameters with each other. In both cases the considerations were based on the results obtained at three selected time instances, marked in Figure 4.20.

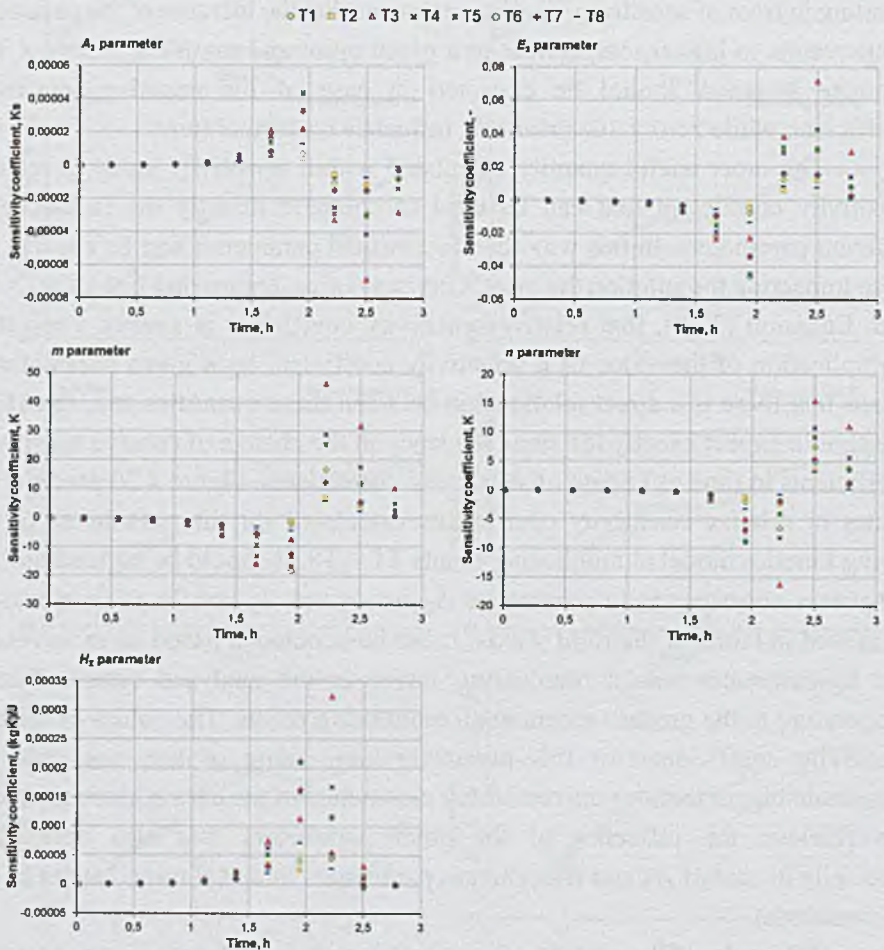


Figure 4.19: Sensitivity coefficients calculated for the parameters of the curing kinetics model at points T1 ÷ T8.

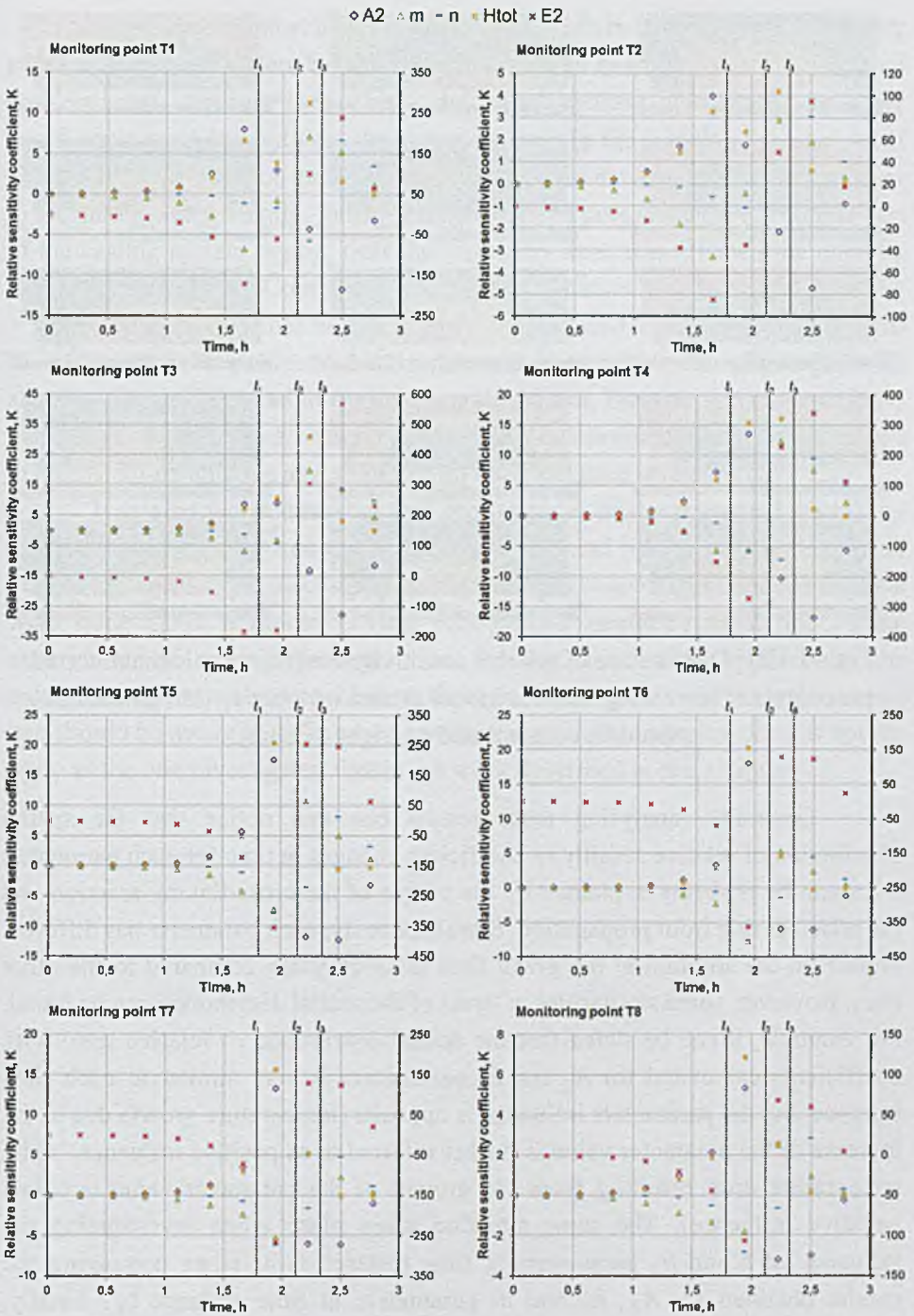


Figure 4.20: Relative sensitivity coefficients calculated for the parameters of the curing kinetics model at points T1 ÷ T8.

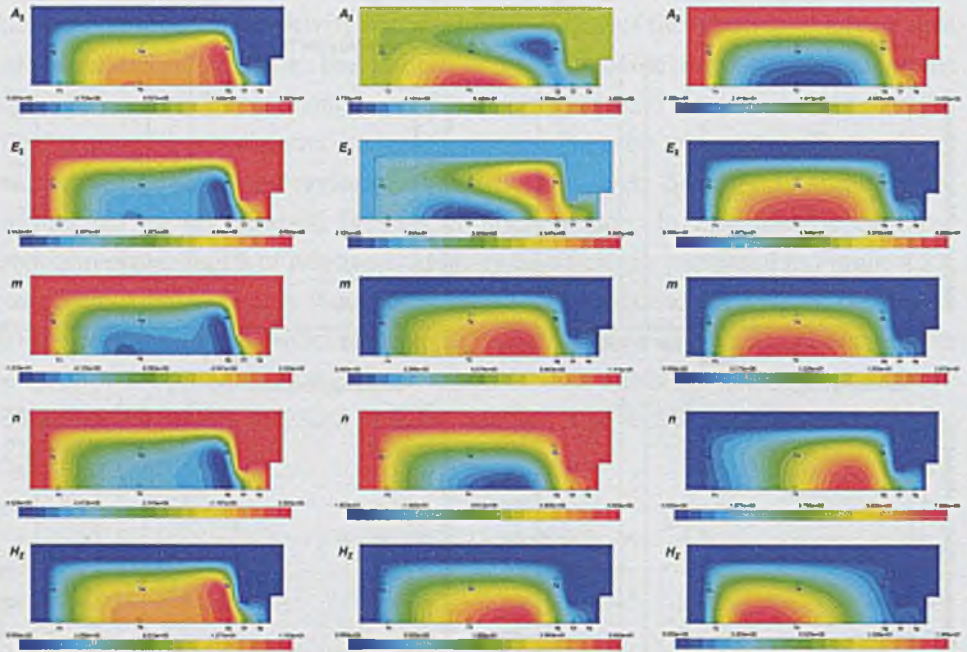


Figure 4.21: Distribution of relative sensitivity coefficient calculated for all parameters of the curing kinetics t model at time instance t_1 (left column), t_2 (middle column) and t_3 (right column).

Generally, analysing these results one can notice that the spatial distribution of relative sensitivity coefficient changes in time for each parameter, what can be probably explained by the course of the cross-linking reaction and the arisen curing front propagation. Simultaneously, each parameter has different impact on the solution at the given time instance when compared to the other ones. However, some similarities in terms of the spatial distribution can be found. For example, it can be stated that the spatial distribution of relative sensitivity coefficients calculated for A_2 and E_2 parameters is very similar at each time instance, but the parameters influence is opposite (temperature growth due to the increase of the parameter value is further referred to as positive influence, while temperature drop resulting from the growth of the parameter value is called negative influence). The same situation takes place when investigating the influence of n and H_x parameters at time instance t_2 or when comparing the results obtained for A_2 , E_2 and m parameters at time instance t_3 . Finally, similarities between all parameters are also visible at time instance t_1 , when parameters A_2 and H_x have positive influence on the solution, whereas E_2 , m and n have negative impact.

Regarding the most influential locations it can be concluded that the upper part of the casting system region was impacted the most at the first considered time instance. At time instance t_2 , the biggest values of relative sensitivity coefficients were located near the symmetry axis in the middle of the height of the casting system region and in the upper part of the casting system region closer to the mould walls. Finally, for the last investigated time instance, the middle part of the casting system region, near the symmetry axis, was affected the most by the parameters values. Comparing that with the location of monitoring points T1 ÷ T8 it can be stated that not all sensors were placed in the optimum regions during the virtual experiment of curing process. However, in case of data gathered at points T3 and T5, used in the inverse calculations, the situation was relatively good, since these sensors were influenced to a considerable degree by the change of almost all parameters and at almost all analysed time instances.

It is also worth stressing that the outcome of the presented sensitivity analysis was partially used to select the number and location of sensors when designing experiments, discussed in the subsequent chapter. These measurements were done using a mould having very similar geometry as in the virtual experiment of curing process. The heating conditions applied in the measurements were also very close to these defined in the virtual study. However, one should be aware that the casting system used in the experiments was not the same as the one investigated within the work described in this chapter.

5. Experimental investigation of curing process

5.1. Goals and assumptions

The goal of the experimental part conducted within the framework of this thesis was triple. Firstly, it was interesting to examine how the composite material structure (combination of casting system and crepe paper) influences the kinetics of curing reaction in comparison to the homogenous sample. Secondly, the performed laboratory experiments allowed checking how the course of polymerization reaction is affected by heating conditions. Finally, the last but not least benefit coming from the curing experiments was the contribution to experimental validation of the curing modelling approach, addressed in chapter 6. On the one side, the measured data was used to build direct numerical model that was applied in inverse analyses aimed at calculation of the parameters of the curing kinetics model. On the other hand, the recorded temperatures constituted the measurement data needed as the input in the mentioned inverse calculations.

It is worth stressing that the basis for all experimental investigations was the strong correlation between the course of curing reaction, resulting in the heat generation, and temperature field monitored by sensors. In other words, the exothermic reaction was represented by peaks in temperature recordings and this allowed tracing the progress of chemical reaction. It should also be mentioned that several simplifications were introduced during the performed curing tests and, hence, they differed from typical vacuum casting process, described in subchapter 2.3. First of all, the filling stage was excluded from considerations and the measurements were conducted only during the curing stage. It was assumed in this case that the curing reaction was not initiated due to relatively short filling process (dozens of seconds) that was additionally performed in ambient temperature. Hence, it is very likely that the start of polymerization was delayed in such conditions and the reaction was initiated probably at the beginning of the curing stage when temperature was raised. Besides that the curing process was performed under ambient pressure instead of vacuum. The second simplification resulted from the fact that vacuum conditions are applied in industrial production mainly for trouble-free filling. On this basis it was assumed that the ambient pressure does not influence the cross-linking process. All above allowed simplifying both the measurement stand and the experimental procedure applied during tests. In addition to that the numerical model simulating the performed

experiments and used in the inverse calculations was less complex what was very important from the computational time perspective.

5.2. Experimental stand

The measurement stand used in the laboratory experiments is presented in Figure 5.1. The main element of the experimental rig was electric oven (VENTICELL 404) with aluminium mould (refer to Figure 5.2) that was filled with the investigated sample and placed in the central point of the oven chamber. The electric oven maintained air temperature inside the chamber at the level defined by using the oven controller. It was possible to specify arbitrary heating program consisted of many stages with variable temperature levels. The uniformity of air temperature inside the oven was ensured by fan forcing the hot air circulation in the whole chamber volume and accelerating the stabilization of temperature. In turn, the forced hot air convection influenced the heating conditions on the mould walls, so it can be concluded that the mould boundary conditions were defined indirectly.

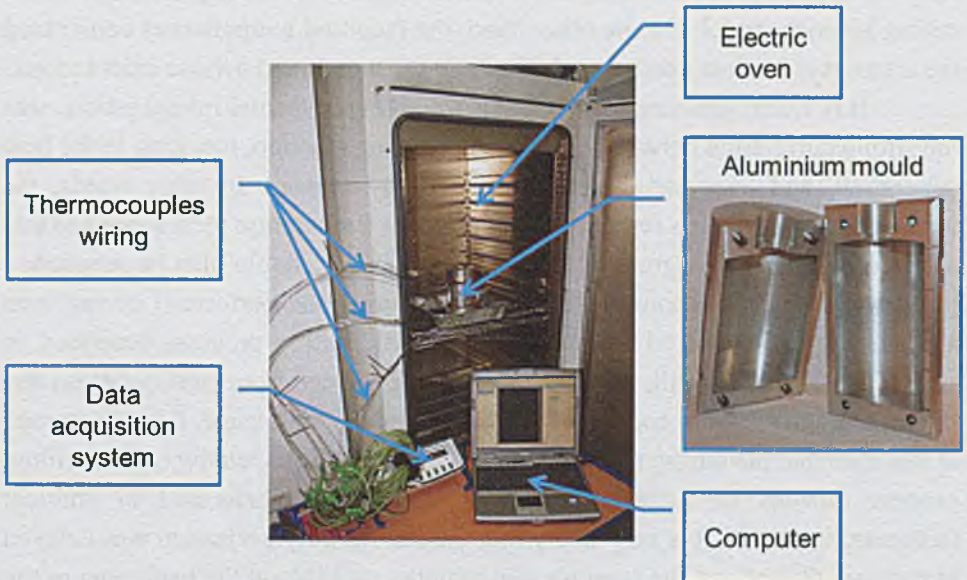


Figure 5.1: Experimental stand used in curing experiments.

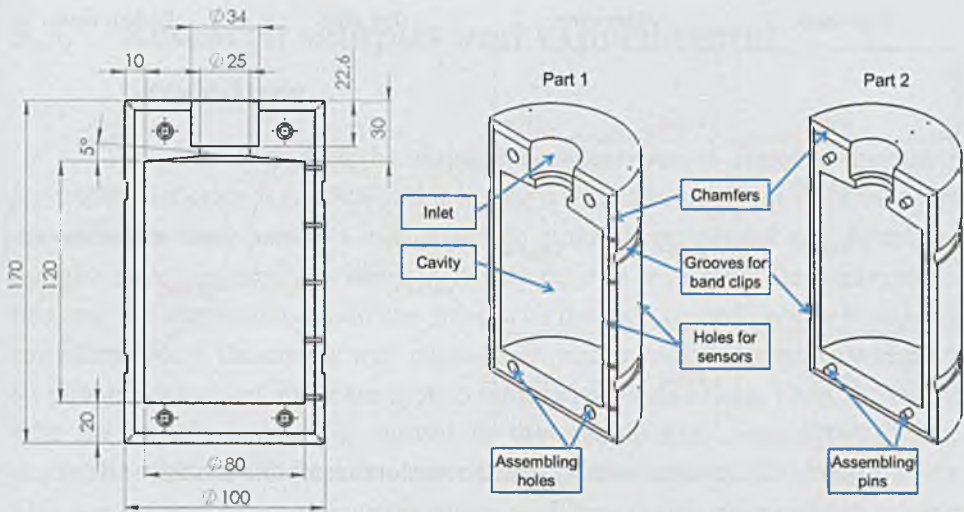


Figure 5.2: Design and main dimensions of experimental mould.

Consequently, 21 temperature sensors (K type thermoelements) were placed inside the mould walls (about 3 mm depth) in order to record the exact temperature profile. Their location is presented in Figure 5.3. It is worth stressing that the mould was made of PA6 aluminium characterized by relatively high thermal conductivity at the level of 134 W/mK [54]. In this way the heat delivered to the mould was immediately transferred through the mould walls to the cavity, filled with the investigated sample, and vice versa. Thermoelements were also placed inside the mould cavity, as shown in Figure 5.4, in order to monitor the response of the system to the curing reaction manifested by heat generation. All thermal sensors were connected with data acquisition system (National Instruments CompactDAQ) collecting signals and passing them to computer. Next, these data were processed and recorded in a dedicated data-logging software (National Instruments LabView SignalExpress).

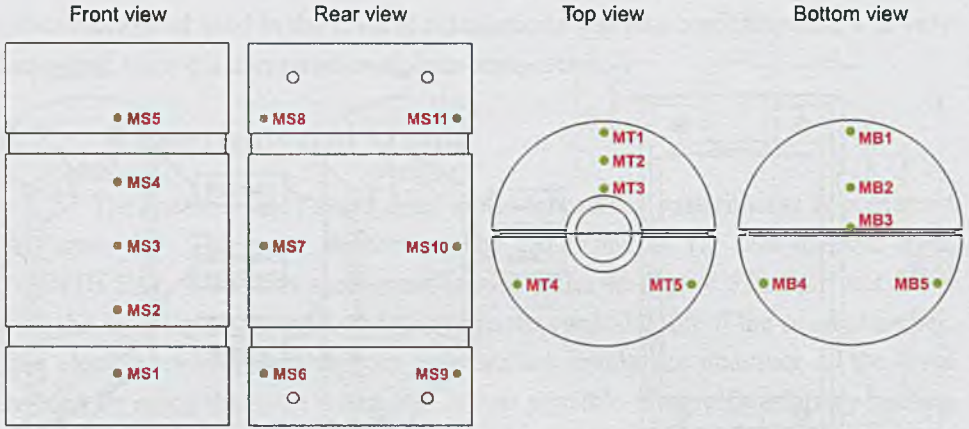


Figure 5.3: Location of temperature sensors inside the mould walls.

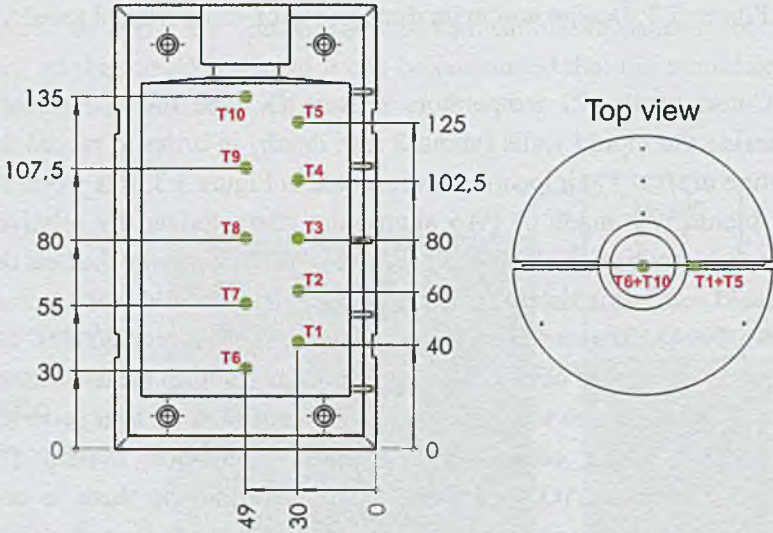


Figure 5.4: Location of temperature sensors inside the mould cavity.

It should be emphasized that the position of the sensors assembled inside the mould cavity was chosen with the help of information gained in the sensitivity analysis, performed within the virtual experiment of curing process (refer to subchapter 4.6). This was done in spite of different casting systems used in the virtual and real experiments. However, both cases were very similar when considering geometrical dimensions, initial condition and boundary conditions. For this reason it was assumed that the most critical regions of the experimental mould, i.e. affected to the highest degree by the progressing curing reaction, should be close to these recognized within the virtual study.

5.3. Research samples and experimental procedure

The general target of the curing experiments was to compare the curing process for different samples. For this reason it was extremely important to ensure the same starting conditions in each of the curing experimental and, hence, all samples were prepared according to strictly defined procedure. Basically, in the first step the aluminium mould was filled with the investigated sample in ambient conditions. Next, the sample was degassed in vacuum chamber in order to remove air bubbles entrapped inside the system during the mould filling. Then, the mould with the sample inside was moved to the electric oven, connected to data acquisition system and kept at elevated temperature equal to 50°C for 5 hours. This was enough to equalize temperature at all monitoring points and to achieve steady-state. In this way the same initial temperature field was defined at the beginning of each curing experiment. On the other hand, this level of preheating temperature was still not high enough to activate the curing reaction according to the Hexion casting system datasheet [53] and, consequently, the uniformity of the initial field of degree of curing was ensured.

The matrix of all conducted experiments is presented in Table 5.1. It can be seen that six experimental runs were made in total, although the essential part of this experimental study were the measurements done for the Hexion casting system (mixture of epoxy resin and hardener) and for the composite sample (coil of crepe paper impregnated with the Hexion casting system), marked as EXP_B.1 and EXP_C respectively. This was the basis for the investigation focused on the influence of the composite structure on the curing reaction. Two other tests, marked as EXP_B.2 and EXP_B.3, were done to check how the curing reaction is influenced by the changed heating conditions (modified heating rate and curing temperature as shown in Figure 5.5). Finally, the remaining two experiments were conducted to verify how the cross-linking phenomenon is affected by the moisture in the paper coil (EXP_D) and to build the numerical model of heat and mass flow, excluding the curing related effects (EXP_A with the Hexion epoxy resin without hardener).

Table 5.1: Summary of experimental runs.

Sample	Heating profile 1 (original)	Heating profile 2 (modified)	Heating profile 3 (modified)
Epoxy resin without hardener	EXP_A		
Hexion casting system	EXP_B.1	EXP_B.2	EXP_B.3
Dried paper coil impregnated with the Hexion casting system	EXP_C		
Moist paper coil impregnated with the Hexion casting system	EXP_D		

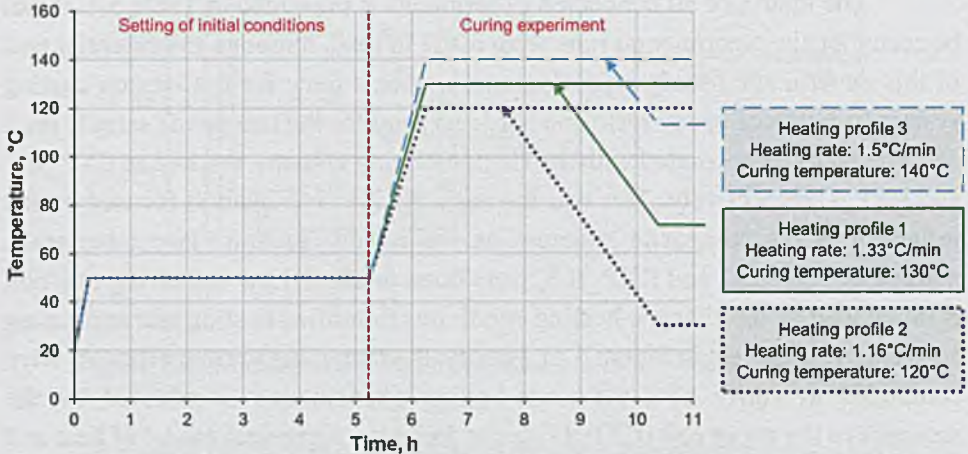


Figure 5.5: Heating profiles applied in curing experiments.

The selected research samples are illustrated in Figure 5.6. One can notice that the external diameter of the paper coil was smaller than the internal diameter of the mould what resulted in 5 mm gap formed in between them. In this case two different regions were created after the mould filling, namely the composite one in the prevailing volume of the mould and the one occupied only by the casting system (in the mentioned gap and in the inlet part of the mould due to the intended material excess).

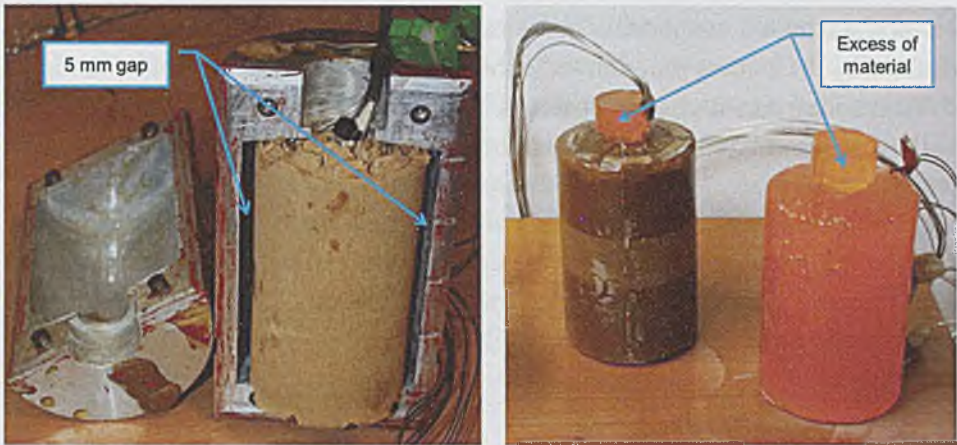


Figure 5.6: Selected research samples (left - paper coil before impregnation, right – paper coil and standard casting system after curing experiment).

5.4. Experimental results

5.4.1. Course of curing reaction at different monitoring points

The first issue investigated based on the results of the curing experiments was the course of the curing reaction depending on the location inside the mould cavity. Figure 5.7 depicts temperatures measured by all thermocouples located in the mould cavity for selected experimental runs. This allowed defining the most crucial regions, i.e. places where the exothermic effect of the curing reaction was the most significant.

Results from EXP_A (with epoxy resin without hardener, i.e. without curing reaction) allowed stating that there was temperature distribution inside the cavity that was not caused by the exothermic cross-linking process. The maximum difference in temperatures values detected during this experimental run was slightly above 7°C. The highest temperatures were measured successively at monitoring point T6, T5 and T4, while the lowest values were observed by thermal sensors T1, T2 and T9. It is probable that this temperature distribution developed due to non-uniform heating of the mould and/or due to the changes of the epoxy resin density resulting from temperature variations, what finally caused gravitational movement of the epoxy resin inside the cavity. Temperature field became uniform in the final part of this experiment, when the steady-state condition was achieved. It was also concluded that the curves representing temperatures inside the cavity reflected the course of the curve corresponding to the average mould temperature (solid black curve in Figure 5.7).

In turn, the mould temperature curve can be interpreted as the heating condition defined by the heating program set in the electric oven (dotted red curve in Figure 5.7). Besides that it can be observed that the determined temperature curves follow a pattern typical for the transient heat conduction/convection problem.

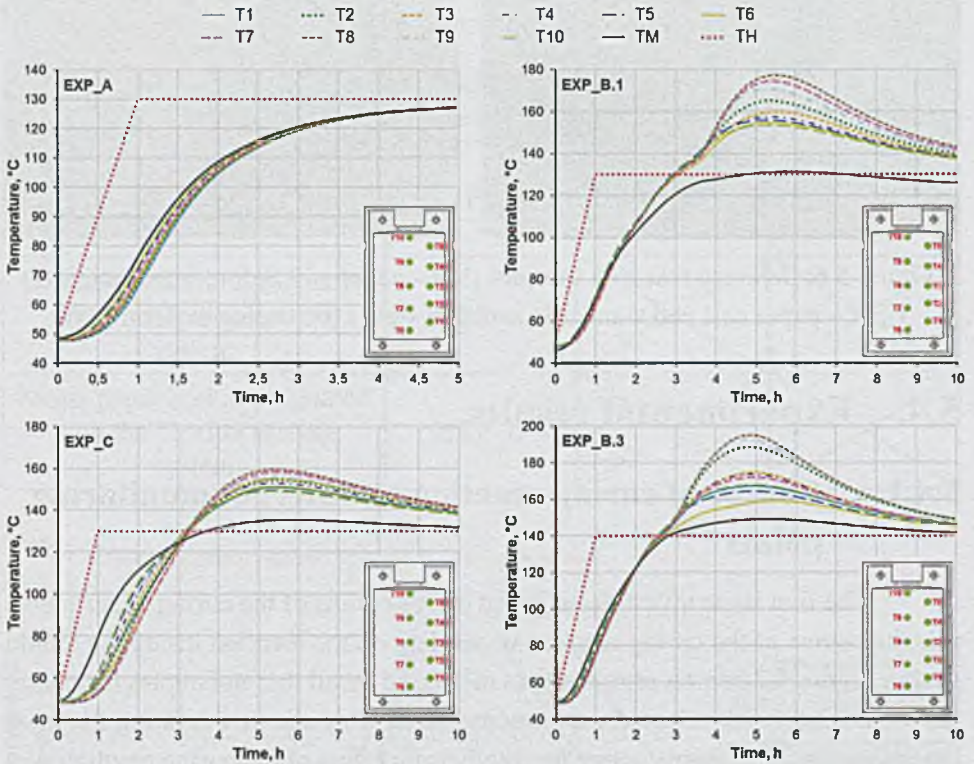


Figure 5.7: Temperatures measured at monitoring points inside the mould cavity during selected experimental runs.

Analysing the results of the remaining experiments it is clearly visible that the values and distribution of temperatures were highly dependent on the sample, on the heating conditions and on the heat generation resulting from the cross-linking process. It was also recognized that considering single experiment the curing rate was not homogenous in the whole cavity domain. For example, in case of EXP_B.1 the highest temperature peak coming from the exothermic reaction was detected more or less in the middle of the epoxy resin volume at monitoring points T7, T8 and T9. The maximum value observed at point T8 was at the level of 177°C, where the maximum heating temperature set in the oven during this experiment was equal to 130°C. Surprisingly, very high temperature was also recorded by thermocouple T2 located near the mould wall. This is in opposition to EXP_A, for which T2 and T9 were among the coolest regions. It is

suspected that the heat generated in the middle of the epoxy resin region could not be freely released due to relatively low thermal conductivity of the Hexion casting system (around 0.2 W/mK) and this caused more intensive heating in this area. It can also be noticed that the characteristic temperature peak caused by the curing reaction occurred for the remaining monitoring points. Additionally, it can be concluded that the curing reaction initiated uniformly in the whole epoxy resin domain, since temperature started to increase almost at the same time for all investigated points. Generally, similar tendencies regarding temperatures variations can also be seen in case of EXP_B.3 conducted in higher ambient temperature than EXP_B.1, although the values were naturally not the same due to different heating conditions.

Finally, the modification of temperatures distribution (comparing to EXP_A) is also visible in case of the experiment done for the composite material in the form of paper impregnated with the Hexion casting system (EXP_C). However, the maximum temperatures captured in this particular case were lower ($149 \div 159^{\circ}\text{C}$) than for EXP_B.1 ($153 \div 177^{\circ}\text{C}$) performed for the standard Hexion casting system. This proved that the presence of the crepe paper influenced the spatial distribution of temperatures inside the cavity, probably due to different physical and thermal properties of the considered samples.

5.4.2. Influence of sample structure

The examination of the sample structure influence on the course of the curing reaction was the main goal of the experimental part. For this purpose the results obtained for the standard epoxy resin mixture by means of Hexion casting system (EXP_B.1) were compared with data recorded for the composite sample in the form of crepe paper impregnated with the Hexion mixture (EXP_C). In addition to that the outcome of EXP_A was used as the reference in this part of study, since in this test the measured temperatures were only determined by the heat transfer capabilities of the pure epoxy resin and, consequently, its response to the ambient conditions (not by the exothermic curing reaction). It is worth stressing that data from the monitoring points T2, T7, T8 and T9 were used to compare different experimental runs discussed further in this chapter, since these locations were affected the most by the exothermic curing reaction.

The obtained results presented in Figure 5.8 revealed different temperature fields built up during the curing experiments performed for the two mentioned samples. Significant increase of temperature caused by the intensive heat production due to the curing process was observed for the Hexion casting system after 2 hours of the experiment, when the average temperature in the cavity reached about 105°C . Another quite dramatic rise of temperature was

detected after 3.5 hours of the experiment. This could be the effect of two-stage curing reaction that characterizes the investigated Hexion casting system as already mentioned in subchapter 2.3. The highest temperatures close to 180°C were observed in this experiment more or less after 5.5 hours counting from the test beginning. It is probable that at this moment the curing reaction has already been advanced and, simultaneously, the system was not able to release the generated heat in an efficient way due to relatively low value of the material thermal conductivity.

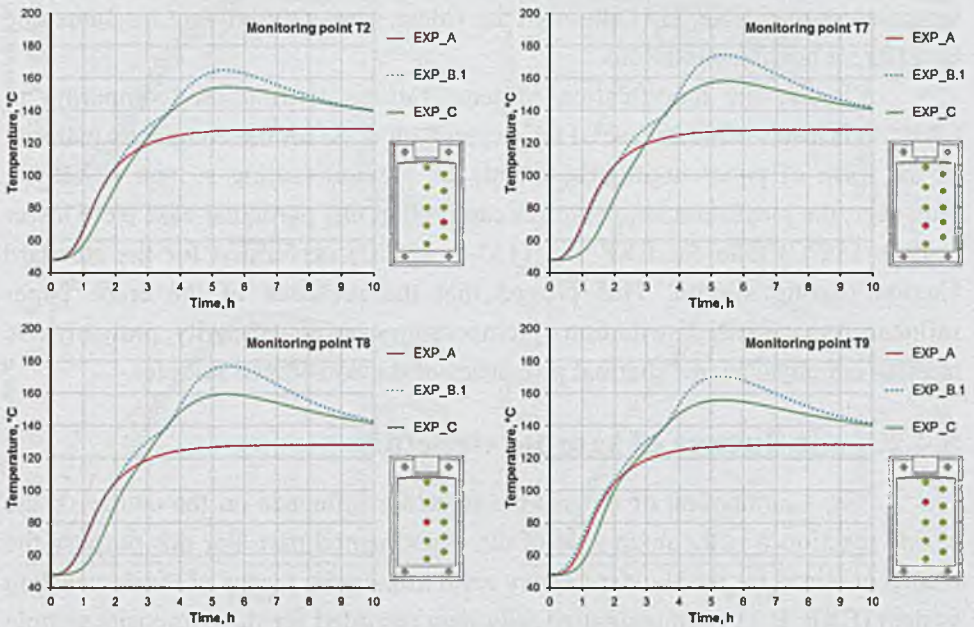


Figure 5.8: The influence of the sample structure on temperatures measured at selected monitoring points.

In case of the paper-epoxy resin composite it can be concluded that the curing phenomenon was initiated more or less at the same time as for the casting system (after 2 hours). However, this time the rate of temperature increase was stable during the whole temperature rise period (the clear change in temperature growth rate observed in EXP_B.1 after 3.5 hours was not detected). The maximum temperature levels were recorded in the composite sample also after about 5.5 hours, but the values of the maximum temperatures were lower than in the experiment conducted for the casting system. It is possible that the introduction of the crepe paper coil modified the effective physical and thermal properties of the system (refer to Table 2.1 and Table 2.2). This could result in different heat conduction/convection mechanism (due to changed thermal

conductivity value) and in different amount of heat that the system was able to accumulate (due to changes in the density and specific heat values). Another explanation is that the porous structure of the crepe paper was not perfectly filled with the casting mixture and, consequently, some volume of pores was still filled with air after the impregnation process, what could limit the heat transfer within the composite structure significantly due very low thermal conductivity of air (around 0.025 W/mK at 20°C).

The differences mentioned above raised the question whether the kinetics of curing reaction determined for the standard casting system is also valid for the composite structure in the form of crepe paper impregnated with the epoxy resin mixture. The answer is not so obvious, since the mentioned discrepancy stated in the temperature fields could be caused by different curing kinetics, by different material properties or, what is the most probable, by both these aspects. This issue is among others the subject of the study described in chapter 6.

5.4.3. Influence of heating conditions

Additional value coming from the experimental study was the information about the influence of the heating conditions on the course of the curing reaction. According to Equation (3.4) it should be expected that the curing rate depends on temperature and degree of curing. The same sample in the form of standard epoxy resin mixture (Hexion casting system) was investigated in three different heating conditions in order to check this relationship. In each experiment the heating rate and the target heating temperature value was changed (refer to Figure 5.5).

The results of these experimental trials (presented in Figure 5.9) confirmed that the heating conditions influence the course of the curing reaction. It is clearly visible that the increased heating rate results in faster initiation of the curing reaction and in faster occurrence of the temperature peak. The value of the maximum temperature is also determined by the heating procedure. The first observation is that higher heating temperature and heating rate produced higher temperature peak at almost all monitoring points (except point T7). It is also interesting that the difference in the temperature peak value between two selected experimental runs is not the same as the difference in the defined heating temperature value. Moreover, the change of the maximum temperature is not the same comparing the results from the monitoring points even for the same experiment. The probable reason for such situation is that the capability of the investigated sample to transfer the released heat outside the mould is different depending on the location in the cavity. Another possible explanation is the already mentioned relationship between the curing rate and the values of degree

of curing, which definitely changed in each experiment. Finally, one should keep in mind that according to Equation (3.13) the heating rate affects the amount of heat that is generated during the curing reaction.

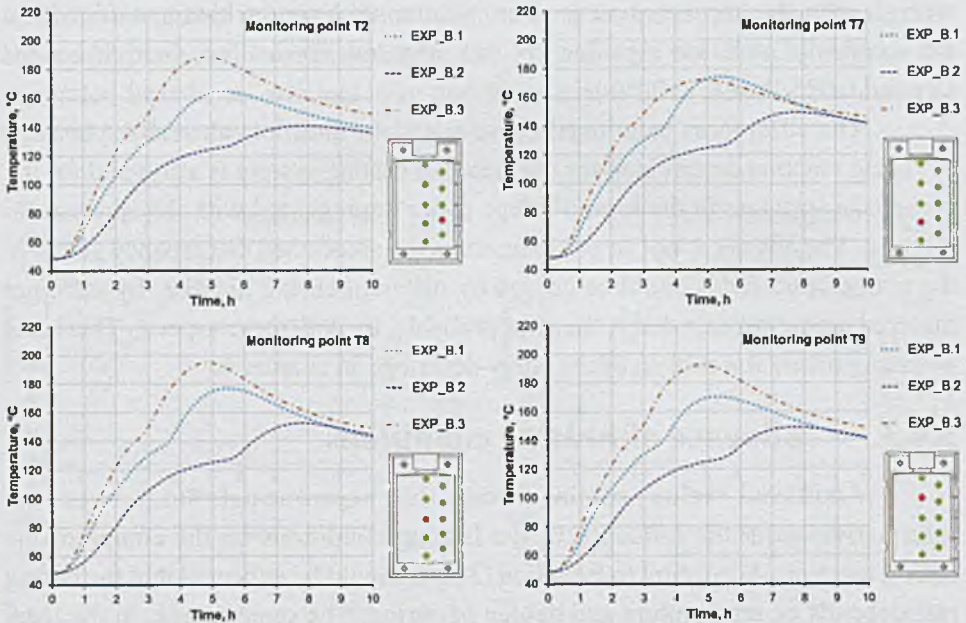


Figure 5.9: The influence of the heating conditions on temperatures measured at selected monitoring points.

5.4.4. Influence of moisture in paper

Other interesting observations were made based on the comparison of results obtained in two experimental runs performed for the composite sample. In the first test (EXP_C) the paper coil was dried for several hours in the oven prior to the curing experiment in order to remove the water from the paper pores. In the other experimental run (EXP_D) the paper coil was not submitted to any pre-treatment, what means that some amount of moisture resulting from the air humidity remained inside the paper during the curing experiment. Temperatures measured in these two trials are illustrated in Figure 5.10. Comparing these two experiments it was confirmed that the water presence in the paper coil influences the curing process significantly. The curing reaction proceeded much faster for the moist paper coil and the value of temperature peak was much higher. These differences in the curing course can be probably connected with the heat released during water evaporation, since the disagreement in the measured temperatures

begins around the temperature level of 100°C, which is the water boiling temperature in the atmospheric pressure (101325 Pa).

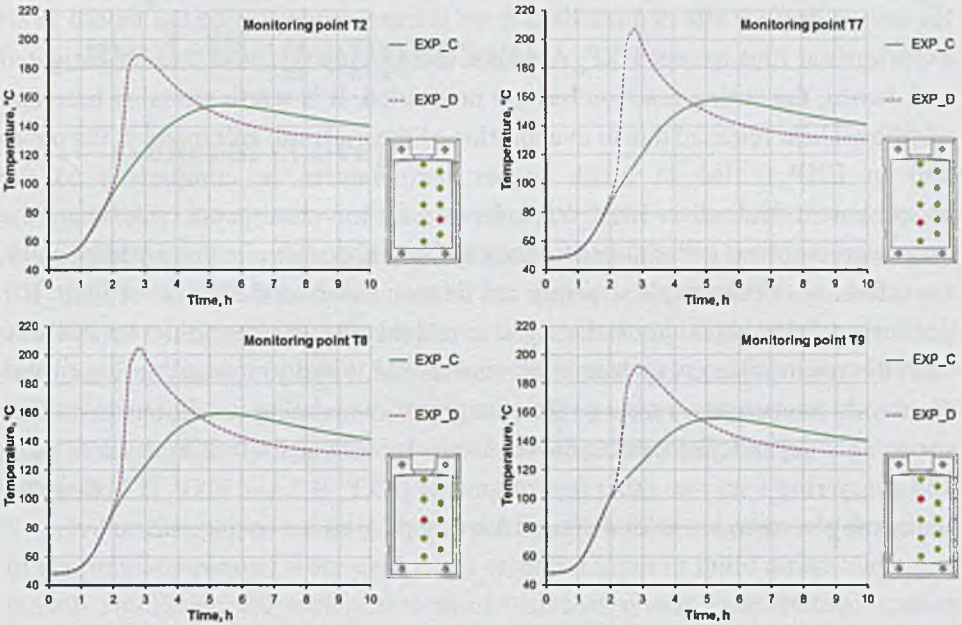


Figure 5.10: The influence of the moisture in the paper coil on temperatures measured at selected monitoring points.

5.4.5. Mould temperature

The last issue investigated based on the results of the curing experiments was the mould temperature. 21 thermocouples assembled in different locations inside the mould walls allowed checking two things. Firstly, it was possible to verify if the mould temperature was uniform in the whole mould volume as expected due to relatively high thermal conductivity of the mould material (aluminium PA6). The second issue observed was the influence of the heat generated during the curing of different samples and in different heating conditions on the mould temperature.

The obtained results revealed the maximum difference in temperature considering all thermal sensors inside the mould walls in the range of 1.6 ÷ 3.4°C depending on the experimental run. This means that the mould temperature was close to uniformity in all measurements and, hence, the values averaged for each mould wall were used to define boundary conditions in the computer simulations of the curing experiments (refer to subchapter 6.3.3).

Meanwhile, the average value calculated based on the recordings taken by all sensors was used to compare the mould temperature for different experimental runs as can be seen in Figure 5.11. Generally, the heat released in the curing process affected readings from thermocouples inside the mould in all experimental runs except EXP_A where the pure epoxy resin was investigated and, hence, the curing reaction has not proceeded. It is worth stressing here that additional heat released due to evaporation of the moisture entrapped in the paper coil in EXP_D led to much higher temperatures in comparison to the measurement denoted as EXP_C, performed for the dried paper coil, where the only source of heat generation was the exothermic curing reaction. Additionally, the influence of the sample structure can be seen based on the results of EXP_B.1 performed for the Hexion casting system and the already mentioned EXP_C run with the resin-paper composite inside the mould. Finally, it was confirmed that the mould temperature reacts to the changes of the heating conditions inside the oven. This dependence can be observed when treating EXP_B.1 as a reference and comparing with two other measurements (EXP_B.2 and EXP_B.3) done for the casting system, but with different heating profiles set in the electric oven.

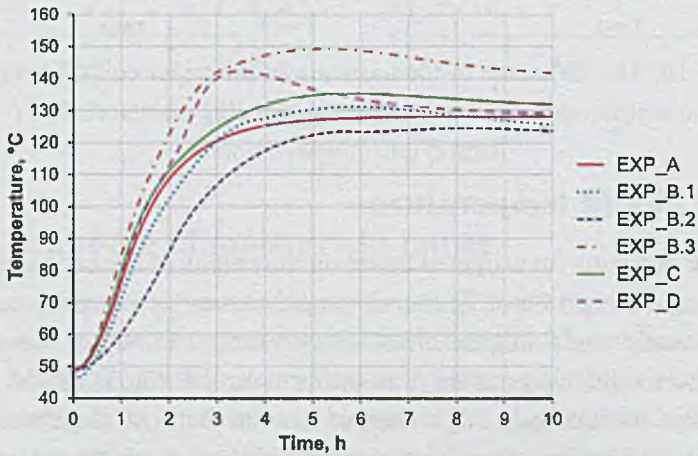


Figure 5.11: Averaged mould temperature observed during all experimental runs.

6. Experimental validation of the curing modelling approach

6.1. General concept

One of the objectives defined within the framework of this thesis was to develop inverse methodology allowing one to calculate the curing kinetics data for composite structures that could be applied successfully in computer simulations of the real industrial systems like for example high-voltage electrical bushings. In this connection, it was extremely important to perform experimental validation of the worked out curing modelling approach and to prove the effectiveness of the proposed tool in solving experimentally-based engineering problems.

For this purpose data gathered during the curing experiments described in the previous chapter were used as an essential input to build direct numerical models simulating the curing process of different systems under consideration (standard casting mixture and composite system). In addition to that the experimental results constituted the point of reference during the inverse calculations of the curing kinetics. The applied validation procedure can be divided into the following stages:

- stage 1 – numerical modelling of heat (neglecting curing effects) and mass transfer for the pure epoxy resin,
- stage 2 – numerical modelling of heat (neglecting curing effects) and mass transfer for the standard casting system by extending the model built up at stage 1,
- stage 3 – numerical modelling of heat (neglecting curing effects) and mass transfer for the composite system by extending the model built up at stage 2,
- stage 4 – application of the model prepared at stage 2 in inverse calculations of the curing kinetics data for the standard casting system,
- stage 5 – application of the curing kinetics data optimized at stage 4 in the curing simulation (including curing effects) of the standard casting system, based on the numerical model developed at stage 2, and of the composite system, based on the numerical model developed at stage 3,
- stage 6 – application of the model prepared at stage 3 in inverse calculations of the curing kinetics data for the composite system,

- stage 7 – application of the curing kinetics data optimized at stage 6 in the curing simulation (including curing effects) of the composite system, based on the numerical model developed at stage 3.

6.2. Mathematical modelling of the composite curing

Detailed description of the mathematical modelling of curing process for the standard casting system has been discussed in subchapter 4.2 of this thesis. However, consideration of the composite structure in the form of a porous crepe paper impregnated with the casting system required modifications in the mathematical model. In the proposed solution the composite structure is reflected by the porous media model available in ANSYS Fluent [92]. It is depicted in Figure 6.1 that the consideration of the porous media model affects the remaining phenomena modelled during the curing simulations. One should notice that it was assumed that the porous structure of the crepe paper is fully filled with the casting mixture and no air gaps are present in the considered system material.

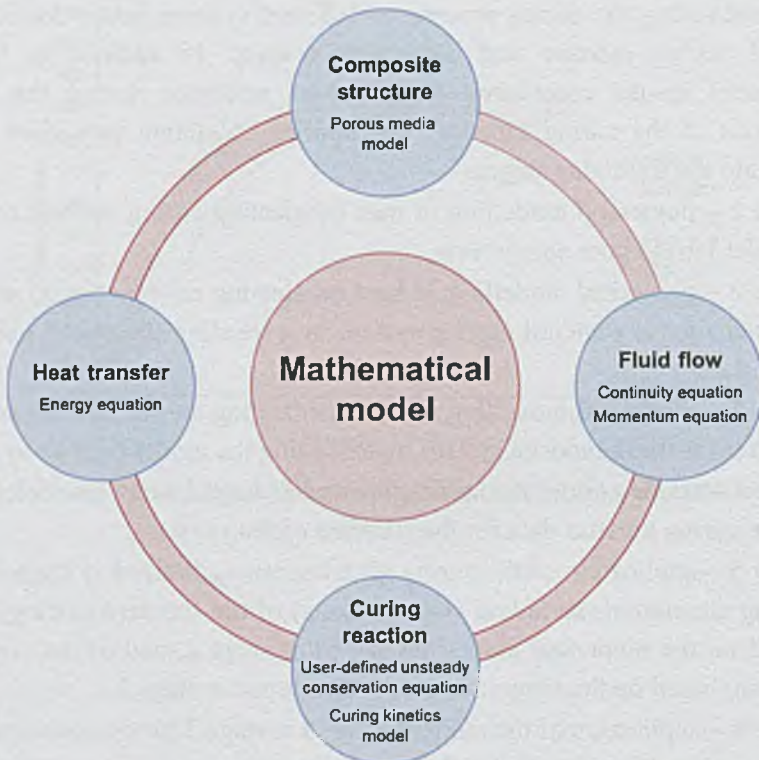


Figure 6.1: Mathematical model applied in the computer simulations of the composite curing.

The flow of fluid through porous medium is modelled by the introduction of the momentum source term expressed by vector \mathbf{S} into the standard fluid flow equation:

$$\frac{\partial(\rho_f \mathbf{w})}{\partial t} + \nabla \cdot (\rho_f \mathbf{w} \mathbf{w}) = \mu \cdot \nabla^2 \mathbf{w} - \nabla p + \rho_f \mathbf{g} + \mathbf{S} \quad (6.1)$$

where ρ_f is density of the fluid flowing through the porous medium.

This momentum source term describes the pressure drop due to flow through porous material [92] and is calculated according to the following relationship:

$$\mathbf{S} = -D\mu\mathbf{w} - \frac{\rho_f |\mathbf{w}| \mathbf{C}}{2} \mathbf{w} \quad (6.2)$$

where the first term on the right-hand side of the equation above is so-called viscous loss term and the second one is known as inertial loss term, D stands for the viscous resistance tensor and C denotes the inertial resistance tensor.

The same approach based on the Ergun equation as presented in [51] and [92] was applied to describe the flow resistance through the analysed porous structure of the crepe paper. However, this formula is dedicated to the calculation of the pressure gradient in densely packed beds and was adapted to the considered system due to the lack of more suitable formula. According to the Ergun equation the pressure drop due to flow through densely packed bed is calculated as:

$$\frac{\partial p}{\partial l_j} = -\frac{150\mu(1-\gamma)^2}{d_p^2\gamma^3} w_j - \frac{1.75\rho_f(1-\gamma)|\mathbf{w}|}{d_p\gamma^3} w_j \quad (6.3)$$

where l_j refers to the length of the packed bed in a given direction j , d_p denotes the diameter of particles constituting the packed bed, w_j is the component of the velocity vector in a given direction j and γ stands for porosity that is defined as:

$$\gamma = \frac{V_p}{V_p + V_s} \quad (6.4)$$

where V_p is the volume occupied by pores and V_s is the volume of solid material (crepe paper in this case).

For laminar flows as in the considered case the inertial resistance term in Equation (6.3) may be dropped and the Ergun equation takes the form of the Blake-Kozeny equation [92]:

$$\frac{\partial p}{\partial l_j} = - \frac{150\mu(1-\gamma)^2}{d_{p,j}^2\gamma^3} w_j \quad (6.5)$$

The diameter of particles constituting the packed bed d_p is replaced in the investigated problem with the characteristic diameter of pores inside the crepe paper $d_{p,j}$ in a given direction j . Finally, comparing Equations (6.2) and (6.5) the viscous resistance coefficient D_j in a given direction j can be expressed as:

$$D_j = \frac{150(1-\gamma)^2}{d_{p,j}^2\gamma^3} \quad (6.6)$$

Heat transfer within the porous medium is modelled assuming thermal equilibrium between the porous medium and the flowing fluid. In such an approach the heat transfer is described by using standard form of energy equation, but with modifications made in the conduction flux and transient terms (refer to Equation (4.3)). In case of the conduction flux term an effective value of thermal conductivity λ_e is used, while the transient term includes thermal inertia of solid region on fluid medium as can be seen in the formula below [92]:

$$\frac{\partial[\gamma\rho_f E_f + (1-\gamma)\rho_s E_s]}{\partial t} + \nabla \cdot [\mathbf{w}(\rho_f E_f + p)] = \nabla \cdot (\lambda_e \nabla T) + \dot{q}_{v,r} \quad (6.7)$$

where E_f is the total energy of fluid, E_s denotes the total energy of solid (porous medium), ρ_s stands for the solid density and the value of effective thermal conductivity λ_e is calculated as follows [92]:

$$\lambda_e = \gamma\lambda_f + (1-\gamma)\lambda_s \quad (6.8)$$

where λ_f is the thermal conductivity of fluid and λ_s is the thermal conductivity of solid.

Porous media modelling has also an impact on the time-derivative term in continuity and scalar transport equations as presented below [92]:

$$\frac{\partial \gamma \rho_f}{\partial t} + \nabla \cdot (\rho_f \mathbf{w}) = 0 \quad (6.9)$$

$$\frac{\partial (\gamma \rho_f \alpha)}{\partial t} + \nabla \cdot (\rho_f \mathbf{w} \alpha) = \rho_f \dot{\alpha} \quad (6.10)$$

6.3. Numerical modelling of curing experiments

6.3.1. Geometrical models

Different samples were tested in the experimental part of this thesis, namely: pure epoxy resin (without hardener), two-component casting system composed of epoxy resin and hardener and, finally, the composite structure in the form of crepe paper impregnated with the two-component casting system. For this reason two different geometrical models presented in Figure 6.2 had to be applied in computer simulations of the experiments. In case of the first geometry the aluminium mould (described in details in subchapter 5.2) was filled with homogenous medium, either pure epoxy resin or two-component casting system. In the second geometrical model the mould cavity was divided into two separate regions, i.e. the prevailing one occupied by the paper coil impregnated with the casting system and the other one located near the side mould wall and in the top region of the mould cavity that was filled only with the casting system. The thin (5 mm thick) layer of the casting system between the paper coil and the side mould wall appeared because of the mismatch in the paper coil and the mould cavity dimensions (uneven diameters), what can be observed in Figure 5.6. In turn, an excess of the casting system in the inlet region of the mould resulted from the target level of the mould filling, the same for each experimental run.

Additionally, it can be noticed that several simplifications were introduced into the geometrical models comparing to the real systems described in subchapters 5.2 and 5.3. First of all, thermocouples and their wiring system were not included in the model. Besides that many geometrical features of the mould were neglected (chamfers, holes for thermocouples assembling, pins and holes for the connection and positioning of the two parts of the mould, grooves for band clips for the mould clamping). Finally, in case of the composite sample the irregularity of the top and the bottom surfaces of the paper coil was omitted and ideally flat surfaces were modelled instead. It was assumed that all details mentioned above would not affect significantly the heat transfer in the considered

system. On the other side, such an approach allowed simplifying the geometry to 2D axisymmetric case, what made the geometry discretization easier and resulted in smaller number of the mesh elements shortening consequently the computational time.

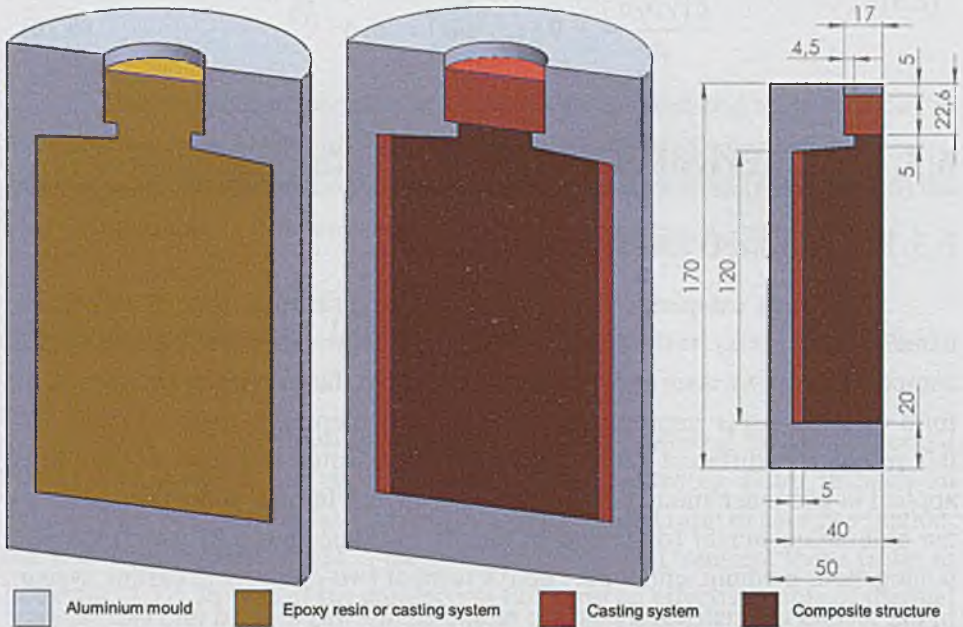


Figure 6.2: Geometrical models of experimental samples (left – pure epoxy resin or casting system, middle – composite sample, right – main dimensions).

6.3.2. Computational meshes and numerical time-steps

Similar methodology as already described in subchapter 4.3.2 was applied during the discretization of both considered geometrical models. Namely, Quad Elements Scheme with Pave Type Scheme was used to mesh the region occupied by the epoxy resin/casting system, whereas Quad Elements Scheme with Submap Type Scheme was utilized in case of the aluminium mould region. It is worth stressing that different cell sizes, i.e. 0.75 mm, 1.5 mm and 3 mm, were applied in calculations to prove that the numerical solution is not influenced by the mesh resolution (mesh-independent solution). In all cases unstructured numerical mesh with varying number of the mesh elements (depending on the mentioned default cell size) was generated as depicted in Figure 6.3. The number of elements obtained for each of the meshes is presented in Table 6.1, while the mesh quality judged based on the value of the Equivalent Size Skewness parameter (calculated according to Equation (4.6)) is gathered in Table 6.2.

Generally, the mesh quality was relatively good for each of three cases, although the quality worsened together with higher number of the mesh elements. The results of the mentioned mesh independence study and of the analysis of the influence of the time-step size are discussed in subchapter 6.4.2.

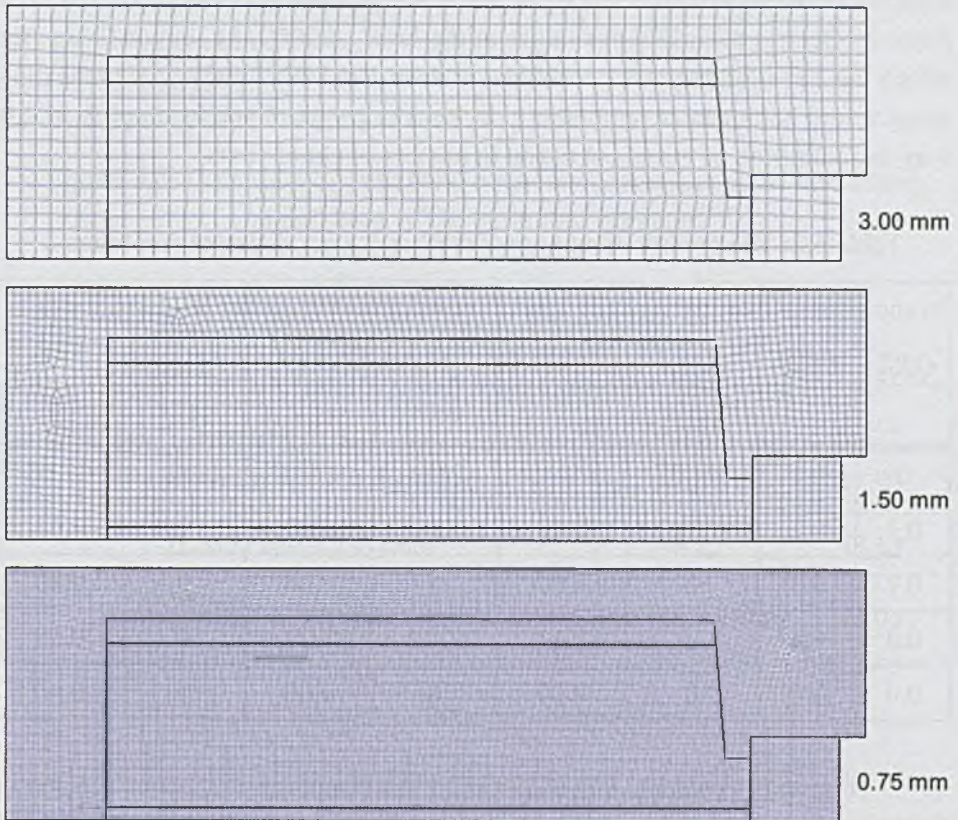


Figure 6.3: Different mesh resolutions used in numerical calculations.

Table 6.1: The number of mesh elements obtained for different cell sizes.

Cell size, mm	Number of mesh elements, -		
	Total	Mould	Cavity
0.75	15103	5653	9450
1.5	3735	1350	2385
3	957	353	604

6.3.3. Initial and boundary conditions

Measurement data recorded during the curing experiments was used to define both the initial and boundary conditions. As described in subchapter 5.3, in each experimental run the mould was firstly filled with the investigated sample material to the level shown in Figure 6.2. Then each sample was preheated for 5 hours in electric oven in temperature at the level of 50°C, i.e. in conditions for which the cross-linking process could not be initiated. The goal of the preheating stage was to homogenize temperature in the whole system and to simplify in this way the definition of initial condition in numerical simulations.

Table 6.2: The quality of numerical meshes having different resolutions.

Q_{EVS}^{\min}	Q_{EVS}^{\max}	0.75 mm cell size		1.5 mm cell size		3 mm cell size	
		# of cells	%	# of cells	%	# of cells	%
0	0.1	15007	99.36	3481	93.20	948	99.06
0.1	0.2	73	0.48	234	6.27	9	0.94
0.2	0.3	7	0.05	9	0.24	0	0.00
0.3	0.4	16	0.11	11	0.29	0	0.00
0.4	1.0	0	0.00	0	0.00	0	0.00

Figure 6.4 presents initial condition and boundary conditions defined in the numerical simulations of the curing experiments as well as the location of temperature monitors corresponding to thermal sensors used in the experiments (see Figure 5.4). In case of initial condition 0% degree of curing was prescribed in the whole volume occupied by the curing system. The actual values of temperatures treated as initial ones were slightly different for each experimental trial and are presented in Table 6.3. It can be noticed that separate initial fields of temperature were defined in the mould and cavity regions. Average value from sensors located either in the mould walls or inside the mould cavity was used for this purpose. In total three different boundary conditions of temperature kind were defined on the external edges of 2D model accordingly to temperatures measured by sensors located inside the mould walls (see Figure 5.3). It is worth mentioning that the heating profiles were prescribed individually for each investigated sample as shown in Figure 6.5.

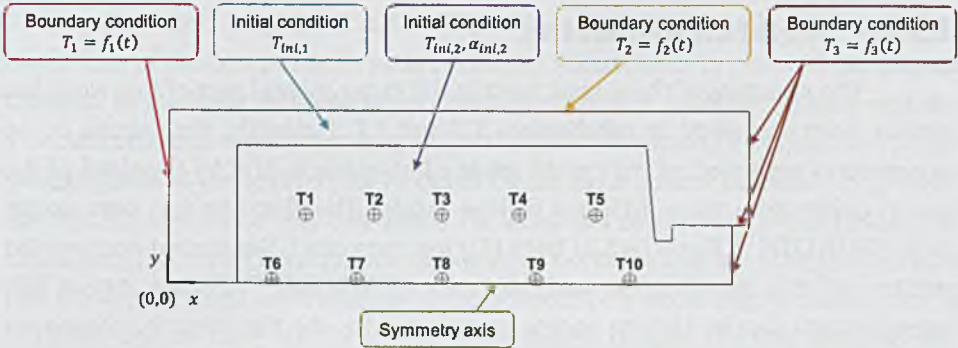


Figure 6.4: Definition of initial and boundary conditions in the numerical simulations of the curing experiments.

Table 6.3: Initial values of temperature defined in the numerical simulations of the curing experiments.

Sample	$T_{ini,1}$	$T_{ini,2}$
Epoxy resin without hardener	48.07	47.99
Hexion casting system	48.25	48.13
Dried paper coil impregnated with the Hexion casting system	48.36	48.06

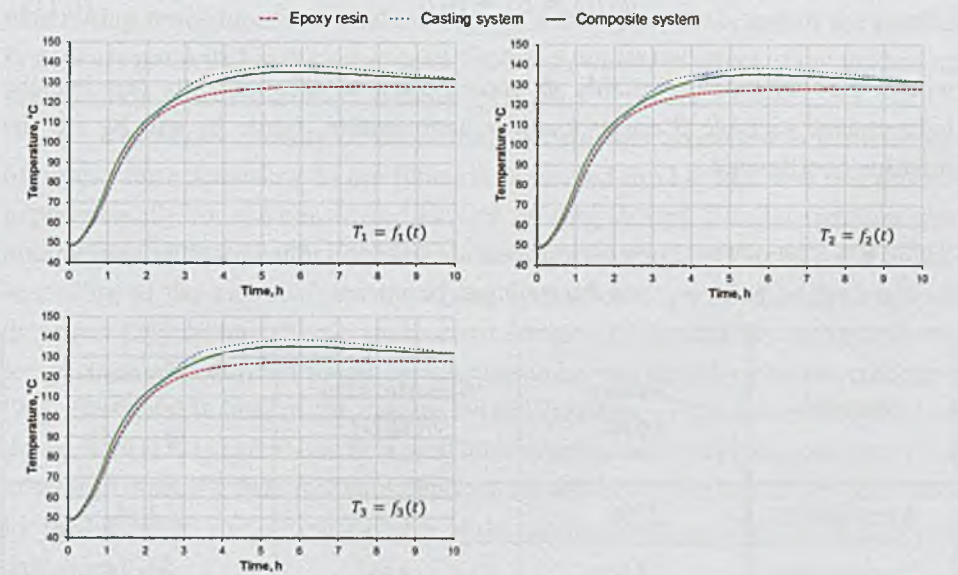


Figure 6.5: Temperature profiles defined as boundary conditions in the numerical simulations of the curing experiments.

6.3.4. Material properties

The structure of the system used in the experimental part of this work has already been explained in subchapters 5.2 and 5.3. Basically, the sample in the experiments consisted of the mould made of aluminium of PA6 type and of the mould cavity with three different fillings inside. The first one was pure epoxy resin (EPIKOTE™ Resin 04820 from Hexion company), the second one was the mixture of this epoxy resin and hardener (EPIKURE™ Curing Agent 860 manufactured also by Hexion company) and, finally, the third was the composite structure in the form of crepe paper (delivered by ARIMER Oy company) impregnated with the Hexion mixture consisted of the epoxy resin and the hardener mentioned earlier.

The properties of solids defined in the curing simulations performed within the experimental procedure are gathered in Table 6.4. It was assumed in case of aluminium and crepe paper that temperature dependence of density, specific heat and thermal conductivity is negligible and, hence, constant values were defined based on data provided by one of the aluminium suppliers [54] and on the cellulose properties found in literature [51]. The value of specific heat, thermal conductivity and viscosity of fluids was defined again according to piecewise-linear function described by Equation (4.7) [92], whereas the fluids density was described by using the linear function expressed in its general form by the equation below [92]:

$$\phi(\beta) = B_1 + B_2\beta \quad (6.11)$$

where the dependent variable ϕ corresponds in this case to density, the independent variable β corresponds to temperature, while B_1 and B_2 are the function coefficients.

Table 6.4: The material properties of solids defined in the computer simulations of the curing experiments.

Material	Density kg/m ³	Specific heat J/(kgK)	Thermal conductivity W/(mK)
Aluminium	2790	873	134
Crepe paper	1550	1340	0.335

As already explained in subchapter 6.2, the applied method of numerical modelling of the composite structure requires additional properties of the porous material in the form of crepe paper. Among them the material porosity and the viscous resistance coefficient have to be defined. The porosity of the crepe paper was assumed at the level of 0.816 based on the information found in [52], while the viscous resistance was calculated for axial and radial direction according to Equation (6.6). The characteristic diameter of pores was assumed to be 0.42 mm and 0.1 mm in axial and radial direction respectively according to data found in [51] that was worked out for similar crepe paper. In case of axial direction this diameter corresponds to the measured distance between the paper layers in the paper coil, while the radial dimension is just an assumption due to the lack of better data. The final value of the viscous resistance coefficient defined in the computer simulations for the composite system was equal to $5.29856E+07$ $1/m^2$ in axial direction and $9.34666E+08$ $1/m^2$ in radial direction.

In case of fluids the constant values of material properties were initially assumed based on the casting system datasheet [53]. However, not all needed data were found there and, moreover, most of the properties were not temperature dependent. Meanwhile, the curing experiments revealed big variations of temperature during the considered process and it was expected that the material properties of the epoxy resin or of the casting system change with temperature. It was also confirmed by the first computer simulations. Consequently, the constant values were replaced with the results of measurements, with the combination of measurements and datasheet values or with the values obtained as an effect of data tuning procedure. The final properties of the epoxy resin and of the casting system are presented in the mentioned Table 6.5, while the effect of the properties optimization is also discussed in subchapter 6.4.1.

Eventually, density of the casting system was expressed in dependence of temperature according to the function presented in [11] that was determined experimentally for the considered Hexion casting system. Similar function was also applied to describe the epoxy resin density, but B_1 coefficient was modified according to the value of density of the epoxy resin specified in the material datasheet [53]. In turn, the dependence of the specific heat of the epoxy resin on temperature was defined based on the measurements done by Hexion company [97]. The specific heat of the casting system (mixture of the epoxy resin and of the hardener) was calculated as a weighted average value utilizing data from the mentioned specific heat measurements (done separately for the epoxy resin and for the hardener) and information about the mixing ratio specified in the material datasheet [53]:

$$\phi_{mix}(T) = \frac{m_{res} \cdot \phi_{res}(T) + m_{har} \cdot \phi_{har}(T)}{m_{res} + m_{har}} \quad (6.12)$$

where ϕ_{mix} is the dependent variable corresponding in this case to the property of the mixture of epoxy resin and hardener, m_{res} and m_{har} is the mass of epoxy resin and hardener respectively, while ϕ_{res} and ϕ_{har} is the dependent variable expressing in this case the property of epoxy resin and hardener respectively.

Again, piecewise-linear function explained already before (refer to Equation (4.7)) was used to define the influence of temperature on the specific heat of the epoxy resin and of the casting system. Thermal conductivity of both materials was tuned iteratively in computer simulations, although not exceeding the range given in the material datasheet [53]. One can notice that the same values of thermal conductivity were obtained in this tuning procedure both for the epoxy resin and for the casting system. Finally, the epoxy resin viscosity was read directly from the graph available in the material datasheet [53], while the casting system viscosity was obtained as a weighted average value, similarly to the specific heat, according to Equation (6.12). It should be emphasized that the influence of temperature on the value of thermal conductivity and viscosity of both materials was expressed by using the mentioned piecewise-linear function (see to Equation (4.7)).

For the modelling of the curing kinetics of the Hexion casting system a two-stage reaction model expressed by Equation (3.8) was chosen. This was dictated by the specific course of curing process of the considered system as already explained in subchapter 2.3. The initial values of the model parameters were defined according to the results of calorimetric measurements done for the same casting system [11]. The only exception was the total heat of reaction H_{Σ} , which was expressed in the cited publication [11] as a function of the heating rate v_h , whereas in the presented study constant value was assumed. The set of curing model parameters given in Table 6.6 was treated as a starting point in the inverse calculations performed within the framework of this thesis (refer to subchapter 6.5). However, it should be stressed that in one of the performed inverse analyses the total heat of reaction was also defined in dependence on the heating rate v_h . In this case the coefficients of the function expressing the relationship between the total heat of reaction H_{Σ} and the heating rate v_h were subjected to optimization instead of the value of the total heat of reaction H_{Σ} (more details can be found in subchapter 6.5).

Table 6.5: The material properties of fluids defined in the computer simulations of the curing experiments.

Material	Density kg/m ³	Specific heat J/(kgK)		Thermal conductivity W/(mK)		Dynamic viscosity kg/(ms)	
		T, °C	Value	T, °C	Value	T, °C	Value
Pure epoxy resin	$B_1 = 1170.0$ $B_2 = -0.74945$	20 ≤	1810	60 ≤	0.175	≤ 25	0.4500
		30	1830	≥ 100	0.15	30	0.2500
		40	1860			40	0.1250
		60	1880			50	0.0750
		70	1910			60	0.0500
		80	1940			70	0.0300
		90	1960			80	0.0200
		100	1960			90	0.0150
		110	1960			100	0.0100
		120	1980			≥ 110	0.0070
		130	2010				
		140	2030				
		≥ 145	2040				
Source	[11] and [53]	[97]		[53] + data fitting		[53]	
Casting system (epoxy resin + hardener)	$B_1 = 1397.2$ $B_2 = -0.74945$	20 ≤	1736	60 ≤	0.175	≤ 25	0.2467
		30	1761	≥ 100	0.15	30	0.1370
		40	1786			40	0.0685
		60	1811			50	0.0411
		70	1836			60	0.0274
		80	1862			70	0.0164
		90	1882			80	0.0110
		100	1882			90	0.0082
		110	1882			100	0.0055
		120	1902			≥ 110	0.0038
		130	1927				
		140	1952				
		≥ 145	1971				
Source	[11]	[97]*		[53] + data fitting		[53]*	

* weighted average value

Table 6.6: Initial curing kinetics model used as a starting point in inverse calculations.

Parameter	Unit	Value
A_1	1/s	1.6484E+03
A_2	1/s	1.1108E-01
E_1	K	5.4522E+04
E_2	K	8.1601E+03
m_1	-	7.4816E-01
m_2	-	9.9224E-01
n_1	-	1.1895E+00
n_2	-	1.9707E+01
k_{02}	-	3.7248E-04
H_{Σ}	J/kg	2.7547E+05

6.4. Numerical simulations of pure heat and mass transfer

The first step made in the approach to the numerical modelling of the curing process were the simulations including only heat and mass transfer calculations, i.e. not taking into account the curing reaction. The goal of these simulations was to tune the numerical model in order to describe accurately the mentioned processes for each of the investigated samples, namely for epoxy resin, casting system and composite system. The numerical results were compared with the experimental data, but only the first 1 hour and 45 minutes of the process was considered at this stage, since the curing related effects were not observed in this period of time. This is confirmed by the results of the curing experiments included in subchapter 5.4. For example, Figure 5.8 shows clearly that the course of the measured temperature curves for the epoxy resin and for the casting system is very similar unless the samples temperature reaches around 100°C (more or less after the mentioned 1 hour and 45 minutes of the experimental time). It is worth stressing that it was important to neglect the curing modelling in this tuning procedure due to lack of reliable curing kinetics data available at this stage of calculations.

6.4.1. Fitting of numerical model

The first simulations of pure heat and mass transfer phenomena showed big discrepancies between the numerical and the experimental data. Consequently, dozens of simulations were performed in order to tune the numerical model and to get good level of agreement with the measurements. The fitting process concerned mainly the material properties as well as initial and boundary conditions. However, it should be stressed that the introduction of temperature dependent material properties (refer to subchapter 6.3.4) contributed the most. The improvement in the correlation of the numerical results with the experimental data due to the model tuning can be seen in Figure 6.6 on the example of few monitoring points, although similar situation was observed for the remaining points located in the mould cavity.

6.4.2. Influence of mesh resolution and time-step size

As already mentioned in subchapter 6.3.2, the influence of the numerical mesh resolution and of the time-step size on the simulation results was verified in computations. Three different mesh densities and three sizes of the numerical time-step were defined in simulations. This allowed observing how the temperature field is affected by these two factors. It was concluded based on the obtained results for all monitoring points that the mesh resolution and the time-step size influences the numerical results in negligibly small degree. For this reason only exemplary results reflecting all performed analyses are presented in Figure 6.7. The influence of the mesh cell size is shown on the example of temperatures recorded at point T3 during the simulations for the casting system, whereas the importance of the time-step size is illustrated based on temperatures captured at point T7 during the simulations for the composite system.

Eventually, it was decided to apply in the next step of computations, i.e. inverse analyses, the mesh element size equal to 1.5 mm. The medium mesh resolution was chosen at the cost of potential profits in computational time (refer to Table 6.7), although coarser mesh gave almost the same results. However, it was assumed that the mesh with 3 mm cell size is too coarse and it could give inaccurate results in case of bigger gradients of temperature and also the resulting quantities like velocity that were expected in the simulations including the curing phenomenon. In case of numerical time-step size two values were used in calculations. Namely, 1 s time-step applied initially in the few first inverse analyses was increased to 2 s in order to accelerate the remaining calculations.

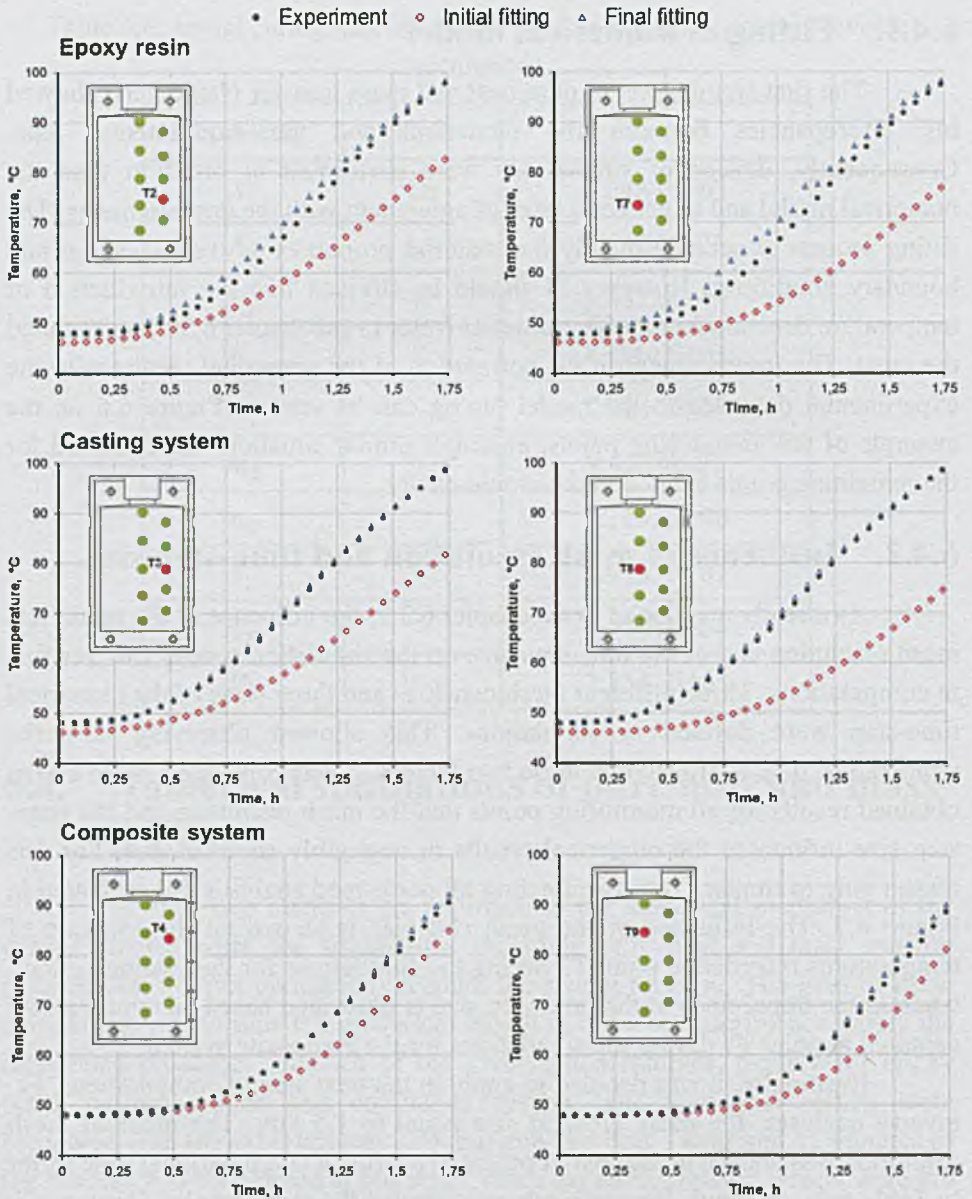


Figure 6.6: Initial and final agreement between the simulations and measurements for each of the investigated samples.

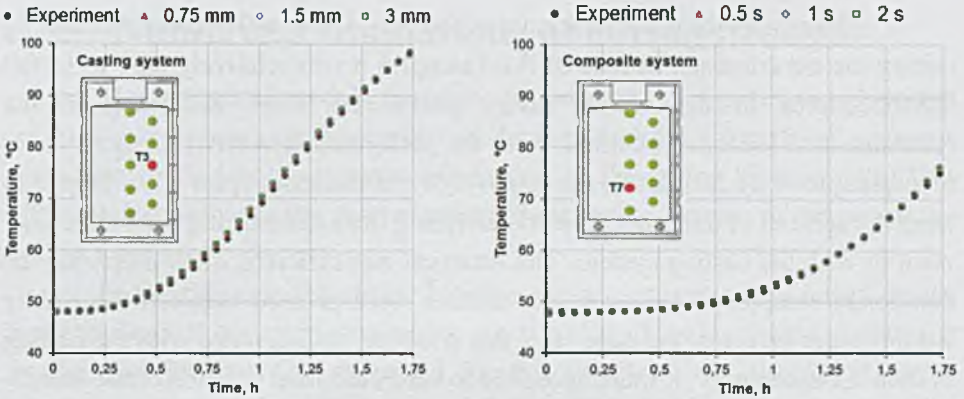


Figure 6.7: The influence of the mesh element size (left) and of the time-step size (right) on temperature field obtained in the simulations.

Table 6.7: Computational time depending on the mesh cell size and on the time-step size.

Mesh cell size, mm	Time-step size, s	Computational time, min		
		Epoxy resin	Casting system	Composite system
1.5	0.5	155	174	183
1.5	2	40	49	45
1.5	1	83	91	90
0.75	1	172	183	215
3	1	65	72	63

6.4.3. Influence of the location of monitoring points

In case of the epoxy resin and the casting system modelling the agreement between the simulation results after the model tuning and the experimental data was on a similar good level at all monitoring points in the mould cavity. The situation was different for the results obtained for the composite system. The correlation between the numerical and the measurement data was worse at some monitoring points (more precisely at T1, T5, T6 and T10 locations) than at the remaining ones. One of the reasons could be different location of monitoring points in the simulations and in the experiments.

The reason for this suspicion was the way of thermal sensors assembling during the experiments. In case of fluid samples it was relatively easy to install thermocouples in the mould cavity positioning them according to the recommended locations obtained from the performed sensitivity analysis (refer to subchapter 4.6). Moreover, the relatively rigid thermocouples wires helped to keep the sensors at unchanged positions during the mould filling with the epoxy resin or with the casting system. The situation was different when preparing the composite sample. In this case the sensors were pressed between the tightly wound paper layers of the paper coil that was later impregnated with the casting system. Consequently, it was impossible to verify the final position of the sensors and, hence, it could happen, especially in case of the bottom (T1 and T6) and top (T5 and T10) thermocouples, that their final position differed from the desirable one.

Consequently, a kind of sensitivity analysis was performed to check how the relocation of the points influences the simulation results. This study confirmed that even few millimetres shifts could make a significant difference in temperature readings due to big temperature gradients at these positions. Figure 6.8 presents the improved agreement between the measured and the computed temperatures at points T5 and T10 after their relocation in the simulation in axial direction (5 mm below their original position). It should be stressed that in spite of better correlation with experimental data, observed for the relocated points, the original positions were kept in the next curing simulations of the composite system, done within the performed inverse analysis.

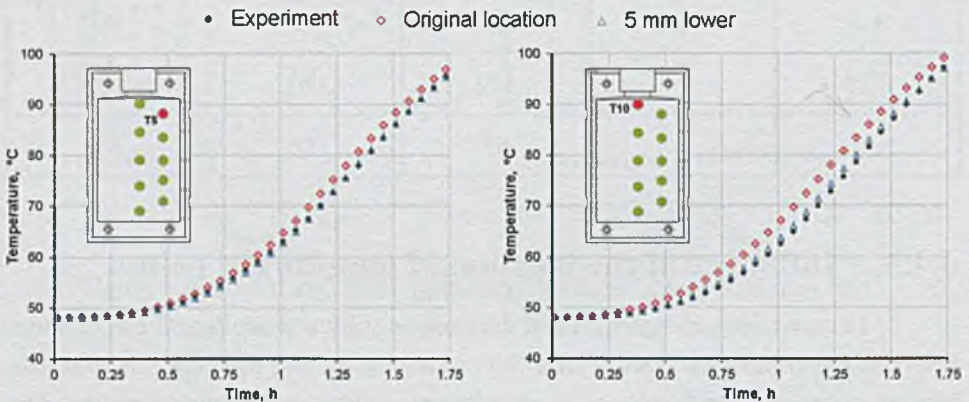


Figure 6.8: The influence of the sensors location on the agreement between the experimental and the simulation results obtained for the composite system.

6.5. Numerical simulations of curing process

The numerical models tuned in the previous step (refer to subchapter 6.4.1) to get an accurate description of the heat and mass transfer phenomena were next applied in the inverse calculations of the curing kinetics data. Two different approaches to the determination of the curing kinetics of the composite system were made.

In the first one the curing kinetics model was optimized based on the numerical model describing the curing process of the Hexion casting system and on the experimental data measured for this sample. Next, the found curing kinetics was directly applied in the model of the curing reaction of the casting system and of the composite system. However, one should remember that the composite sample was built of two materials, i.e. the porous crepe paper and the casting system. This means that the volume of the casting system in the porous composite sample was accordingly lower than in the sample consisted only of the casting system. Hence, two more simulation series were performed to verify how the inclusion of the crepe paper porosity influences the results. In the first series the crepe paper porosity was introduced only in the energy source term to take into account lower amount of energy generated in curing reaction because of smaller volume of the casting system in the composite sample. In the second series the source term of unsteady state conservation equation solved for degree of curing was additionally modified. It is important that the changes were applied in both cases only to regions occupied by the composite material (see Figure 6.2). The original forms of energy equation and unsteady state conservation equation solved for degree of curing are expressed respectively by Equation (6.7) and Equation (6.10), while their modified forms are represented by the following equations:

$$\begin{aligned} \frac{\partial[\gamma\rho_f E_f + (1-\gamma)\rho_s E_s]}{\partial t} + \nabla \cdot [w(\rho_f E_f + p)] \\ = \nabla \cdot (\lambda_e \nabla T) + \gamma \dot{q}_{v,r} \end{aligned} \quad (6.13)$$

$$\frac{\partial(\gamma\rho\alpha)}{\partial t} + \nabla \cdot (\rho w\alpha) = \gamma\rho\dot{\alpha} \quad (6.14)$$

The second approach used to determine the curing kinetics of the composite system was based on data recorded during the curing experiment done for this sample and on inverse analysis utilizing the numerical model of the curing process of the composite system. This means that in this case the material porosity

has already been taken into account in the numerical model applied during the optimization of the curing kinetics data.

6.5.1. Inverse calculations of the kinetics of curing reaction

The optimization procedure performed to calculate the curing kinetics data consisted of several runs of inverse analysis with the IRACKLIS software developed specially for this purpose (refer to subchapter 3.3.2). Only Levenberg-Marquardt algorithm was applied during the inverse calculations and Particle Swarm optimization was excluded from considerations. The reason for this was twofold. First of all, Levenberg-Marquardt method turned out to be more efficient during the trials performed earlier within the study referred to as virtual experiment of curing process (refer to subchapter 4.4). Secondly, the computational time for each inverse analysis was relatively long as it took between few days to few weeks depending on the analysis setup.

Table 6.8 presents the full list of inverse analyses that were conducted to optimize the curing kinetics model. One can notice that most of analyses were done utilizing the numerical model of the casting system curing (IA_1 + IA_3.1 and IA_4 + IA_8). The only inverse analysis executed using the numerical model of the composite system curing was IA_3.2. The remaining settings of this inverse analysis were the same as in case of IA_3.1 and, hence, this pair of calculations allowed checking if the curing kinetics data obtained for the casting system correlates with the curing kinetics data found for the composite system.

It can also be seen in the mentioned Table 6.8 that other settings of inverse analysis were submitted to changes in the consecutive runs of computations. The total number of iterations was set at the level of 10 in each analysis, however in some cases the computations were stopped before reaching the target number of iterations due to the solution divergence problem (caused by the modified values of the investigated curing kinetics parameters). The changes of the time-domain range and the time-step size were dictated by the search of savings in computational time due to the mentioned time-consuming process of inverse calculations.

In case of the heating conditions it was doubtful whether the boundary conditions obtained during the experiment for the pure epoxy resin or the ones measured during the test done for the casting system should be used when modelling the curing of the casting system. On the one side, the heating conditions got for pure epoxy resin (without the exothermic effects) described different process than the one modelled in the curing simulations of the casting system. On the other hand, inclusion of the exothermic effects in the heating

conditions recorded for the casting system meant that some portion of the curing kinetics data has already been described by the boundary conditions and it was not obvious how it should be reflected in the curing kinetics model. Consequently, it was decided to run the first two inverse analyses with the same input data except the heating conditions defined either according to data measured for the pure epoxy resin or for the casting system. Finally, the application of the heating conditions obtained during the experiment for the casting system resulted in better agreement between the measured temperatures and the simulation data obtained for the final, i.e. optimized, curing kinetics parameters. Hence, these boundary conditions were defined in the remaining inverse analyses performed for the casting system.

The other difference between the conducted inverse analyses was the choice of the monitoring points used to compare the experimental and the simulation data. Also the selection of the curing kinetics parameters submitted to optimization was not always the same (either few parameters or all of them were fitted in the inverse analysis). Eventually, the change factor applied to modify the parameters values during the calculation of sensitivity matrix varied within the performed inverse analyses.

The next issue were the initial values of the curing kinetics parameters. It can be seen that the parameters presented in Table 6.6 were set as an input only in the part of inverse analyses (IA_1, IA_2, IA_3.1 and IA_3.2), while in the remaining ones the parameters obtained in the inverse calculations marked as IA_2 were applied. Furthermore, in the last approach (IA_8) the constant value of the total heat of reaction was replaced by the linear function expressing its dependence on the heating rate according to Equation (6.11) [11] (the dependent variable ϕ corresponds in this case to the total heat of reaction H_x , while the independent variable β corresponds to the heating rate v_h). It should be noticed that different initial values of the kinetics parameters resulted in different temperature results obtained at the very beginning of the iterations. This means that the initial value of the objective function was also not the same in all inverse analyses. Both initial and final values of the considered parameters as well as the initial and final values of the objective function obtained in each inverse analysis are presented in Table 6.9.

Table 6.8: Different settings of the performed inverse analyses.

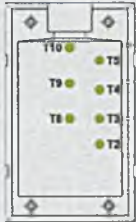
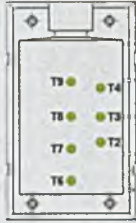
Inverse analysis	Sample	Measured temperatures	Mould heating conditions	Time-domain, s	Time-step size, s	Number of iterations	Monitoring points	Optimized parameters	Parameters change
IA_1	Casting system	EXP_B.1	EXP_A	0+21000	1	10		E_1, E_2, m_2	10%
IA_2	Casting system	EXP_B.1	EXP_B.1	0+21000	1	10		E_1, E_2, m_2	10%
IA_3.1	Casting system	EXP_B.1	EXP_B.1	0+21000	1	8		A_1, A_2, E_1, E_2, m_2	10%
IA_3.2	Composite system	EXP_C	EXP_C	0+21000	1	7		A_1, A_2, E_1, E_2, m_2	10%
IA_4	Casting system	EXP_B.1	EXP_B.1	6000+21000	2	10		All	10%
IA_5	Casting system	EXP_B.1	EXP_B.1	6000+21000	2	10	E_1, E_2	10%	
IA_6	Casting system	EXP_B.1	EXP_B.1	6000+21000	2	10		$A_1, A_2, m_1, m_2, n_1, n_2, k_{02}, (E_1, E_2)$	10% (1%)
IA_7	Casting system	EXP_B.1	EXP_B.1	6000+21000	2	7		All (E_1, E_2)	10% (1%)
IA_8	Casting system	EXP_B.1	EXP_B.1	0+21000	2	4		B_1, B_2	10%

Table 6.9: Results of the performed inverse analyses.

Inverse analysis	Sample	Value	A_1 1/s	A_2 1/s	E_1 K	E_2 K	m_1 -	m_2 -	n_1 -	n_2 -	k_{O_2} -	H_I J/kg	G K ²	IF %
IA_1	Casting system	Initial	1648.4340	0.1111	54522.4700	8160.0500	0.7482	0.9922	1.1895	19.7071	0.0004	275467.2000	162857	21
		Final	1648.4340	0.1111	51501.6449	26924.7322	0.7482	1.3694	1.1895	19.7071	0.0004	275467.2000	129263	
IA_2	Casting system	Initial	1648.4340	0.1111	54522.4700	8160.0500	0.7482	0.9922	1.1895	19.7071	0.0004	275467.2000	162857	15
		Final	1648.4340	0.1111	53094.4697	15035.9368	0.7482	1.5904	1.1895	19.7071	0.0004	275467.2000	137935	
IA_3.1	Casting system	Initial	1648.4340	0.1111	54522.4700	8160.0500	0.7482	0.9922	1.1895	19.7071	0.0004	275467.2000	162857	54
		Final	9287.3800	0.0224	61708.6600	12704.3100	0.7482	0.9922	1.1895	19.7071	0.0004	1353189.0000	74925	
IA_3.2	Composite system	Initial	1648.4340	0.1111	54522.4700	8160.0500	0.7482	0.9922	1.1895	19.7071	0.0004	275467.2000	69070	60
		Final	1464.6240	0.0182	54646.6900	9473.1540	0.7482	0.9922	1.1895	19.7071	0.0004	299219.6000	27825	
IA_4	Casting system	Initial	1648.4340	0.1111	53094.4697	15035.9400	0.7482	1.5904	1.1895	19.7071	0.0004	275467.2200	137935	47
		Final	912.5692	0.1100	54328.3722	14589.8545	0.8921	1.4953	0.8359	7.6956	0.0021	1233611.7310	72834	
IA_5	Casting system	Initial	1648.4340	0.1111	53094.4697	15035.9400	0.7482	1.5904	1.1895	19.7071	0.0004	275467.2000	137935	5
		Final	1648.4340	0.1111	52168.5200	30399.0400	0.7482	1.5904	1.1895	19.7071	0.0004	275467.2000	131042	
IA_6	Casting system	Initial	1648.4340	0.1111	53094.4697	15035.9400	0.7482	1.5904	1.1895	19.7071	0.0004	275467.2000	137935	13
		Final	1753.8585	0.0842	52898.8439	15883.1177	0.7440	1.7072	0.6083	23.8224	0.0001	275467.2000	120685	
IA_7	Casting system	Initial	1648.4340	0.1111	53094.4697	15035.9400	0.7482	1.5904	1.1895	19.7071	0.0004	275467.2000	137935	30
		Final	1745.8625	0.0704	52913.9163	16156.9707	0.7477	1.7514	0.5067	26.0724	0.0001	416828.8680	96577	
IA_8	Casting system	Initial	1648.4340	0.1111	53094.4697	15035.9400	0.7482	1.5904	1.1895	19.7071	0.0004	$B_1 = 23.94$ $B_2 = 390.5$	118754	33
		Final	1648.4340	0.1111	53094.4697	15035.9400	0.7482	1.5904	1.1895	19.7071	0.0004	$B_1 = 22.41$ $B_2 = 1164.3$	80025	

6.5.2. Results of inverse calculations

Three aspects affected the evaluation of the outcome of inverse calculations. The first one was the final value of objective function expressing the agreement between the experimental and simulation data after the curing kinetics optimization. This final value of objective function allowed one to determine the value of improvement factor calculated according to Equation (4.10). Both the initial and final values of objective function and the improvement factors are included in the already cited Table 6.9. It should be noted that all performed inverse analyses led to the curing kinetics model giving better agreement with experimental data than before optimization, what generally justifies validity of the developed inverse methodology. The biggest improvement of temperatures fitting was obtained for the inverse analysis done for the curing model of the composite system (IA_3.2). Hence, these calculations and three other inverse analyses performed for the casting system that were finished with highest improvement factor, namely IA_3.1, IA_4 and IA_8, were selected for further analysis.

In the second step of the results analysis temperature curves generated in the numerical simulations utilizing the optimized curing kinetics parameters (in the inverse analyses done for the casting system) were taken into account and compared with the experimental curves (see Figure 6.9). In these charts the curve marked as EXP_A refers to the experiment conducted for pure epoxy resin (without curing reaction), the curve titled EXP_B.1 is the experiment done for the casting system including curing phenomenon and, finally, the curve denoted as 'Initial' represents the outcome of the simulation done with the input (not optimized) values of the curing kinetics model parameters (refer to Table 6.6).

The first observation made based on the results of the simulation with the initial curing kinetics model is that the reaction was activated too early comparing to the experimental data. Higher temperatures due to the occurring exothermic polymerization reaction were visible in this case already in the first hour, while according to the measurements 2 hours passed before the reaction started and the generated heat influenced the sensors readings (it is clearly visible when compared the results of EXP_A and EXP_B.1). The location of this characteristic increase of temperature was shifted in time in case of all three simulations with the optimized curing kinetics models giving better agreement with the performed experiment. However, a dramatic increase of temperature similar to the one observed in the experiment was clearly visible only for the kinetics model optimized in IA_8, while for the other two cases temperatures curves had a relatively flat course. On the other hand, one should remember that IA_3.1 and IA_4 turned out to be superior to IA_8 when taking into account the mentioned

objective function and improvement factor. Consequently, it was impossible to conclude unambiguously which of the performed inverse analyses gave the best results in the simulations modelling the curing of the casting system.

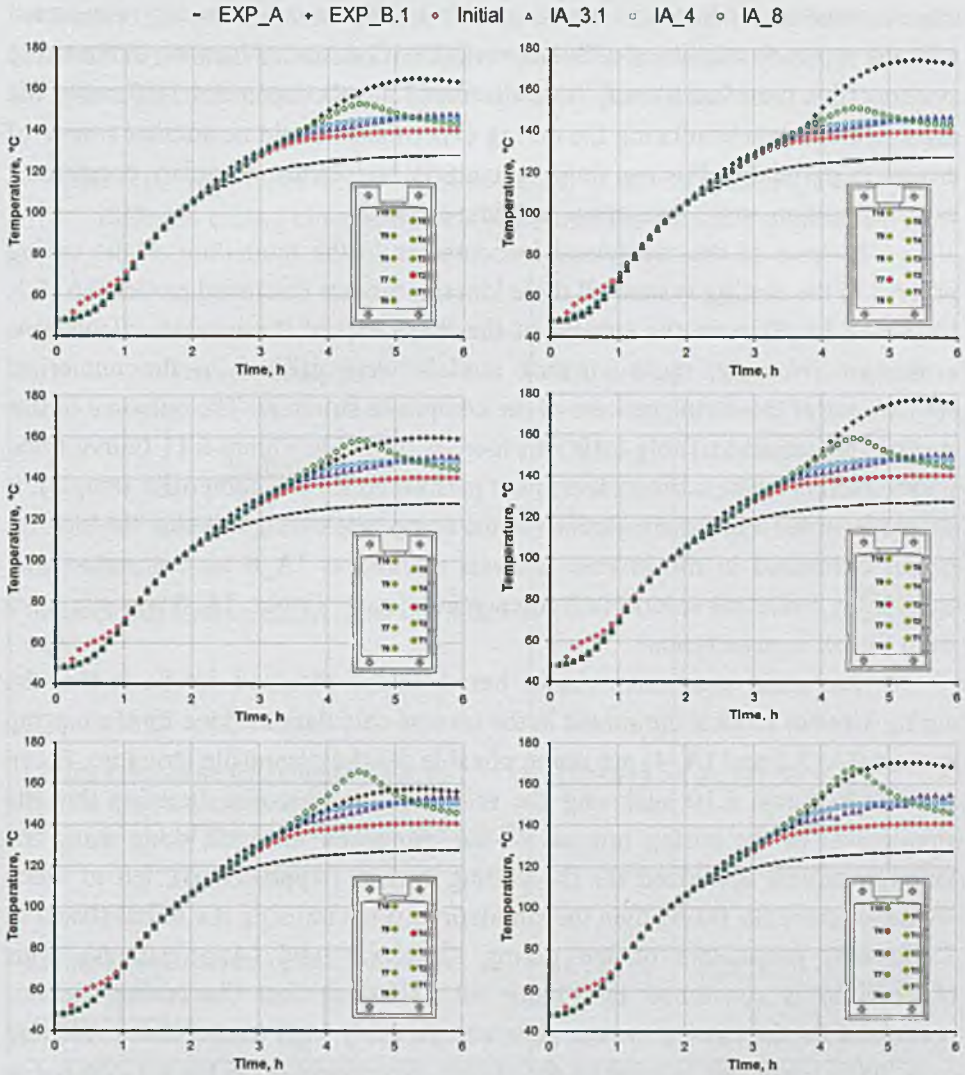


Figure 6.9: Temperature agreement at selected points near the mould wall (left) and in the middle of the mould cavity (right) for the casting system.

Besides that one can notice, especially analysing the results obtained for IA_8, that temperatures values were overestimated at some points, while for the others they were underestimated. This means that it could be impossible to obtain good agreement between experimental and simulation data at all points simultaneously. There are several probable reasons for that. One of them can be

the wrongly chosen curing kinetics model. Hence, evaluation of other multi-stage curing kinetics model can be a subject of further studies. Additionally, investigation of the dependence of the total heat of reaction on the heating rate should be continued. The other explanation of differences between the experimental and simulation results can be measurement errors, e.g. connected with the accuracy of thermal sensors or with their inaccurate location in the tested systems (this issue has already been discussed in subchapter 6.4.3). Finally, the numerical models simulating the curing experiments could be another source of errors. In particular, this can concern material properties, boundary conditions, initial condition, mesh resolution and time-step size.

In spite of the mentioned inaccuracies in the modelling of the curing process of the casting system all three kinetics models discussed earlier (IA_3.1, IA_4 and IA_8) were the subject of the third step of the inverse calculations evaluation. Namely, these kinetics models were utilised in the numerical simulations of the curing process of the composite structure. The outcome of this study is presented in Table 6.10, in Figure 6.10 and in Figure 6.11 (curve titled EXP_C refers to the curing experiment performed for the composite sample). It should be noted that the simulations of the composite curing utilizing the kinetics model optimized in the inverse analysis marked as IA_8 were instable and, eventually, led to the solution divergence in all runs. Hence, IA_8 was excluded from further considerations.

The main conclusion drawn based on the obtained results is that the curing kinetics models optimized in the inverse calculations done for the casting system (IA_3.1 and IA_4) are not applicable for the composite structure. It can be seen in Table 6.10 analysing the values of the objective function that the simulations of the curing process of the composite material, done using the kinetics models optimized for the casting system (Approach B), led to much worse temperature fitting than the simulations done utilising the initial (listed in Table 6.6) parameters of the curing kinetics model (Approach A). This observation is confirmed by Figure 6.10 showing that the curing kinetics optimized for the casting system gave unreasonably high temperatures reaching over 200°C, whereas in case of the curing experiment done for the composite sample the maximum temperatures were recorded below 160°C. One of the probable reasons of that was overestimation of the total heat of reaction. The amount of heat generated during the composite sample should be lower, since the volume of the casting system in the porous crepe paper was considerably smaller than in case of the casting system sample. This presumption was at least partially confirmed by the results obtained in the simulations, in which the influence of the material porosity was reflected either only in the energy equation (Approach C) or both in the energy equation and in the unsteady state conservation equation

representing the curing kinetics model (Approach D). In both cases the agreement between the simulation and experimental curves was improved comparing to Approach B as can be seen in Figure 6.11 and, consequently, the value of the objective function was also lowered (refer to Table 6.10). Nevertheless, the correlation between the results of the measurements and the numerical data generated by using Approach C and Approach D was still much worse than for the initial (not optimized) curing kinetics model (Approach A).

Table 6.10: Results of the curing simulations of the composite system with different curing kinetics models optimized for the casting system.

Inverse analysis	G, K^2		
	IA_3.1	IA_4	IA_8
Sample	Casting system	Casting system	Casting system
Approach A Initial curing kinetics model (refer to Table 6.6)	69070	69070	Solution divergence
Approach B Curing kinetics model optimized for the casting system (refer to the final parameters of IA_3.1, IA_4 and IA_8 listed in Table 6.9)	3323518	2469229	Solution divergence
Approach C Curing kinetics model optimized for the casting system and porosity included in the energy equation	1678218	1232855	Solution divergence
Approach D Curing kinetics model optimized for the casting system and porosity included in the energy and unsteady state conservation equations	3277937	1762863	Solution divergence

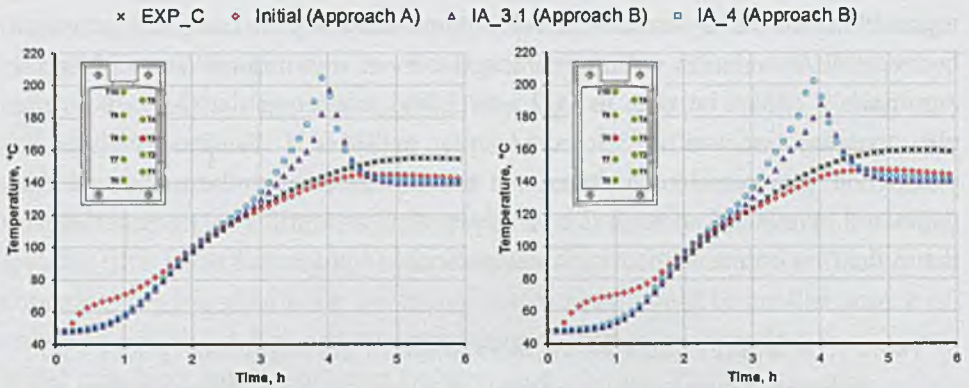


Figure 6.10: Temperature agreement at selected points for the composite sample modelled with the curing kinetics optimized for the casting system.

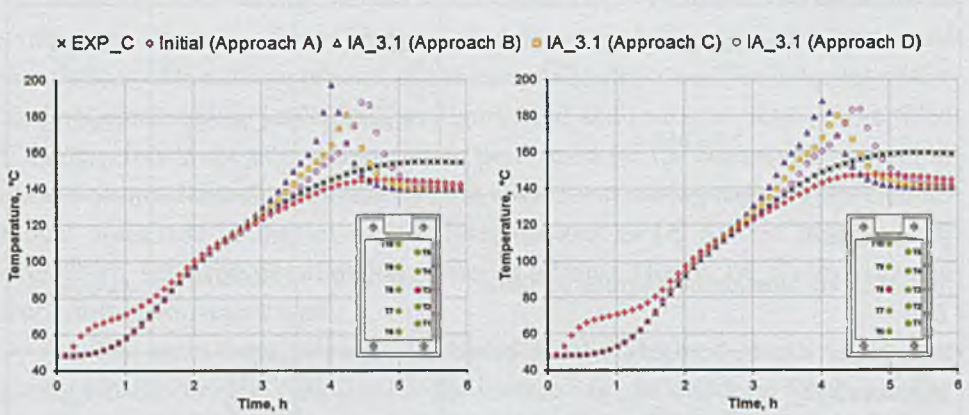


Figure 6.11: Temperature agreement at selected points for the composite sample modelled with the curing kinetics optimized for the casting system and with the porosity related corrections.

Further analysis of the results revealed considerable improvement of the agreement between the experimental data and the simulation results obtained with the kinetics model optimized in the inverse analysis utilizing the numerical model of the composite curing (IA_3.2). In this case the objective function was decreased by 60% comparing to the initial state thanks to the applied optimization procedure (refer to Table 6.9). The representation of the experimental temperature field obtained in the simulation with the improved kinetics model was much better than before optimization as shown in Figure 6.12. It is especially visible in the first 2 hours analysed, since too early activation of the curing reaction observed in the simulation done for the initial kinetics model was shifted in time in the simulation done for the optimized curing kinetics data. Consequently, the maximum temperatures occurred around 5 hour counting from

the simulation start, which was very similar to the experimental results. The values of maximum temperatures were also closer to these measured experimentally.

This confirmed that the proposed approach to determination of the curing kinetics data of composite structures works effectively and can be used together with thermal experiments to analyse the curing process of systems having heterogeneous structure and complex geometry. Besides that it can be stated that the kinetics model describing the curing of epoxy resin mixture (like the tested Hexion casting system) cannot be directly applied to the modelling of the cross-linking phenomenon of the composite structure in the form of crepe paper impregnated with this epoxy resin mixture. This conclusion was proved both by the curing experiments that showed differences in the course of polymerization reaction of these two samples and by the inverse calculations, since the kinetics model derived for the casting system was different than the one optimized for the composite material.

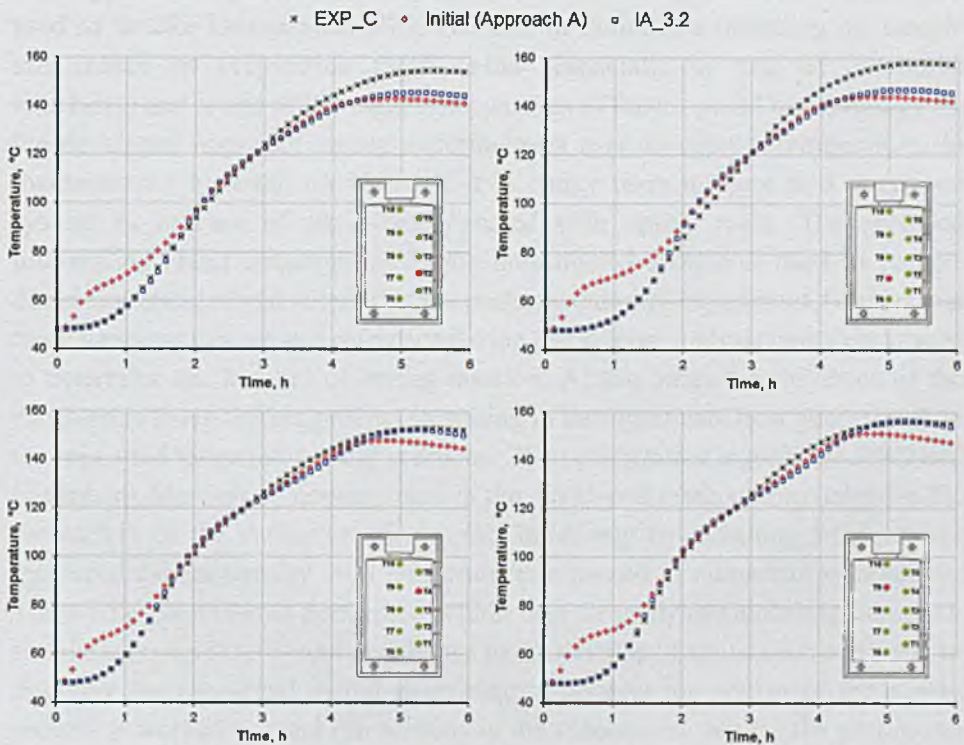


Figure 6.12: Temperature agreement at selected points for the composite sample modelled with the curing kinetics optimized for the composite system.

7. Conclusions and further work

7.1. Conclusions

In this thesis two main issues were comprehensively investigated. The first one was the new approach to determination of the kinetics of curing reaction of cross-linking materials, with the focus on the composite structure in the form of crepe paper impregnated with epoxy resin. Secondly, the possibilities of numerical modelling of the curing process occurring in this kind of composite materials were examined.

The approach to determination of the kinetics of curing reaction proposed within this thesis combines temperature measurements with numerical simulations and inverse methods. It is dedicated to the analysis of more detailed and bigger scale geometries than in case of standard experimental techniques used so far like for example DSC. The lack of limitations regarding the sample size makes its preparation much easier (especially in case of composite structures) and is one of the biggest advantages of the proposed methodology. In the developed approach curing experiment is used to capture temperatures in thermosetting material, no matter if it is epoxy resin mixture or a combined system as in case of paper impregnated with epoxy resin. The recorded information about temperatures in the investigated sample is used to prepare direct numerical model simulating the performed curing experiment. Besides that these temperatures act as a reference during the inverse analysis being performed to determine the kinetics of curing reaction. At this stage the influence of the exothermic cross-linking process (resulting in the significant heat generation) on the measured temperature field is crucial. The optimization algorithms (PSO and Levenberg-Marquardt) implemented in the developed methodology improve the parameters of the curing kinetics model iteratively by matching temperatures measured experimentally with temperatures obtained in numerical simulations. The whole calculations performed within inverse analysis (including computer simulations) are fully automated thanks to the developed application software. In this way the numerical model describing accurately the course of the curing process is worked out and can be used in the subsequent step for the purpose of optimization of the curing process.

The developed inverse methodology was subjected to many tests to evaluate the reliability and efficiency of the mentioned optimization algorithms constituting the core of the proposed approach. In the preliminary verification step both methods were applied to determine the coefficients of simple

polynomial and more complex Rastrigin functions. It allowed finding the optimum configurations of PSO and Levenberg-Marquardt algorithms that were employed in the subsequent stage utilizing the developed inverse methodology to determine the unknown parameters of the curing kinetics model. In this study the needed measured temperature data were generated virtually by using the mentioned direct numerical model of the curing process and the known information about the curing kinetics of the analysed material (obtained in DSC measurement). Hence, this part of investigations was referred to as virtual experiment of curing process. The optimized curing kinetics models were further evaluated in computer simulations utilizing modified geometries of the analysed systems, different resolutions of computational meshes and changed boundary conditions. Moreover, the effectiveness of both optimization algorithms was tested in inverse calculations including errors introduced into the synthetically prepared measurement data.

The preparation of experimental stand and the execution of curing experiments for different research samples was the next substantial element of this thesis. Both systems with relatively simple and uniform structures like in case of standard epoxy resin as well as complex composite specimens in the form of the mentioned resin impregnated paper were investigated. It is worth stressing that the location of thermal sensors in these experiments was defined utilizing information gained in sensitivity analysis. The main goal of the experimental part was to qualify the influence of the considered sample structure on the course of the cross-linking reaction and to capture data needed in the experimental validation of the developed numerical approach to curing modelling of cross-linking structures.

The final step taken in this thesis constituted the mentioned experimental validation of the curing modelling approach with the kinetics of curing reaction calculated with the use of the developed inverse methodology. The validation was performed both for the epoxy resin sample as well as for the resin-paper composite. For this purpose the direct numerical model built out within the mentioned virtual experimental study was extended with additional models in order to take into account the porous structure of crepe paper impregnated with epoxy resin. This time the temperatures measured in the curing experiments were utilized in two ways, i.e. to define and tune the numerical models and as an additional (reference) information required in the inverse analyses to determine the parameters of the curing kinetics models. The fundamental part of the validation procedure were the inverse calculations done independently to determine the curing kinetics model of the epoxy resin and of the resin-paper composite sample. It should be stressed at this point that the optimization was done this time only by using the Levenberg-Marquardt algorithm.

The main outcome of the research summarized above is that the hypothesis formulated at the beginning of this work has been confirmed, i.e.:

- the numerical model of the curing process of the resin-paper composite system has been developed,
- the kinetics of curing reaction occurring in the resin-paper composite structure has been determined by the combination of inverse methods, computer simulations and temperature measurements carried out during the curing process of the considered composite sample.

Moreover, all tasks defined in subchapter 1.3, leading to the statements above, have been accomplished and the following conclusions have been drawn based on investigations done within the framework of this thesis:

- the correctness of the principle of working and the effectiveness of the proposed methodology of the curing kinetics determination has been confirmed in inverse analyses performed within the study referred to as virtual experiment of curing process,
- Levenberg-Marquardt method turned out to be more effective in these virtual tests in comparison to PSO,
- the problem of inverse determination of the parameters of the curing kinetics model turned out to be ill-conditioned as the obtained results were not unique, i.e. good temperature agreement was obtained for more than one set of the curing kinetics parameters,
- the validity of the curing kinetics data obtained in the inverse calculations based on the virtual experiment has been proved in a series of tests including boundary conditions, geometry and mesh independence studies,
- the analysis of error influence carried out in the inverse calculations based on the virtual experiment revealed that the effectiveness of both considered optimization algorithms depends on errors in the input data,
- the sensitivity analysis being a part of the inverse calculations based on the virtual experiment provided information about the dependence of temperature field on the parameters of the curing kinetics model that was further used to define the optimum location of sensors in the experimental part (design of experiment),
- different course of curing reaction of the epoxy resin and of the resin-paper composite has been confirmed in temperature measurements carried out during the curing experiments,
- the influence of heating conditions and of moisture in the paper on the course of curing reaction has been proved as well in the mentioned experiments,
- the numerical model of the curing process developed based on the real experiments has been evaluated in a series of tests confirming that the

- numerical solution is independent on mesh and time-step size, but at the same time is strongly influenced by the location of temperature monitoring points,
- the kinetics of curing reaction of the epoxy resin sample and of the resin-paper composite, optimized by using the developed inverse methodology, improved the correlation between the simulation results and experimental data measured for a given material,
 - the curing simulation done for the resin-paper composite with the kinetics model obtained for the epoxy resin led to poor correlation with experimental data what confirmed that the curing kinetics valid for the epoxy resin sample cannot be applied to describe the cross-linking process of the composite structure in the form of the crepe paper impregnated with this epoxy resin,
 - the kinetics of curing reaction determined for the resin-paper composite was different than the one obtained for the epoxy resin sample.

7.2. Further work

The overall effectiveness of the developed inverse methodology of determination of the curing kinetics was proved, since the optimized kinetics models improved agreement between temperatures calculated in the numerical simulations and measured during the curing experiments. However, the accuracy of the representation of the curing reaction course was on different level depending on the measurement point. There are several potential reasons of such a situation that could be examined as a continuation of the research done within the framework of this thesis.

The first one is the already mentioned relatively big influence of the location of temperature monitoring points on results. It is probable that thermal sensors were not in the desired positions during experiments. Consequently, one could consider the repetition of measurements with improved control on the location of thermocouples, especially in the composite sample, to get more reliable measurement data for inverse calculations.

The next point that could be investigated is the kinetics model applied in the modelling of the curing reaction of the Hexion casting system. The choice of this specific two-stage reaction model was an assumption and other curing kinetics models could be evaluated in the next steps. For example, the inclusion of the dependence between the heating rate and the total heat of reaction gave promising results in one of the inverse analyses performed for the epoxy resin. However, the numerical simulation with such modified model was unstable and, eventually, was not applied successfully in the simulation of the composite curing. Hence, further development of the numerical approach utilizing this kinetics model should be considered.

The other issue is the chosen Hexion casting system that according to the performed measurements is characterized by relatively complex two-stage curing reaction. Hence, other thermosetting systems cross-linking in one-stage manner could also be studied with the developed inverse methodology.

Finally, the inverse calculations constituting the part of the experimental validation procedure were performed only by using the Levenberg-Marquardt method due to long computational time. Hence, it would be worth running the inverse analyses by using the stochastic PSO algorithm or a combination of both implemented optimization methods to compare the effectiveness of these approaches in inverse calculations utilizing the measured data.

Appendix

CD with results

CD with results, attached to the internal face of the back cover of this book, contains data organized in the following folders:

1. IRACKLIS software
 - a. IRACKLIS_ver_24.01.2011 – version used in the inverse calculations done to determine the kinetics of curing reaction (within the virtual experiment of curing process)
 - b. IRACKLIS_ver_18.05.2011 – version used in the inverse calculations done for the analysis of error influence (within the virtual experiment of curing process)
 - c. IRACKLIS_ver_24.07.2012 – version used in the inverse calculations done within the experimental validation of the curing modelling approach
2. Numerical model of the virtual curing experiment
 - a. Original model
 - b. Geometry independence study
 - c. Mesh independence study
 - d. Boundary conditions independence study
 - e. Analysis of error influence
 - f. Sensitivity analysis
3. Numerical model of the experiment run with the pure epoxy resin
 - a. Original model
 - b. Mesh independence study
 - c. Time-step size independence study
4. Numerical model of the curing experiment run with the casting system
 - a. Original model
 - b. Mesh independence study
 - c. Time-step size independence study
5. Numerical model of the curing experiment run with the resin-paper composite
 - a. Original model
 - b. Mesh independence study
 - c. Time-step size independence study
 - d. Influence of the monitoring points location

Bibliography

- [1] K. Ellis, *Bushings For Power Transformers: A Handbook For Power Engineers*, AuthorHouse, 2011.
- [2] J. H. Harlow, *Electric Power Transformer Engineering*, CRC Press, 2004.
- [3] L. Jonsson, R. Johansson, *High-voltage bushings: 100 years of technical advancement*, ABB Review, Volume 3, pp. 66-70, 2009.
- [4] D. M. Getson, *High voltage bushings*, ABB Document, 2002.
- [5] L. A. Canova, *Silica Filler For Epoxy Encapsulants And Epoxy Encapsulants Containing Same*, US Patent no. 4738892, 1988.
- [6] J. Stabik, M. Szczepanik, A. Dybowska, L. Suchon, *Electrical properties of polymeric gradient materials based on epoxy resin filled with hard coal*, Journal of Achievements in Materials and Manufacturing Engineering, Volume 38, Issue 1, pp. 56-63, 2010.
- [7] H. Wang, Y. Bai, S. Liu, J. Wu, C. P. Wong, *Combined effects of silica filler and its interface in epoxy resin*, Acta Materialia, Volume 50, pp. 4369-4377, 2002.
- [8] H. Parry, R. Hewitt, *Effect of Fillers on Epoxy Resins*, Industrial and Engineering Chemistry, Volume 49, No. 7, pp. 1103-1104, 1957.
- [9] *Swedish Bushings Plant Sees Growth in RIP Designs*, Insulation News & Market Report, Issue 68, Volume 13, No. 2, 2005.
- [10] W. L. Oberkampf, T. G. Trucano, *Verification and Validation in Computational Fluid Dynamics*, Progress in Aerospace Sciences, Volume 38, Issue 3, pp. 209-272, 2002.
- [11] Z. Bulinski, *Numerical Modelling and Credibility Analysis of Free Surface Flows in Selected Industrial Processes*, Ph.D. Thesis, Silesian University of Technology, 2010.
- [12] www.grc.nasa.gov, *Tutorial on CFD Verification and Validation*, NPARC Alliance Verification and Validation Web Site, September 18th 2012.
- [13] R. Sekula, P. Saj, T. Nowak, K. Kaczmarek, K. Forsman, A. Rautiainen, J. Grindling, *3-D modeling reactive molding processes: From tool development to industrial application*, Advances in Polymer Technology, Volume 22, Issue 1, pp. 42-55, 2003.
- [14] M. R. Kamal, S. Sourour, *Kinetics and Thermal Characterization of Thermoset Cure*, Polymer Engineering and Science, Volume 13, Issue 1, pp. 59-64, 1973.

- [15] M. R. Kamal, S. Sourour, M. Ryan, *Integrated Thermo-Rheological Analysis of the Cure of Thermosets*, Proceedings of the 31st Annual Technical Conference, pp. 187-191, Quebec, Canada, 1973.
- [16] J.-S. Le Brizaut, D. Delaunay, B. Garnier, Y. Jarny, *Implementation of an inverse method for identification of reticulation kinetics from temperature measurements on a thick sample*, International Journal of Heat and Mass Transfer, Volume 36, Issue 16, pp. 4039-4047, 1993.
- [17] J.-M. Vergnaud, I.-D. Rosca, *Rubber Curing and Properties*, CRC Press, 2008.
- [18] S. Li, R. Vatanparast, H. Lemmetyinen, *Cross-linking kinetics and swelling behaviour of aliphatic polyurethane*, Polymer, Volume 41, Issue 15, pp. 5571-5576, 2000.
- [19] J. M. Laza, C. A. Julian, E. Larrauri, M. Rodriguez, L. M. Leon, *Thermal scanning rheometer analysis of curing kinetic of an epoxy resin: 2. An amine as curing agent*, Polymer, Volume 40, Issue 1, pp. 35-45, 1999.
- [20] L. Pilato, *Phenolic Resins: A Century of Progress*, Springer, 2010.
- [21] X. Ramis, J. M. Salla, C. Mas, A. Mantecon, A. Serra, *Kinetic study by FTIR, TMA, and DSC of the curing of a mixture of DGEBA resin and γ -butyrolactone catalyzed by ytterbium triflate*, Journal of Applied Polymer Science, Volume 92, Issue 1, pp. 381-393, 2004.
- [22] P. Bartolomeo, J. F. Chailan, J. L. Vernet, *Curing of cyanate ester resin: a novel approach based on FTIR spectroscopy and comparison with other techniques*, European Polymer Journal, Volume 37, Issue 4, pp. 659-670, 2001.
- [23] T. G. Neiss, E. J. Vanderheiden, *Solution and solid-state NMR analysis of phenolic resin cure kinetics*, Macromolecular Symposia, Volume 86, Issue 1, pp. 117-129, 1994.
- [24] M. C. Kazilas, I. K. Partridge, *Exploring equivalence of information from dielectric and calorimetric measurements of thermoset cure – a model for the relationship between curing temperature, degree of cure and electrical impedance*, Polymer, Volume 46, Issue 16, pp. 5868-5878, 2005.
- [25] D. Mulligan, *Cure Monitoring for Composites and Adhesives*, Rapra Review Reports, Volume 14, No. 8, Report 164, 2003.
- [26] W.-B. Xu, S.-P. Bao, S.-J. Shen, G.-P. Hang, P.-S. He, *Curing kinetics of epoxy resin-imidazole-organic montmorillonite nanocomposites determined by differential scanning calorimetry*, Journal of Applied Polymer Science, Volume 88, Issue 13, pp. 2932-2941, 2003.
- [27] D. Rosu, C. N. Cascaval, F. Mustata, C. Ciobanu, *Cure kinetics of epoxy resins studied by non-isothermal DSC data*, Thermochemica Acta, Volume 383, Issues 1-2, pp. 119-127, 2002.

- [28] S. Han, H. G. Yoon, K. S. Suh, W. G. Kim, T. J. Moon, *Cure kinetics of biphenyl epoxy-phenol novolac resin system using triphenylphosphine as catalyst*, Journal of Polymer Science Part A: Polymer Chemistry, Volume 37, Issue 6, pp. 713-720, 1999.
- [29] E. Majchrzak, B. Mochnecki, J. S. Suchy, *Kinetics Of Casting Solidification – An Inverse Approach*, Scientific Research of the Institute of Mathematics and Computer Science at Czestochowa University of Technology, No. 1 (6), pp. 169-178, 2007.
- [30] D. Szeliga, J. Gawad, M. Pietrzyk, *Parameters Identification Of Material Models Based On The Inverse Analysis*, International Journal of Applied Mathematics and Computer Science, Volume 14, No. 4, pp. 549-556, 2004.
- [31] A. A. Skordos, I. K. Partridge, *Inverse heat transfer for optimization and on-line thermal properties estimation in composites curing*, Inverse Problems in Science and Engineering, Volume 12, Issue 2, pp. 157-172, 2004.
- [32] Y. C. Jarny, *Inverse Heat Transfer Problems And Thermal Characterization Of Materials*, 4th International Conference on Inverse Problems in Engineering, Rio de Janeiro, Brazil, 2002.
- [33] Nowak A. J., Bulinski Z. P., Kasza K., Matysiak L., *Inverse thermal problems in computational modelling of the paper vacuum drying process*, Inverse Problems in Science and Engineering, Volume 19, Issue 1, pp. 59-73, 2011.
- [34] Bulinski Z. P., Nowak A. J., Kasza K., Matysiak L., *Retrieving of the initial moisture field in porous material based on temperature measurements during drying*, Inverse Problems in Science and Engineering, Volume 20, Issue 5, pp. 691-705, 2012.
- [35] www.incontext.indiana.edu, December 28th 2013.
- [36] *Dissipation factor ($\tan \delta$) over the main insulation on high voltage bushings. Product Information*, ABB Document, 2002.
- [37] *Resin Impregnated Paper bushing technology at its best. Features and benefits*, ABB Document, 2006.
- [38] S. C. M. Park, D. J. Lee, I. S. Park, S. S. Seol, *Numerical and Experimental Investigation on Hot Vacuum Drying for Insulating Materials of 154 kV SF₆ Gas Insulated Transformer*, 13th International Heat Transfer Conference (IHTC-13), Sydney, Australia, 2006.
- [39] K. Kasza, L. Matysiak, R. Sekula, *Experimental verification of the numerical model for paper vacuum drying process*, ABB Report, 2008.
- [40] *Micafil Bushings. RIP Technology*, ABB Document, 2003.
- [41] *Bushings for High Voltage AC Applications. Selection guide*, ABB Document, 2006.

- [42] P. Saj, K. Kasza, R. Sekula, *Influence of aluminum foil and paper layers packing on curing process of RIP bushings*, ABB Report, 2005.
- [43] *Resin impregnated paper bushings. Product information*, ABB Document, 1997.
- [44] I. Hamerton, *Recent Developments in Epoxy Resins*, Rapra Review Reports, Volume 8, No. 7, Report 91, 1996.
- [45] *PERP Program – Epoxy Resins. New Alert*, Nexant Chem Systems, 2006.
- [46] www.researchinchina.com, *Global and China Epoxy Resin Industry Chain Report, 2011- 2012*, 2012.
- [47] www.prweb.com, September 10th 2012.
- [48] J. C. Salomone, *Polymeric Materials Encyclopedia*, CRC Press, 1996.
- [49] *EPIKOTE™ Resin 04820*, Material Safety Data Sheet (in Polish), Hexion Specialty Chemicals, 2010.
- [50] *EPIKURE™ Curing Agent 860*, Material Safety Data Sheet (in Polish), Hexion Specialty Chemicals, 2010.
- [51] A. J. Nowak, Z. Bulinski, *Preliminary study of numerical modelling of vacuum paper drying process*, Report within the cooperation with ABB Corporate Research, Institute of Thermal Technology, Silesian University of Technology, 2006.
- [52] K. Kasza, *Numerical modeling of paper vacuum drying process in Fluent software*, ABB Report, 2007.
- [53] *EPIKOTE™ Resin 04820 + EPIKURE™ Curing Agent 860. 2-Component Casting System for Reaction Injection Moulding and Conventional Casting*, Technical Data Sheet, Hexion Specialty Chemicals, 2010.
- [54] www.dostal.com.pl, October 6th 2012.
- [55] K. Kasza, L. Matysiak, R. Sekula, *Study on improvement of drying process of high voltage bushings*, ABB Report, 2008.
- [56] R. Sekula, K. Kaczmarczyk, T. Nowak, P. Saj, K. Forsman, A. Rautiainen, *Method of determining the hardening degree of thermosetting plastics, in particular of epoxy resins* (in Polish), PL Patent no. 192991 B1, 2000.
- [57] P. Panchaipetch, V. Ambrogio, M. Giamberini, W. Brostow, C. Carfagna, N. A. D'Souza, *Epoxy+liquid crystalline epoxy coreacted networks: I. Synthesis and curing kinetics*, Polymer 42, Issue 5, pp. 2067-2075, 2001.
- [58] Z. Ma, J. Gao, *Curing Kinetics of o-Cresol Formaldehyde Epoxy Resin and Succinic Anhydride System Catalysed by Tertiary Amine*, Journal of Physical Chemistry B, Volume 110, Issue 25, pp. 12380-12383, 2006.
- [59] A. Cosgrove, L. Lopez, J. Hernandez-Ortiz, T. Osswald, E. Camacho, *Modeling the Vulcanization Process of High Consistency Rubber And Liquid Silicon Rubber*.

- [60] A. J. Nowak, Z. Bulinski, *Estimation of Kinetic Parameters of the Resin Composite Curing Utilising Inverse Methodology*, Report within the cooperation with ABB Corporate Research, Institute of Thermal Technology, Silesian University of Technology, 2009.
- [61] A. Yousefi, P. G. Lafleur, R. Gauvin, *Kinetic studies of thermoset cure reactions: A review*, Polymer Composites, Volume 18, Issue 2, pp. 157-168, 1997.
- [62] K. Pielichowski, K. Flejtuch, *Kinetic study of the cross-linking process of epoxy resins based on differential scanning calorimetry (DSC) measurements*, Report within the cooperation with ABB Corporate Research, Cracow University of Technology, 2004.
- [63] T. Hatakeyama, F. X. Quinn, *Thermal Analysis. Fundamentals and Applications to Polymer Science*, John Wiley & Sons Ltd, 1999.
- [64] M. R. Kamal, *Thermoset Characterization for Mobility Analysis*, Polymer Engineering and Science, 14, pp. 231-239, 1974.
- [65] K. Pielichowski, J. Pagacz, *DSC and heat capacity measurement of resin mixture* (in Polish), Report within the cooperation with ABB Corporate Research, Cracow University of Technology, 2011.
- [66] M. N. Ozisik, H. R. B. Orlande, *Inverse Heat Transfer. Fundamentals And Applications*, Taylor & Francis, 2000.
- [67] Z. Ostrowski, *Application of Proper Orthogonal Decomposition to the Solution of Inverse Problems*, Ph.D. Thesis, Silesian University of Technology, 2006.
- [68] O. M. Alifanov, *Inverse Heat Transfer Problems*, Springer-Verlag, 1994.
- [69] A. Tarantola, *Inverse Problem Theory. Methods for Data Fitting and Model Parameter Estimation*, Elsevier Science B. V., 1987.
- [70] A. Kirsch, *An Introduction to the Mathematical Theory of Inverse Problems*, Springer Science+Business Media LLC, 2011.
- [71] K. Kurpisz, A. J. Nowak, *Inverse Thermal Problems*, International Series on Computational Engineering, Computational Mechanics Publications, 1995.
- [72] C. W. Groetsch, *Inverse Problems. Activities for Undergraduates*, Cambridge University Press, 1999.
- [73] C. Vogel, *Regularization Methods. An Applied Mathematician's Perspective*, Proceedings of SAMSI Workshop on Inverse Problem Methodology in Complex Stochastic Models, North Carolina, USA, 2002.
- [74] L. Matysiak, Z. Bulinski, A. J. Nowak, *Inverse Approach For Curing Kinetics Analysis Of Composites*, ECCOMAS International Conference on Inverse Problems in Mechanics of Structure and Materials (IPM 2011), Rzeszow-Sieniawa, Poland, 2011.

- [75] J. Kennedy, R. C. Eberhart, Y. Shi, *Swarm Intelligence*, Academic Press, 2001.
- [76] J. Kennedy, R. Eberhart, *Particle Swarm Optimization*, Proceedings of the 1995 IEEE International Conference on Neural Networks, pp. 1942-1948, Perth, Australia, 1995.
- [77] R. Eberhart, J. Kennedy, *A New Optimizer Using Particle Swarm Theory*, Proceedings of the Sixth International Symposium on Micro Machine and Human Science, pp. 39-43, Nagoya, Japan, 1995.
- [78] D. Bratton, J. Kennedy, *Defining a Standard for Particle Swarm Optimization*, Proceedings of the 2007 IEEE Swarm Intelligence Symposium (SIS 2007), 2007.
- [79] J. C. Bansal, P. K. Singh, M. Saraswat, A. Verma, S. S. Jadon, A. Abraham, *Inertia Weight Strategies in Particle Swarm Optimization*, Proceedings of the 2011 Third World Congress on Nature and Biologically Inspired Computing (NaBIC), pp. 633 – 640, Salamanca, Spain, 2011.
- [80] M. I. A. Lourakis, *A Brief Description of the Levenberg-Marquardt Algorithm Implemented by levmar*, 2005, www.ics.forth.gr, December 28th 2013.
- [81] A. Ranganathan, *The Levenberg-Marquardt Algorithm*, 2004, www.ananth.in, July 4th 2014.
- [82] D. de Souza, *Neural Network Learning by the Levenberg-Marquardt Algorithm with Bayesian Regularization (part 1)*, www.codeproject.co, September 17th 2012.
- [83] www.mathworld.wolfram.com, September 17th 2012.
- [84] A. J. Nowak, *Sensitivity analysis and specification of crucial parameters of lumped diffusion model of vacuum paper drying process*, Report within the cooperation with ABB Corporate Research, Institute of Thermal Technology, Silesian University of Technology, 2006.
- [85] K. Kasza, L. Matysiak, L. Malinowski, *Method to Describe Curing in Large Epoxy Samples*, *Advances in Polymer Technology*, Volume 28, Issue 4, pp. 267-275, 2009.
- [86] A. J. Nowak, Z. Bulinski, *Development of Numerical Model of Vacuum Paper Drying Process. Part III. Inverse Analysis*, Report within the cooperation with ABB Corporate Research, Institute of Thermal Technology, Silesian University of Technology, 2008.
- [87] S. Siltanen, *MAT-52506 Inverse Problems*, 2009, matriisi.ee.tut.fi, December 28th 2013.
- [88] A. Wirgin, *The inverse crime*, arxiv.org, December 28th 2013.
- [89] *Inverse problems: an introduction*, Math lectures, Geothe University Frankfurt, www.math.uni-frankfurt.de, December 31st 2013.

- [90] *ANSYS Fluent 12.0/12.1 Documentation*, ANSYS Inc., 2009.
- [91] A. J. Nowak, *Advanced Numerical Techniques in Energy Transfer. International Workshop for PhD Students*, Silesian University of Technology, 2004.
- [92] *ANSYS Fluent 14.0 Help*, ANSYS Inc., 2011.
- [93] R. W. Johnson, *The Handbook Of Fluid Dynamics*, CRC Press LLC, 1998.
- [94] B. Andersson, R. Andersson, L. Hakansson, M. Mortensen, R. Sudiyo, B. van Wachem, *Computational Fluid Dynamics for Engineers*, Cambridge University Press, 2012.
- [95] *GAMBIT 2.4 Documentation*, Fluent Inc., 2007.
- [96] K. Kasza, L. Malinowski, *Computer simulations and optimization of the curing process of 123kV RIF bushing*, ABB Report, 2008.
- [97] *Measurements data*, Hexion Specialty Chemicals, 2012.

Experimental Analysis and Inverse Approach in Numerical Modelling of Curing Process of Composite Materials

Abstract

Curing reaction is an inseparable phenomenon connected with the processing of thermosetting materials like for example epoxy resins. These materials constitute an excellent electrical barrier and, additionally, represent very good mechanical and thermal properties. This is the main reason why epoxy resins are widely used in energy industry, where strict requirements are set for power products regarding their reliability and quality, since this affects directly the operation of the whole power transmission and distribution system. One can find electrical bushings, current and voltage transformers, sensors, cable joints, etc. among the products, where epoxy resins are used as electrical insulation.

Such wide application of these thermosets means that the material properties must be tailored to the specific product. For this reason inorganic fillers like silica are used to modify the material properties. Addition of filler can result in higher hardness of the mixture, in lower shrinkage during the mixture curing, in decreased heat generation during the exothermic curing reaction, in the material transparency or its specific colour or, finally, in the improvement of other parameters influencing the material processing and its further exploitation as well as in lower cost of the material. Unfortunately, utilization of fillers is connected with the risk of sedimentation phenomenon that, consequently, can lead to anisotropic properties of electrical insulation what is highly undesirable.

This problem concerns mainly the power products having big dimensions like high-voltage electrical bushings reaching in some cases even more than ten meters of height. This is one of the reasons why the standard epoxy resin insulation has been replaced in the mentioned high-voltage bushings with the composite material in the form of crepe paper impregnated with epoxy resin. Consequently, the manufacturing of electrical insulation, including course of the curing reaction, has changed because of the difference between the material properties of standard epoxy resin and paper-resin composite. Meanwhile, the right execution of the cross-linking process is one of the main aspects influencing the final properties of electrical insulation, mainly because of strong exothermic character of the cross-linking reaction. For example, too high heat generation during the production of epoxy resin insulation can lead to the material

overheating and, simultaneously, to the degradation of the material insulation properties.

The complexity of the curing reaction makes its experimental analysis highly difficult, even in case of epoxy resin mixtures with relatively simple structure. Usually, Differential Scanning Calorimetry (DSC) is used to determine the kinetics of the cross-linking reaction, however, this measurement method is limited by a small size of the investigated sample (few milligrams). Hence, it is doubtful if such little sample is representative for much bigger systems having composite structure like in case of the mentioned paper impregnated with epoxy resin present in high-voltage bushings.

In the connection to above it was decided to make an attempt within the presented thesis to work out an alternative method of determination of the curing reaction kinetics of complex and big composite structures. For this purpose numerical modelling and inverse methodology supported with experimental measurements was proposed. It was possible, since the computational time is not the limiting factor anymore due to, observed already in the 80's, dynamic development of the mentioned inverse methods, of commercial software dedicated to numerical simulations and of processor capacity offered by modern.

The scope of this Ph. D. thesis includes among others the literature review focused on the application of inverse methods, utilizing numerical modelling and experiments, for determination of the kinetics of the phase change process, similar to the curing reaction. Information about electrical bushings and electrical insulation applied in these devices is also a part of introduction. The theoretical basics of inverse analysis and the mathematical description of the curing reaction kinetics can be found as well. Finally, the mentioned DSC, as one of the most famous measurement methods of the curing kinetics determination, is also described.

The preparation of the experimental stand and the execution of the curing experiments for different research samples was the substantial element of this thesis. Both systems with relatively simple and uniform structures like in case of standard epoxy resin as well as complex composite specimens in the form of the mentioned resin impregnated paper were investigated. The goal of this experimental part was twofold, i.e. to qualify how the structure of the investigated samples influences course of the cross-linking reaction and to capture data needed in the subsequent stages of the thesis.

The built up of the mathematical and numerical models describing the performed curing experiments was one of them. In particular, the model of the curing reaction kinetics had to be developed at this stage. For this purpose the inverse analysis was proposed. Basically, in this approach the temperatures recorded during the course of the curing process were applied to determine the

parameters of the mentioned model. At this stage the influence of the exothermic curing reaction (resulting in the significant heat generation) on the measured temperature field was important. Additionally, application software was developed within the worked out inverse approach to fully automate the optimization procedure (including computer simulations) executed in each inverse analysis. The application was based on two optimization algorithms, namely Levenberg-Marquardt method and Particles Swarm Optimization.

The developed approach to curing modelling, utilizing the inverse methodology to find the curing kinetics data, was subjected to credibility analysis. In the first step the preliminary tests were conducted to work out the optimum configuration of the optimization algorithms. For this purpose the coefficients estimation problem was solved for two benchmark functions. The goal of the next study, referred to as the virtual curing experiment, was to calculate the unknown curing kinetics parameters within inverse analysis. At this stage the needed measured temperatures were generated by using the mentioned numerical model of the curing process and the known curing kinetics data (so-called simulated measurement). The found curing kinetics model improved the correlation of results with the measurement data confirming the correctness of the principle of working of the proposed inverse methodology.

The next step constituted the experimental validation and this time the temperatures measured in the curing experiment were utilized as additional information required in inverse analysis to determine the parameters of the kinetics model of the cross-linking reaction. It should be noticed that two different kinetics models were worked out at this stage, namely the one describing the course of the curing reaction of the investigated epoxy resin and the second one dedicated to the composite structure consisted of the crepe paper impregnated with the mentioned epoxy resin. In both cases the applied inverse methodology led to the curing kinetics data giving an improved agreement between the simulation and experimental results. Additionally, it was concluded that the model describing the curing kinetics of the epoxy resin cannot be directly applied to the modelling of the cross-linking process of the resin-paper structures.

Badania Eksperymentalne oraz Numeryczna Analiza Odwrotna Procesu Utwardzania Materiałów Kompozytowych

Streszczenie

Reakcja utwardzania jest nieodłącznym zjawiskiem towarzyszącym procesom wytwarzania z wykorzystaniem materiałów termoutwardzalnych, do których zalicza się między innymi żywice epoksydowe. Stanowią one doskonałą barierę elektryczną, przy okazji reprezentując bardzo dobre własności mechaniczne i termiczne. Jest to jedna z głównych przyczyn powszechnego stosowania żywic epoksydowych w branży energetycznej. Ma to związek z wysokimi wymaganiami stawianymi produktom energetyki w kwestii ich bezawaryjności i jakości, których spełnienie jest krytyczne z punktu widzenia niezawodności całego systemu energetycznego. Do takich produktów zalicza się między innymi przepusty elektryczne, przekładniki prądowe i napięciowe, sensory, złącza kablowe, itd.

Szerokie zastosowanie żywic epoksydowych wiąże się z koniecznością dostosowania jej własności do konkretnej aplikacji. W tym celu wykorzystuje się różnego rodzaju wypełniacze nieorganiczne, na przykład krzemionkę, których dodatek może skutkować wzrostem twardości mieszanki, zmniejszeniem skurczu mieszanki podczas utwardzania, mniejszą generacją ciepła w egzotermicznej reakcji utwardzania, uzyskaniem przezroczystości lub konkretnego koloru mieszanki, czy wreszcie poprawą innych parametrów wpływających na przetwórstwo materiału i jego późniejszą eksploatację oraz obniżenie kosztu samego materiału. Niestety stosowanie wypełniaczy wiąże się także z ryzykiem wystąpienia zjawiska sedymentacji, w wyniku którego uzyskuje się anizotropowe własności izolacji elektrycznej, co jest wysoce niepożądane.

Problem ten dotyczy w głównej mierze produktów energetycznych o dużych gabarytach, jak wysokonapięciowe przepusty elektryczne osiagające w niektórych przypadkach kilkanaście metrów wysokości. Między innymi w celu przeciwdziałania zjawisku sedymentacji, standardową izolację żywiczną we wspomnianych przepustach wysokonapięciowych zastąpiono materiałem kompozytowym w postaci papieru marszczonego impregnowanego żywicą epoksydową. Pociągnęło to za sobą również zmiany w procesie wytwarzania izolacji elektrycznej, w tym w przebiegu samej reakcji utwardzania ze względu na różne własności materiałowe standardowej mieszanki żywicznej i żywiczno-papierowego kompozytu. Tymczasem, właściwy przebieg procesu sieciowania

jest jednym z najbardziej istotnych aspektów wpływających na końcowe własności izolacji elektrycznej, głównie ze względu na silnie egzotermiczny charakter reakcji sieciowania. Przykładowo, zbyt wysoka generacja ciepła w czasie wytwarzania izolacji żywicznej może prowadzić do przegrzania układu i tym samym do degradacji własności izolacyjnych materiału.

Złożoność reakcji utwardzania powoduje jednak, że analiza eksperymentalna tego zjawiska jest niezwykle trudna, nawet w przypadku mieszanin żywicznych o stosunkowo prostej strukturze. Zazwyczaj, w celu określenia kinetyki reakcji sieciowania, wykorzystuje się skaningową kalorymetrię różnicową (ang. Differential Scanning Calorimetry – DSC), która ograniczona jest jednak niewielkim rozmiarem badanej próbki (kilka miligramów). Wątpliwe jest, czy tak niewielkich rozmiarów próbka jest reprezentatywna dla większych układów o strukturze kompozytowej, jak w przypadku wspomnianego papieru impregnowanego żywicą epoksydową.

W związku z powyższym postanowiono w ramach niniejszej pracy podjąć próbę opracowania alternatywnej metody wyznaczania kinetyki reakcji utwardzania złożonych struktur kompozytowych o większych gabarytach, z wykorzystaniem modelowania numerycznego oraz metodyki odwrotnej wspieranej pomiarami eksperymentalnymi. Stało się to możliwe, ponieważ czas obliczeń nie stanowi obecnie przeszkody ze względu na, obserwowany już w latach 80-tych, dynamiczny rozwój wspomnianych metod odwrotnych, komercyjnych narzędzi do symulacji numerycznych oraz mocy obliczeniowych współczesnych komputerów.

Zakres pracy doktorskiej obejmuje między innymi przegląd literaturowy ukierunkowany na zastosowanie metod odwrotnych, wykorzystujących modelowanie numeryczne i eksperymenty, do wyznaczania kinetyki procesu przemiany fazowej, podobnego do reakcji utwardzania. Znaczną część wstępu teoretycznego stanowi wprowadzenie do zagadnień dotyczących przepustów elektrycznych oraz izolacji elektrycznej stosowanej w tych urządzeniach. Ponadto, w pracy zawarto podstawy teoretyczne analizy odwrotnej, a także przedstawiono opis matematyczny kinetyki reakcji utwardzania i wspomnianą skaningową kalorymetrię różnicową, jako jedną z najpopularniejszych metod pomiarowych służących do wyznaczania kinetyki reakcji sieciowania.

Istotnym elementem pracy doktorskiej było przygotowanie stanowiska pomiarowego oraz wykonanie eksperymentów utwardzania z wykorzystaniem próbek badawczych o stosunkowo prostej, jednorodnej strukturze jak w przypadku standardowych układów żywicznych, jak również skomplikowanych struktur kompozytowych w postaci wspomnianego papieru krepowanego, impregnowanego żywicą epoksydową. Miało to na celu określenie wpływu

budowy badanych próbek na przebieg reakcji sieciowania oraz zebranie danych potrzebnych w kolejnych etapach pracy.

Opracowanie modelu matematycznego i numerycznego opisującego przeprowadzone eksperymenty utwardzania było jednym z nich. Etap ten wymagał w szczególności przygotowania modelu kinetyki reakcji utwardzania. W tym celu zaproponowane zostało podejście odwrotne, w którym parametry wspomnianego modelu matematycznego zostały wyznaczone na podstawie informacji o temperaturach zarejestrowanych w układzie podczas przebiegu procesu utwardzania. Istotny był tutaj wpływ wspomnianej egzotermicznej reakcji, z którą wiąże się generacja dużych ilości ciepła, na mierzone temperatury. Dodatkowo, w ramach opracowanego podejścia odwrotnego przygotowano aplikację w celu pełnego zautomatyzowania procedury optymalizacyjnej (w tym symulacji komputerowych) przeprowadzanej w ramach każdej analizy odwrotnej. Aplikacja ta została oparta na dwóch algorytmach optymalizacyjnych, mianowicie na metodzie Levenberga-Marquardta oraz metodzie roju cząstek.

Rozwinięte podejście odwrotne zostało poddane analizie wiarygodności. W pierwszym kroku przeprowadzono wstępne testy, które posłużyły do opracowania optymalnej konfiguracji algorytmów optymalizacyjnych. Polegały one na wyznaczeniu współczynników dwóch funkcji benchmarkowych. Celem kolejnego studium, nazwanego wirtualnym eksperymentem utwardzania, było opracowanie modelu kinetyki reakcji sieciowania dla przykładowego systemu żywicznego przy wykorzystaniu analizy odwrotnej. Na tym etapie wymagane dane pomiarowe zostały wygenerowane w ramach tzw. symulowanego pomiaru, tj. bazując na modelu numerycznym procesu utwardzania i na informacji o kinetyce utwardzania pochodzącej z pomiaru DSC. W wyniku przeprowadzonej analizy odwrotnej otrzymano parametry modelu kinetyki reakcji utwardzania, które użyte w symulacji komputerowej procesu utwardzania badanego materiału, pozwoliły poprawić korelację temperatur uzyskanych w tych obliczeniach ze sztucznie spreparowanymi danymi pomiarowymi, potwierdzając poprawność działania zaproponowanej metodologii odwrotnej.

Kolejny etap stanowiła właściwa walidacja eksperymentalna, w której temperatury zmierzone podczas eksperymentu utwardzania posłużyły za dodatkową informację niezbędną do przeprowadzenia analizy odwrotnej i do wyznaczenia w ten sposób parametrów modelu kinetyki reakcji sieciowania. Należy zauważyć, że na tym etapie wyznaczono dwa osobne modele kinetyki sieciowania, z których jeden opisywał przebieg reakcji utwardzania badanej żywicy epoksydowej, a drugi był dedykowany strukturom kompozytowym złożonym z papieru krepowanego, impregnowanego wspomnianą żywicą epoksydową. W obydwu przypadkach zastosowanie zaproponowanej

metodologii odwrotnej pozwoliło opracować modele kinetyki utwardzania dające lepszą zgodność pomiędzy wynikami symulacyjnymi i eksperymentalnymi. Dodatkowo stwierdzono, że model opisujący przebieg reakcji utwardzania żywicy epoksydowej nie może zostać bezpośrednio użyty do modelowania procesu sieciowania struktur żywiczno-papierowych.

Silesian University of Technology
Gliwice, Poland, 2014
ISBN 978-83-61506-24-9

